ETH
Eidgenössische Technische Hochschule Zürich
Swiss Federal Institute of Technology Zurich

eeh power systems laboratory

Fernando De Samaniego Steta

Modeling of an Advanced Adiabatic Compressed Air Energy Storage (AA-CAES) Unit and an Optimal Model-based Operation Strategy for its Integration into Power Markets

Master Thesis
PSL1003

EEH – Power Systems Laboratory
Swiss Federal Institute of Technology (ETH) Zurich

Expert: Prof. Dr. Göran Andersson
Supervisors: Dipl.-Ing. Andreas Ulbig and
Dipl.-Ing. Stephan Koch

Zurich, October 2010

Preface

This master thesis is the result of a six-month research project in which I was involved under the supervision of Andreas Ulbig and Stephan Koch at the Power Systems Laboratory (PSL) of ETH Zürich.

The main idea of this project was to develop a model of an Advanced Adiabatic Compressed Air Energy Storage (AA-CAES) system and to assess its operation capabilities within power markets.

The relevance of this project comes from the fact that AA-CAES systems are one of the few technologies that can store energy in the order of gigawatt days (GWd) without using fossil fuels. Hence, these systems are an attractive load balancing solution in a possibly carbon-constrained future, where the integration of intermittent renewable energy sources into the electric grid is a major challenge.

This thesis, and in general my whole postgraduate studies, would not have been possible without my always supportive parents Federico and Concha, which have always encouraged me to follow my dreams and to work hard for them.

The success of this project would not have been possible without the valuable advices and comments from Andreas and Stephan, thanks to whom these last six months were a satisfying learning experience.

Other important pillars without which my master would not have been completed are my dear friends Josch, Criss, Madis, Eva, Kaia, Frank and Teresa. With them I enjoyed wonderful moments during these last two years.

I would also like to thank my tutor Prof. Dr. Roland Scholz, who supported me in all the projects I was interested in along my master studies.

It is worth mentioning that my postgraduate studies would not have taken place without the scholarship awarded by the Mexican National Council of Science and Technology (CONACYT).

Abstract

A model of an advanced adiabatic compressed air energy storage (AA-CAES) plant is presented. The overall efficiency of the model is 57 % and it is composed of a 64 MW compression train, a thermal energy storage (TES) system, an 85 MW expansion train, and a cavern for the storage of compressed air, which is large enough to reversibly store mechanical energy in the order of gigawatt days (GWd). The compression and expansion trains have heat exchangers to transfer heat between the air and a heat transfer fluid. The latter one is used to charge and discharge the TES system. Energy losses occur at the cavern walls, and between the TES and the environment. The AA-CAES model has three different operation states: expansion, compression and idle. The main physical processes occurring in each operation stage are represented by the model while taking into account the energy losses. Four time-dependent differential equations govern this dynamical system, which are solved for each time step of the simulation.

A model-based optimal operation strategy is presented as a benchmark for future inclusion of these storage systems within given power market regimes. The optimization is done via an MPC (Model Predictive Control) scheme using a benchmark price profile, and the hourly price profile of the European Power Exchange (EPEX) electricity spot market for the year 2007. Two approaches were considered for the calculation of the optimal operation strategy by using two different linear models inside the MPC optimizer. The first and second approach correspond to the state-space representation of a discrete linear-time invariant (LTI) system and a piece-wise affine (PWA) system, respectively. The calculated operation strategies maximize the plant's revenue within the imposed constraints following both price profiles.

Kurzfassung

Die vorliegende Arbeit stellt ein Modell für eine adiabatische Druckluftspeicher-Anlage (AA-CAES) vor. Der Gesamtwirkungsgrad des Modells beträgt 57 % und beinhaltet einen 64 MW Kompressionsantriebsstrang, einen thermischen Energiespeicher (TES), einen 85 MW Expansionsantriebsstrang und eine Druckluftspeicherkaverne, die mechanische Energie in der Grössenordnung von Gigawattagen (GWd) speichern kann.

Die Kompressions- und Expansionsantriebsstänge verfügen über je einen Wärmetauscher, welcher die Wärme zwischen der Luft und einer Wärmeträgerflüssigkeitü berträgt. Das Laden und Entladen des TES-Systems erfolgt über die Wärmeträgerflüssigkeit. An den Wänden der Druckluftspeicherkaverne und zwischen dem TES und der Umwelt treten Energieverluste auf. Das AA-CAES-Modell verfügt über drei verschiedene Betriebszustände: Expansion, Kompression und Leerlauf. Das Modell bildet die wichtigsten physikalischen Prozesse des jeweiligen Betriebszustandes, unter Berücksichtigung der Energieverluste, ab. Vier zeitabhängige Differentialgleichungen, die für jeden Zeitschritt der Simulation gelöst werden, bestimmen dieses dynamische System.

Das Modell umfasst auch eine optimale Betriebsstrategie, welche für die künftige Integration dieser Speichersysteme in bestehende Strommärkte verwendet werden könnte. Die Optimierung erfolgt über ein MPC (Model Predictive Control) System, welches ein Pauschalpreis-Grundprofil, sowie das Stundenpreis-Profil des European Power Exchange (EPEX) Spotmarktes von 2007 benutzt. Für die Berechnung der optimalen Betriebsstrategie wurden zwei Ansätze verfolgt, die zwei unterschiedliche lineare Modelle innerhalb des MPC-Optimierers berücksichtigen. Der erste und zweite Ansatz entspricht der Zustandsraum-Darstellung des diskreten, linearen zeitinvarianten Systems (LTI) und jeweils einem stückweise affinen (PWA) System. Die berechnete Betriebsstrategie maximiert die Einnahmen der Anlage innerhalb der gegebenen Rahmenbedingungen.

Contents

List of Acronyms

AA-CAES	Advanced Adiabatic Compressed Air Energy Storage
BTU	British Thermal Unit
CAES	Compressed Air Energy Storage
CFTOC	Constrained Finite-Time Optimal Control
GWd	Gigawatt day
GWh	Gigawatt hour
GW	Gigawatt
HHV	High Heating Value
HPT	High Pressure Turbine
HTF	Heat Transfer Fluid
HX	Heat Exchanger
kWh	Kilowatt hour
kW	Kilowatt
MJ	Megajoule
MPC	Model Predictive Control
MW	Megawatt
LPT	Low Pressure Turbine
LTI	Linear Time Invariant
PHS	Pumped Hydroelectric Storage
PWA	Piece-Wise Affine
RES	Renewable Energy Sources
TES	Thermal Energy Storage
TJ	Terajoule
VAR	Volt-Ampere Reactive

List of Symbols

Symbol	Description	Unit
a	Thermal conductivity	$[\mathrm{W/m \cdot K}]$
c_p	Specific heat capacity at constant pressure	$[\mathrm{J/kg \cdot K}]$
c_v	Specific heat capacity at constant volume	$[\mathrm{J/kg \cdot K}]$
$\dot{m}$	Mass flow	$[\mathrm{kg/s}]$
n	Polytropic index	[-]
N	Prediction Horizon	[h]
p	Pressure	[bar]
t	Time	[h]
T	Temperature	[K]
V	Volume	$[\mathrm{m}^3]$
α	Heat transfer coefficient	$[\mathrm{W/m^2 \cdot K}]$
β	Compression ratio	[-]
η	Efficiency	[-]
ρ	Density	$[\mathrm{kg/m}^3]$

List of Sub- and Superscripts

Subscript	**Description**
a	Air
c	Compression, Compressor
ct	Compressor train
e	Expansion
HTF	Heat Transfer Fluid
i	idle
rs	Rock-salt
sc	Salt cavern
t	Expansion train
TES	Thermal Energy Storage

Superscript	**Description**
in	Inflow of a fluid in a process
out	Outflow of a fluid in a process

Chapter 1

Introduction

The discovery of a vast supply of fossil fuels in the 19^{th} century promoted the industrial revolution and near-exponential growth of the population [1]. Since then, human consumption of fossil fuels has increased abruptly until today, making the modern energy-intensive life of the 21^{st} century highly dependent on them [2]. In 2007, the world's total final energy consumption had a share of fossil fuels close to 70 % [3], which cannot be maintained in the long term since fossil fuels reserves are finite and not equally distributed [4].

These energy security issues related to high fossil fuels dependence together with its association with an accelerated global warming [2], has promoted the exploration of sustainable new renewable energy sources (RES) as an alternative [5–7].

All the same, the replacement of fossil fuels as an energy source is a difficult endeavour because of their high energy density, as well as their versatility and high profitability. These advantages, coupled with the fact that renewable energy sources are generally diffuse, remote from major energy demand centres, variable and uncertain, makes the task of large-scale inclusion even more challenging for these technologies. Therefore, the creation of effective public policies to increase the technical and economic competitiveness of RES has been vital for their deployment. For example, one of the European Union's (EU) main energy policies in the long term is fostering renewable energies for power generation. They will do this through the implementation of regulations that cope with cost disadvantages of these energy sources within liberalized electricity markets [8].

However, fostering renewable energies through improving its technical and economic competitiveness will not necessarily ensure the success of these technologies. Even though there is a lot of room to improve its installed capacity, efficiency and reliability, the major obstacles for large-scale RES integration into the present electric power systems lies in its intermittent nature. In other words, since the electricity produced must match the load at every instant of the day, renewable energies should provide power when needed,

regardless if the sun is shining or the wind blowing. A solution to cope with this problem is provided, among other options, by large-scale energy storage systems. The motivation of this thesis is to present a thermodynamical model of this type of systems together with a benchmark operation strategy, which will allow this system to operate optimally within the existing power market regimes.

This thesis is organized in five chapters. The first one presents an introduction to large-scale energy storage systems, making an emphasis on the compressed air energy storage (CAES) technology together with its inclusion into the electricity value chain. The second chapter introduces a model of an advanced adiabatic CAES (AA-CAES) plant together with the dynamics of the system. Chapter 3 provides the theoretical frame to calculate an optimal operation strategy for the created model using a model predictive control (MPC) scheme. The fourth chapter presents the results of the optimization. The fifth and last chapter discusses the results presented in the previous chapters and concludes this thesis.

The next section presents a comprehensive analysis of the inclusion of these storage systems into the grid making a comparison between the two most promising technologies.

1.1 Large-Scale Energy Storage

1.1.1 Energy storage and its applications

The use of large-scale energy storage plants for bulk electricity management has changed in recent years due to the inclusion of intermittent RES and the market liberalization of the electricity sector. Traditionally, this sector was vertically integrated, which means that companies had to deal with the complete electricity value chain to cover the demand with a quality supply at any minute of the day. In this case, the energy storage systems were owned by each company, using it whenever load leveling was required and for its own economic benefit. After market liberalization, companies were able to offer their energy storage capacity in the power market, which gave the storage plants a value for themselves. This situation, together with the inclusion of RES into the electricity generation mix has fostered interest in large-scale energy storage technologies.

Furthermore, the inclusion of large-scale energy storage systems allows RES to supply power as needed providing quality utility-scale power to the electricity network [7, 9–12]. These storage systems provide support for the intermittent RES, leveling the load in order to maximize the use of the generated electricity, increasing at the same time, the average utilisation of the transmission systems. In order to store utility-scale power to cope with the inclusion of RES, energy storage systems should have a capacity in the order of magnitude of gigawatt days (GWd), which can only be achieved by a

couple of technologies[1] . The following subsections present these technologies compared to all the other electricity storage systems.

Even though large-scale energy storage systems are a good solution to cope with the uncertainty and variability of renewable energies, they are also crucial to maintain the security, reliability and efficiency of the present electric power systems [13]. These energy storage facilities can produce negative and positive regulating power, reduce the spinning reserve[2], assist on grid upgrades and/or prevent them, provide firm capacity, damp price volatility, and provide high-value ancillary services [7, 11, 13–17].

1.1.2 Available large-scale energy storage technologies

Large-scale storage of electricity is a challenging task that is usually tackled by converting electric energy into another type of storable energy like chemical, thermal or potential energy. This energy is then transformed into electricity whenever it is needed. For example, batteries use chemical energy to store electricity whereas CAES uses thermal and potential energy. The available technologies for electricity storage together with their application in the electricity value chain have been extensively reviewed by several authors [7, 13, 16–25]. The application of these technologies as well as their performance depend on their energy and power density, response time, costs and output capacity. Comparisons between storage technologies accounting these latter factors [13, 16, 17] show that compressed air energy storage (CAES) and pumped hydroelectric storage (PHS) are the best options for bulk electricity storage, since they are the ones with the highest energy output capacity and lowest associated costs (see Subsection 1.1.3). The following section presents a discussion about the advantages of CAES over PHS, since the interest of this work is on large-scale energy storage systems.

1.1.2.1 Pumped Hydroelectric Storage (PHS)

The use of potential energy to store electricity is the oldest large-scale storage technology, with the first hydroelectric storage plant built in 1892 in Zürich, Switzerland [21]. Since then these systems have become numerous and their technology is now well developed and globally deployed, having a rated power capacity of over 2000 MW and being able to store energy for more than half a year [17, 26–28]. This storage time depends on the reservoir's size and the availability of the water in the area. Nowadays, there are more than 100 GW of pumped storage in operation, which is about 3 % of the worldwide generation capacity [21, 28].

[1] 1 gigawatt day GWd=86.4 TJ

[2] Use of part-loaded fossil power plants held in readiness to meet sudden and unpredicted demands, as well as power emergencies that arise from the failure of generating units and/or transmission lines [7]

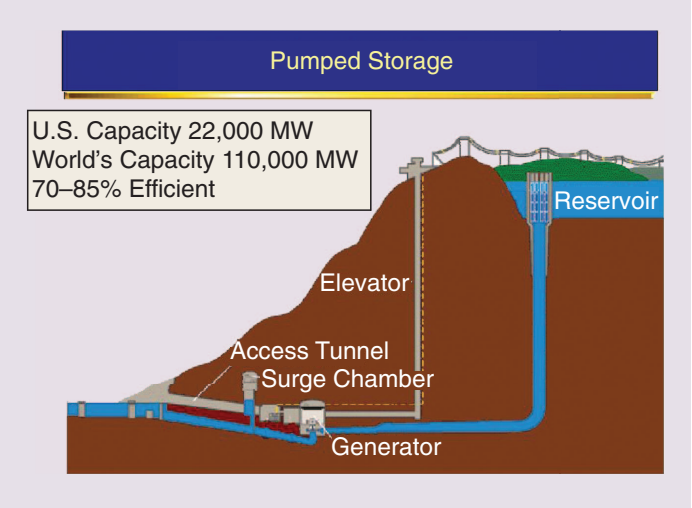

Figure 1.1: Pumped Hydroelectric Storage Plant [21]

PHS systems use surplus electricity to pump water vertically upwards by an altitude h from a lower to an upper reservoir, where it is held until electricity is required again. Whenever this happens, the water is then run downwards through a Francis turbine, which converts the potential energy of the water back into electricity (see Figure 1.1). A height $h = 500$ m between two reservoirs provides an energy density [3] of 4.9 $^{\mathrm{MJ}}/_{\mathrm{m}^3}$ = 1.36 $^{\mathrm{kWh}}/_{\mathrm{m}^3}$. Considering this height difference and an ideal system with no losses, an upper reservoir needs a volume $V = 1000\,\mathrm{m} \cdot 1000\,\mathrm{m} \cdot 50\,\mathrm{m}$ to store 3 GWd.

The main advantage of using PHS systems to store surplus electricity is that it is readily available [17], which from a technical perspective, makes its implementation easier and gives security to investors. The efficiency of these systems, from the point of view of a power network, is between $70 - 85$ % depending on the system characteristics [27]. The recoverable energy content of the reservoir in PHS does not vary drastically with the discharge rate [22], which is an important characteristic for the storage system in order to maintain the quality of the energy output. Finally, these systems can be ready to supply electricity in a matter of minutes.

As for the caveats of PHS systems, the land surface needed to store the pumped water is the main constraint, since sites with suitable topographies for these storage plants are increasingly rare [22, 29, 30]. This has been exacerbated by the fact that the environmental impact of large-scale PHS facilities is becoming more of an issue, and many suitable projects have encountered strong opposition from society [29, 31]. Another problem with

[3] This is calculated for water at 20°C through the following expression: $998.21\ ^{\mathrm{kg}}/_{\mathrm{m}^3} \cdot 9.79\ ^{\mathrm{m}}/_{\mathrm{s}^2} \cdot 500\,\mathrm{m} = 4.9\ ^{\mathrm{MJ}}/_{\mathrm{m}^3}$

these systems is that the rated capacity needs to be bigger than 1000 MW to have competitive capital costs as shown in Table 1.1. Even though these costs are low compared to battery systems, they are always higher than those associated with CAES systems (Table 1.1).

1.1.2.2 Compressed Air Energy Storage (CAES)

Since the research question of this thesis is related to this technology we will place more emphasis on its discussion. The storage of mechanical elastic energy is a technique that has been used since prehistoric times, specially in weapon's construction (for example, the ballista or the bow and arrow). Air is an elastic medium that stores potential energy when it is compressed and releases this energy when it is expanded in a controlled manner. The use of a gas turbine for the controlled air expansion to produce electricity motivated the creation of the CAES technology. The first patent for a compressed air storage system with an underground air-storage cavern was patented by Stal Laval in 1949 [18].

In principle, a CAES system operates very similarly to a conventional gas turbine[4], except that clutches are added so that the compression and expansion stages are separately connected to the generator, thereby taking place at different times. This system can be understood as interrupting the Joule thermodynamic cycle; the compressed air is injected into a cavern instead of sending it directly to the combustor. When electricity is needed, the pressurized air is extracted from the underground reservoir and the cycle is then completed. One important fact of the CAES systems is that they use gas turbines for the generation of electricity, which are energy conversion devices with a very mature technology, with efficiencies between 30 % and 40 % [12, 18, 32]. However, CAES systems have a big advantage over combined-cycle power plants that use gas turbines, since the latter ones use $60\ \% - 70\ \%$ of the generated mechanical energy to drive the air compressor, while the former ones use surplus electricity from the grid [18]. This translates into more electricity generated per unit of gas injected into the CAES system in comparison with a conventional combined-cycle power plant. Ramp rates are also better in CAES systems than in equivalent gas turbine plants [29].

Figure 1.2 shows the basic configuration of a CAES plant, which mainly consists of a compressor train (1), motor-generator unit (2), expansion train (3) and underground insulated reservoir (4) [33]. The CAES storage process is mainly formed by a compression stage, a storage stage and an expansion stage. During the compression stage, surplus electricity of the grid powers a compressor train to compress air to high pressure levels (between $60 - 100$ bar). The storage stage involves the injection of the pressurized

[4]A turbine is a machine consisting of a compressor, a combustor and an expander, which extracts energy from a fuel in a thermodynamic Joule cycle [12].

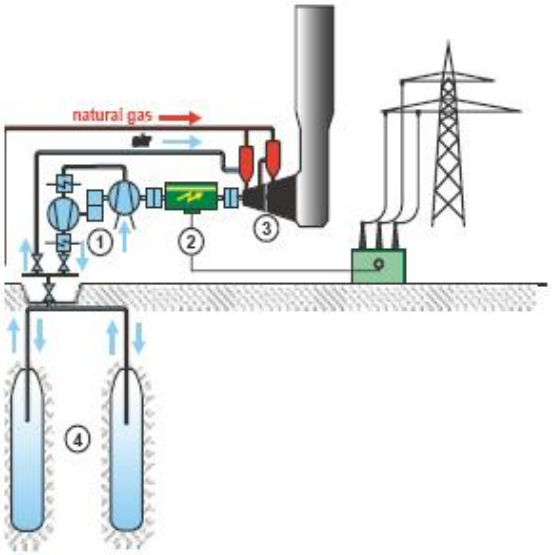

Figure 1.2: Main components of a CAES plant [33]

air into an insulated reservoir (cavern). While the air is being compressed, it passes through inter-coolers and after-coolers to reduce its temperature thereby enhancing the compression efficiency, reducing the storage volume requirement and minimizing thermal stress on the storage volume walls [29]. However, cooling down the air poses a problem at the moment of expansion since the efficiency of the turbines depends on the air temperature and pressure. Thereby, in the expansion stage, fuel is combusted inside the turbines to increase the temperature of the air. The combustion products are then expanded through a turbine train, thus re-generating part of the stored electricity.

The performance of a CAES plant is difficult to asses through a single index due to the presence of two very different energy inputs (gas and electricity). However, if we consider the round trip efficiency (η_{RT})[5], this is typically in the range of $66 - 82$ % [29].

Energy density of compressed air

For an estimation of the energy density of this storage system we will consider air as an ideal binary gas with constant specific heat capacities. Its state equation is called the ideal gas equation, which is given by

$$p \cdot V = n \cdot R \cdot T, \tag{1.1}$$

[5] η_{RT}=(electricity output)/(electricity input) [29].

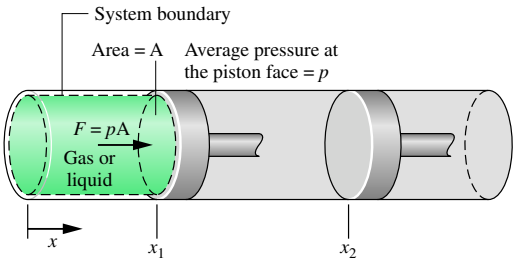

Figure 1.3: Expansion or compression of an ideal gas

where p is the pressure of the gas, V the volume, T the temperature, n the number of moles and R is the universal gas constant[6] [18, 34].

To evaluate the amount of energy that is stored whilst compressing the gas we will consider a closed system, which consists of a piston-cylinder assembly with area A where the gas is compressed (see Figure 1.3). During the compression, the gas exerts a normal force F on the piston, given by

$$F = p \cdot A. \tag{1.2}$$

Thus, the work δW done by the system as the piston is displaced by a distance dx is

$$\delta W = p \cdot A \cdot dx. \tag{1.3}$$

Since the product $A \cdot dx$ in the latter equation equals the change in the volume of the system dV, we can write the work expression as

$$\delta W = p \cdot dV \tag{1.4}$$

When the gas expands, the work at the moving boundary is positive, since dV is positive when the volume increases. However, when the gas is being compressed, dV is negative, and so is the work given by Equation (1.4).

For a volume change from V_1 to V_2, we can obtain the work W by integrating Equation (1.4)

$$W = \int_{V_1}^{V_2} p \, dV \tag{1.5}$$

We will assume an isothermal compression process to calculate the volumetric energy density of compressed air. This assumption transforms the ideal gas equation into the Boyle-Mariotte's law, given by

[6] $R = 8.3145\ {}^{\mathrm{J}}/_{(\mathrm{K \cdot mol})}$

$$p \cdot V = n \cdot R \cdot T = constant, \tag{1.6}$$

hence

$$W = -\int_{V_1}^{V_2} p\, dV = n\, R\, T \int_{V_2}^{V_1} \frac{dV}{V} = n\, R\, T\, ln\left(\frac{V_1}{V_2}\right). \tag{1.7}$$

If we consider that a gas is being compressed in an isothermal process from an initial state with volume $V_0 = 1\ \mathrm{m}^3$ and a pressure $p_0 = 2.03 \cdot 10^5\ \mathrm{Pa} = 20.3$ bar, to a final state with volume $V_1 = 0.4\ \mathrm{m}^3$ and pressure $p_1 = 76.39$ bar, the amount of stored energy is

$$\frac{W}{V_0} = -\frac{n\, R\, T}{V_0} \int_{V_0}^{V_1} \frac{dV}{V} = \frac{p_0\, V_0}{V_0} \int_{V_1}^{V_0} \frac{dV}{V} = p_0\, ln\left(\frac{V_0}{V_1}\right) = 0.186\ \mathrm{MJ/m^3}$$

This value is 21.5 times smaller than the one obtained for the PHS systems, which means that to store the same amount of energy, a CAES system will need a volume 21.5 times larger. Nevertheless, the pressures used in the caverns may vary and the use of underground reservoirs makes the issue of land-use less of a problem. Hence, an important factor for the implementation of these systems is to find geologic formations with an appropriate volume that can withstand the pressures required by the expansion trains of the CAES systems. There are three main geologic formations suitable for this storage technology, which are discussed in the following paragraphs.

Suitable cavern geologies

In large-scale CAES systems the reservoirs where the compressed air is injected are always underground because of the required volumes, hence the name of caverns. The main requirement that needs to be fulfilled by the cavern is that the geologic formation must have sufficient depth to allow safe operation at the required air pressure [13]. The classification for the suitable geologies for these caverns is divided in three categories: salt-, porous- and hard-rock. Over 75 % of the U.S. has geologic conditions that are potentially favorable for underground air storage, which makes CAES a compelling technology [13, 29].

Salt caverns are the most straightforward to develop and operate. The elasto-plastic properties of salt pose a minimal risk of air leakage in these underground reservoirs [29]. These caverns are created by solution mining or dry mining, with costs of USD 1 and USD 10 per kWh of storage capacity respectively [13]. The first one is a technology based on fresh water dissolving salt and becoming saturated with it. This process involves drilling a

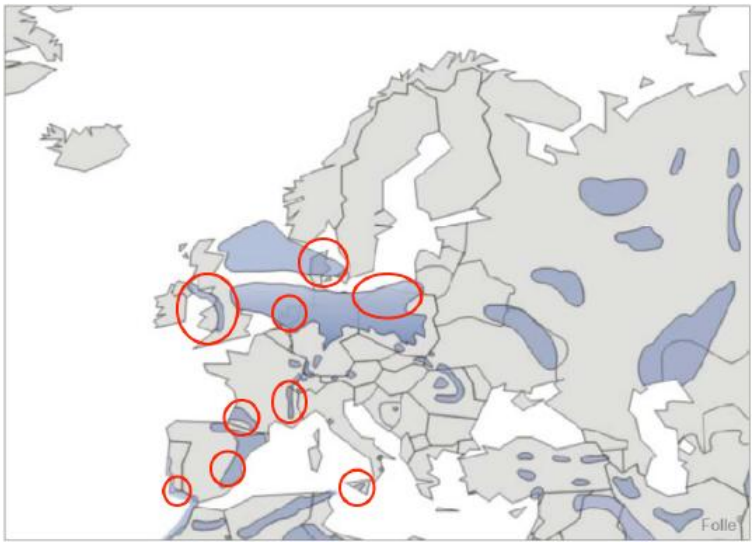

Figure 1.4: Correlation between salt domes and high-quality wind. The circles denote areas investigated for CAES development and the light blue zones depict some high quality wind regions [35].

bore into a salt cavern, cementing the upper side to the surrounding rock, jetting water down a central bore and then removing brine. One of the main problems of this geology is the disposal of brine since it can pollute water reservoirs and it involves other environmental problems [18]. The locations of salt domes are well correlated with high quality wind resources in Europe (see Figure 1.4), while in the United States previous studies show that the wind-rich areas of the Great Plains also have geologies favorable for the installation of CAES units [29].

Underground rock caverns are an option for compressed air storage although the cost of mining a new reservoir is USD 30/kWh of storage capacity created [13]. With respect to the other geologies, these caverns are created by excavating comparatively hard and impervious rock formations. As an alternative to these high costs, there are some existing mines that might be used as a reservoir and in this case the cost will typically be of USD 10/kWh [13]. An advantage of these high-cost reservoirs is the possibility to maintain a constant pressure inside the cavern by using water-compensation ponds [13, 29, 36]. However, this water/air system has a potential hazard called the "champagne effect", which is related to water flow instabilities resulting from the release of dissolved air in the upper portion of the water shaft.

Porous rock formations like sandstone or fissured limestone are found in rock aquifers or depleted gas fields. Depending on the permeability of the porous rock medium, a number of holes has to be drilled into the aquifer to

develop an air bubble that will displace the water contained. The excavation of no less than 50 wells is required to keep pressure losses over a charge-discharge cycle to around 10 $bar - 20$ bar, which will be the most expensive part of the reservoir together with the surface connections [18]. This geology has the potential to be the least costly storage option for large-scale CAES since it typically costs USD 0.10/kWh produced [13]. Porous rock formations are relevant in the literature due to their great availability in central U.S., where most of the high-quality wind resources can be found [13, 29, 37]. Even though the development costs for porous rock formations are low, the suitability of a candidate site requires an extensive characterization.

Existing and Proposed CAES Plants

There are only two working CAES facilities in the world at the moment, and some others that are still in the development stage.

The Huntorf CAES plant is the world's first and longest-operating facility, located near Huntorf in Northern Germany. The 290 MW plant was commissioned in 1978 and was designed to provide black-start[7] services to nuclear units near the North Sea as well as to provide inexpensive peak power [29]. Nowadays, this plant functions primarily for cyclic duty, ramping duty, and as a hot spinning reserve for the industrial customers of the area. Recently it has been successfully leveling the variable power from numerous wind turbine generators in Germany [9, 13, 33]. The underground reservoir of this plant consists of two salt caverns with a total volume of $310,000\,\mathrm{m}^3$ (see Figure 1.5), designed to operate between 48 and 66 bar [33].

The second CAES plant was built in 1991 by the Alabama Electric Cooperative on the McIntosh salt-dome in southwestern Alabama. This plant has 110 MW of rated power and its $560,000\ \mathrm{m}^3$ cavern was designed to operate between 45 bar and 74 bar while providing 26 h of generation at full power [29] (see Figure 1.5). The installation of an advanced recuperator allowed the McIntosh plant to reduce its heat rate[8] by 25 % compared to that one of Huntorf. This recuperator is used to extract thermal energy from the low-pressure expander exhaust to preheat inlet air from the storage cavern before it goes to the inlet of the high-pressure combustor [13, 29, 37]. McIntosh plant performs a wide range of operating functions like load management, ramping duty, generation of peak power, synchronous condenser duty and spinning reserve duty [13]. The ramp rate of this plant is approximately 18 $^{\mathrm{MW}}/_{\mathrm{min}}$, which is about 60 % greater than for typical gas turbines [29].

In the last 15 years the implementation of new CAES plants was very

[7] A black start is the process of restoring a power station to operation without relying on the external electric power transmission network.

[8] The heat rate is the fuel consumed per kWh of output for a CAES system, and its measured in kJ/kWh [29, pp. 37].

CAES plants comparison		
	Huntorf plant	*McIntosh plant*
Equipment Manufacturer	Brown-Boveri	Dresser-Rand
Amount invested (2002 US dollars)	$ 116 million ($400/kWe)	$ 45.1 million ($410/kWe)
Schedule	Commissioned December 1978	Commissioned June 1, 1991
Applications	(1) Peak Shaving (2) Spinning reserve (3) VAR support	(1) Arbitrage (2) Peak Shaving (3) Spinning reserve
Output		
Turbine power [MW]	290	110
Compression power [MW]	60	53
Generation time [hours]	3	26
Compression time [hours]	12	41.6
Ratio Compression/Generation	4	1.6
Reservoir		
Number of caverns	2	1
Geology	Salt	Salt
Air cavern volumes [m^3]	310'000	560'000
Fuel	Gas	Gas/Oil
Air flow rates		
Compression air flow [kg/s]	108	94
Expansion air flow [kg/s]	417	157
air mass flow ratio in/out	0.25	0.6
High pressure expander		
Inlet pressure [bar]	46	43
Inlet temperature [°C]	537	537
Low pressure expander		
Inlet pressure [bar]	11	15
Inlet temperature [°C]	871	871
Heat Rate [BTU/kWh, HHV]	6050	4510
Availability	90%	95%
Starting reliability	99%	99%
Power Requirement	0.82 kWin/kWout	0.75 kWin/kWout
Normal Start [min]	8	10 to 12

Figure 1.5: Comparison between the Huntorf and McIntosh CAES plants [13, 33, 37].

poor and none of the proposed projects was solid enough to arrive to the construction phase. Nowadays, the Iowa Stored Energy Park is the only plant that is under construction and will be ready in 2011. This plant will have a 268 MW CAES system coupled to a wind farm with a capacity of $75 - 100$ MW. The cavern will be an aquifer using a 1000 m deep anticline[9] in a porous sandstone formation [29].

CAES concepts

After the submission of the first CAES patent in 1949, engineers and scientists have made modifications to the conventional cycle of this technology and created hybrids [38–42]. These hybrid systems have in addition another type of energy storage or energy conversion system to the conventional CAES, such as capacitors [42], wind turbines [38], flywheels and thermal energy storages (TES) [40]. As for the modifications to the CAES cycle, its goal is to increase the heat rate of the plant as well as its versatility. These modifications consist in adding or replacing elements of the expansion stage of the thermodynamic cycle, creating new cycles with different applications. A few examples are the recuperated cycle (used in McIntosh plant), steam-injected cycle, compressed air storage with humidification (CASH) and the advanced adiabatic CAES cycle (AA-CAES). Since the main interest of this thesis lies on the latter one, we are going to discuss it in more detail.

The AA-CAES is a promising concept in a carbon-constrained future, since it is free of carbon emissions during its operation and it does not depend on any fossil fuel to recover the stored electricity [39]. The basic idea of this concept is to recover the energy expelled as heat during compression and reuse it later to reheat the stored air during the expansion stage, eliminating the combustor from the conventional cycle (see Figure 1.6) [13,18,43]. A Thermal Energy Storage (TES) stores the heat recovered from the compression stage, where it works as an inter-cooler, reducing the temperature of the compressed air, hence enabling the use of a low-cost underground reservoir. During the discharge regime, the air is reheated to the required temperature by the high pressure turbine inlet. The round-trip efficiency of the AA-CAES varies greatly between different studies with values between 50-75 % [13, 35, 43–45]. This subject is still in discussion due to the different existing models for the TES, which differ considerably depending on the losses of these systems. This is reviewed in more detail on Chapter 2, where a model of an AA-CAES plant is presented. The feasibility of this concept was the object of an EU-funded research project [46], where each component of the AA-CAES system was studied to identify low-cost improvements with available technology [39, 43].

[9] A ridge-shaped fold of stratified rock in which the strata slope downward from the crest.

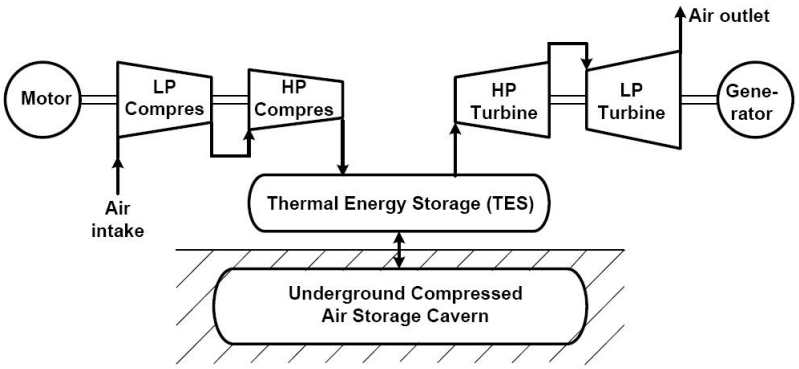

Figure 1.6: Function diagram of an AA-CAES plant (Source: Alstom Power).

The main caveats for this concept are associated with the design of the compression and expansion stage, together with the TES system. The design of the latter one needs to take into account the heat losses within the TES itself, as well as the losses in the cavern. These heat losses reduce the temperature that can be reached while re-heating the air, hence the inlet temperature of the turbine cannot be ensured over the whole discharging time. Since the turbine inlet temperature is decreasing while the system is being discharged, the pressure difference needs to be downsized to avoid low air temperatures at the turbine outlet. This process results in a reduced turbine power output as the AA-CAES is being discharged [36].

1.1.3 Advantages of CAES over other storage technologies

Comparison between different storage technologies in power systems

Figure 1.7 shows the comparison between the energy storage technologies considering their rated power and organizing them in three different groups. The technologies with a rated power of 1–100 kW form a first group that works as uninterrupted power sources (UPS) as well as to keep the power quality of the grid. The second group considers technologies with a rated power of 0.1–10 MW and a discharge time from seconds to hours, which supports the grid as a buffer and emergency storage. Finally, the third group considers the utility-scale technologies. This last group has the highest rated power and discharge times, which implies that the energy output of these systems is the highest one. Therefore, if an output of 1 GWd is needed, CAES and PHS systems are the only available technologies.

The inclusion of each of these storage systems within the present electric

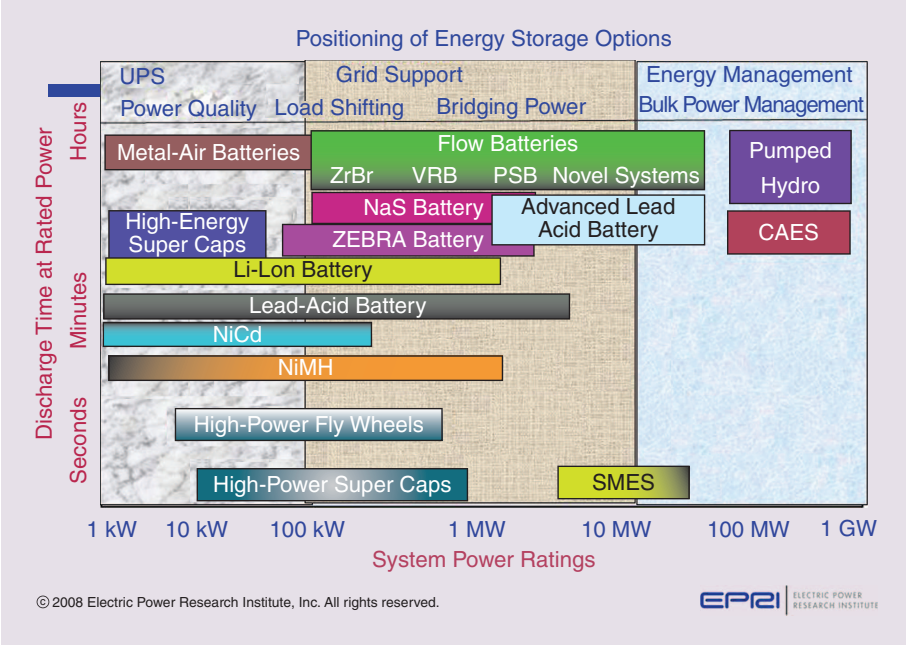

Figure 1.7: Energy storage options and their applications [21].

power systems will vary based on the economics of the technology as well. Therefore, it is important to see the different costs associated with these technologies.

Economic comparison between main energy storage technologies

The costs of the storage systems are difficult to assess and compare because the technical operation of each of them is different. This is particularly important for the CAES technology since the costs are usually calculated using the overall efficiency of the storage system, which is the ratio of the energy outputs over the inputs. Nevertheless, the efficiency value can change since to the gas input and its allocation within the energy system, since different analyses yield different efficiencies [29]. This is not the case for the AA-CAES system since the efficiency of the plant only depends on the electric power input and output (see Subsection 1.1.2.2). A comparison of the total capital costs between storage systems in the Megawatt scale provides a good insight of the economic feasibility of each system (see Table 1.1).

Table 1.1 shows that CAES and PHS have the lowest total capital costs between the compared technologies. However, a more accurate economic comparison needs to take into account the associated variable costs of each technology as well as their energy production. The levelized annual costs[10]

[10] $/kw-yr = Cost of capital (carrying charge of initial purchase) + cost of fixed O&M +

Technology	Capacity ($/kW)	Energy ($/kWh)	Hours of storage	Total Capital Cost ($/kW)
CAES (300 MW)	580	1.75	40	650
PHS (1000 MW)	600	37.5	10	975
Sodium Sulfur Battery (10 MW)	1720-1860	180-210	6-9	3100-3400
Vanadium Redox Battery (10 MW)	2410-2550	240-340	5-8	4300-4500

Table 1.1: Capital costs for medium to large-scale energy storage options [29].

consider the operation and maintenance (O&M) costs, the replacement costs and the consumables of each technology.

Another way to compare the storage technologies is by its per-cycle cost, which represents a meaningful way of evaluating the cost of storing energy in a frequent charge and discharge application, such as load leveling. Figure 1.8 shows the capital cost per cycle in US¢ for different technologies without considering O&M nor replacement costs. In this case the PHS system has the cheapest capital cost per-cycle, thus having an advantage over the other technologies. However, CAES is the second technology on the list and it is important to note that it has a more modest surface footprint than PHS, which reduces the environmental impact and gives more flexibility for its installation.

cost of variable O&M + annualized replacement costs + consumables (fuel and electricity) [47]

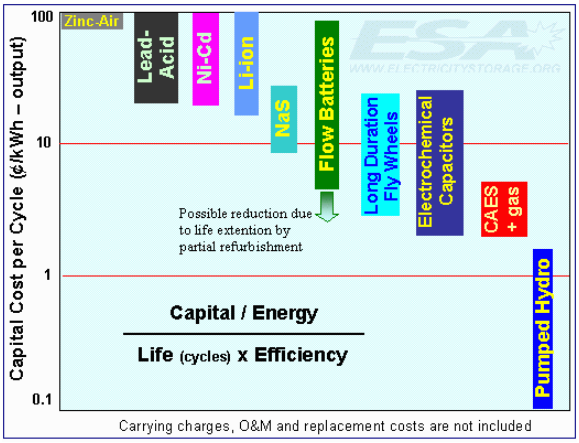

Figure 1.8: Per-cycle costs of different energy storage technologies [48].

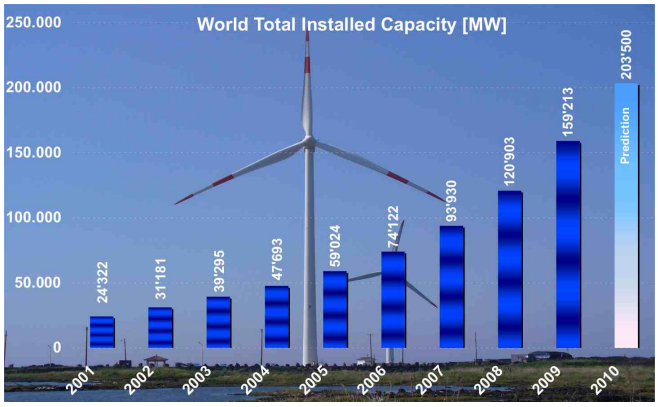

Figure 1.9: World total installed capacity until 2009 [49].

1.2 Wind energy and CAES

During the last decade, the penetration of renewable energy sources into the electricity generation mix has exacerbated the importance of bulk-energy storage [12,13,29,31]. A good example of this can be seen with wind power, which is the most successful source of new renewable energy technologies [31]. Worldwide capacity of wind energy has increased from 24 GW in 2001 to 160 GW by the end of 2009 (see Figure 1.9), where the energy yield of the latter represents 2 % of the global electricity demand, with a value of 340 TWh.

The growth rates of wind capacity installations have been above 20 % during the last decade, and it is very probable that this trend will continue in the following years. This high penetration of wind power into the electric grid has generated a lot of concerns about problems that may occur due

to wind variability and uncertainty [5, 16, 31, 44, 50, 51], since these fluctuations can cause problems to the existing power systems. Furthermore, the reliability of the electricity supply will be only maintained if the generation technologies become more flexible with respect to the penetration of intermittent renewable energies.

A strategy to tackle the caveats of high integration of wind energy sources is to create policies that address the issues of storage and transmission of wind-generated electricity. A good example is to identify as an entity the wind/storage system, or in other words, the output of the wind turbines together with their storage system should be classified as a renewable energy system [31]. Moreover, the co-location of wind generation and a storage system can also improve the capacity factor of the transmission lines needed to deliver the generated power, thereby reducing the amount of transmission capacity together with costs [14].

The inclusion of a properly chosen energy storage system can improve the technical and economic competitiveness of wind electricity to a great extent [5, 7, 12, 13, 18, 41, 44], providing at the same time higher system flexibility to cover the electricity demand [12, 17, 50, 52].

Large-scale electricity storage systems are able to optimize the consumption of wind electricity through load leveling, which means to store the electricity during low-demand periods and supplying it on peak demand periods, transforming non-scheduled low-value electricity into a high-value product.

Within this context CAES systems are very attractive for balancing wind energy, with the great advantage that the construction of the storage plants can be done near the high-quality wind zones in Europe as in the United States. This also copes with the problem that the best exploitable onshore wind resources are often far away from the big load centres [29], which causes significant transmission line losses.

Chapter 2

AA-CAES Model

In the last five years several studies have analyzed the AA-CAES concept extensively [39,43–45], but no AA-CAES plant has yet been constructed. At the beginning of 2010, the project ADELE was launched by RWE, General Electric, Zublin AG, and the German Aerospace Centre (DLR) [53]. The objective of this project is to build and test the world's first AA-CAES plant in Germany. This plant will have a generation capacity of 200 MW and will use a thermal energy storage (TES) made of concrete developed by Züblin AG.

This renewed interest in CAES plants shows that the study of these systems is compelling. Hence, a model of an AA-CAES plant becomes important in order to study further applications of this concept that may be available in the near future.

The following section presents a model of an AA-CAES plant (see Fig. 1.6). The model has four main modules, each of which tries to capture the main physical phenomena occurring in the storage plant (see Appendix C). The first module deals with the compression of atmospheric air and the extraction of the heat expelled because of the compression. The second and third modules represent the heat and air storage, respectively. The fourth one focuses on the re-heating of the air and its expansion through a gas turbine. The thermal energy storage (TES) system is in charge of storing the heat, which is transferred from module one and to module four by a heat transfer fluid (HTF) (see Section 1.1.2.2). It is important to remark that since we are dealing with an adiabatic system, the expansion module does not involve any fuel use (see Fig. 2.1).

The specifications of the AA-CAES model are in accordance with the McIntosh CAES plant as for the cavern size and pressure limits in the cavern (Fig. 1.5). Therefore, the compressed air is stored into a salt cavern, which is an abundant geological formation in Europe and is at the same time the cheapest type of underground storage available [29]. The TES is made of concrete and its properties were obtained from an experimental system

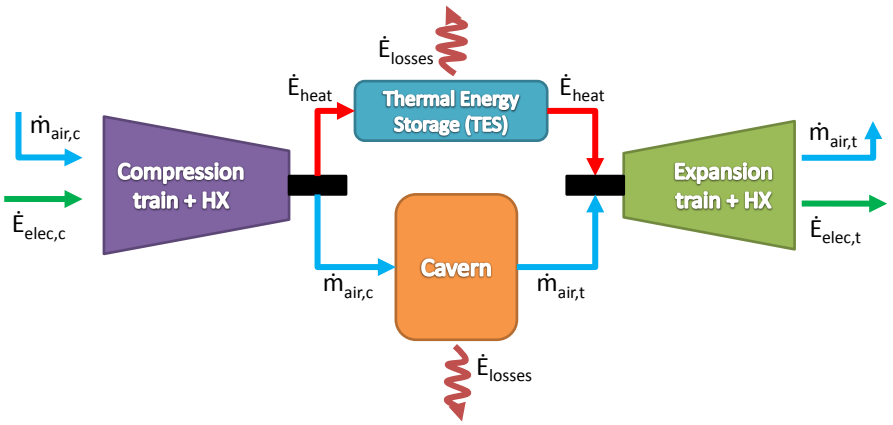

Figure 2.1: Diagram of the CAES model (HX: Heat Exchanger).

constructed by Züblin AG [54–56]. The heat exchangers and the TES work with oil as heat transfer fluid (HTF), with a specific heat capacity of $c_{\mathrm{p,HTF}} = 1260\ ^{\mathrm{J}}/_{\mathrm{kg\cdot K}}$ and a density of $\rho_{\mathrm{HTF}} = 570\ ^{\mathrm{kg}}/_{\mathrm{m}^3}$.

As for the properties of the air, dry air is a mixture that contains roughly 80 % nitrogen (N_2), which is a diatomic gas. Thereby we considered air to be a binary ideal gas with constant specific heat capacities $c_{\mathrm{p,a}} = {}^7/_2$ and $c_{\mathrm{v,a}} = {}^5/_2$. Isothermal and adiabatic transformations are practically not feasible in expansion and compression stages [57] [45], hence we modeled them as polytropic transformations. This holds since there will always be some temperature changes in the gas together with some heat exchange with the surroundings. The compressed air is then cooled down through counter-flow heat exchangers. The pressure of the air in the cavern is the same as the output of the compressor train. No pressure losses are involved in the tubings or heat exchangers. An energy balance of the air in the cavern, following the first law of thermodynamics, shows the air temperature change over time. The heat transfer between the air and the cavern is described by non-stationary heat conduction in a semi-infinite body. A second energy balance of the HTF inside the TES provides the change in temperature of the fluid. No leaking takes place in the tubes transporting the HTF. The air extracted from the cavern is re-heated by the HTF through heat exchangers with an efficiency of 70 %. The pressure of the air is only affected by the turbines through the expansion stage.

The model was built in MATLAB's Simulink environment since the simulation of dynamical systems can be easily implemented there. One of the big advantages of using this platform is the usage of integrators.

The first four sections of this chapter explain the physics behind each of the AA-CAES plant components. More specifically, these sections show the time-dependent differential equations that describe the dynamics of the

air properties at each stage. The last section of this chapter presents the results of the model after a complete cycle of the plant, or in other words, after fully charging and discharging the plant.

2.1 Compression Stage

The compression stage is formed by a compressor train of four compressors and four heat exchangers. Atmospheric air is compressed by the first compressor, then it goes to a heat exchanger where the hot air transfers part of its heat to the HTF. After that, the air goes through the next compressor and the process repeats itself until it arrives at the last compressor. Due to the properties of the salt-cavern, the air cannot be stored at high temperatures [29, 36, 57], hence the air goes through a fourth heat exchanger to reduce its temperature once again before entering into an underground storage.

The compressors operate with an air mass flow of $\dot{m}_{\mathrm{c,a}} = 120\ kg/s$, and have an efficiency of $\eta_{\mathrm{c}} = 88\ \%$. The compression ratio of the compressor train corresponds to the highest permitted pressure in the cavern, which is $\beta_{\mathrm{ct}} = p_{\mathrm{out}}/p_{\mathrm{in}} = 65$ and corresponds to 65 bar. This compression ratio results from multiplying the compression ratios, which are: $\beta_{\mathrm{c},1} = 3.8$, $\beta_{\mathrm{c},2} = 2.6$, $\beta_{\mathrm{c},3} = 2.4$ and $\beta_{\mathrm{c},4} = 2.74$.

The pressure of the air that passes through a compressor increases according to

$$p_{\mathrm{c,a}}^{\mathrm{out}} = p_{\mathrm{c,a}}^{\mathrm{in}}\, \beta_{\mathrm{c}}, \tag{2.1}$$

where $p_{\mathrm{c,a}}^{\mathrm{in}}$ and $p_{\mathrm{c,a}}^{\mathrm{out}}$ are the inlet and outlet pressures of the air, respectively. The superscripts denote the air going into the compressor train (in), and the air that is leaving it (out).

Since we considered the air compression to be polytropic, we have

$$pV^n = constant, \tag{2.2}$$

with n being the polytropic index. The index of the compressor train is $n_{\mathrm{ct}} = 1.6$.

The temperature of the air increases due to the polytropic transformation when it passes through the compression train. From Equation (2.2), it follows that

$$p_{\mathrm{ct,a}}^{\mathrm{in}}\,(V_{\mathrm{ct,a}}^{\mathrm{in}})^{\mathrm{n_{ct}}} = p_{\mathrm{ct,a}}^{\mathrm{out}}\,(V_{\mathrm{ct,a}}^{\mathrm{out}})^{n_{\mathrm{ct}}} \Rightarrow \frac{p_{\mathrm{ct,a}}^{\mathrm{out}}}{p_{\mathrm{ct,a}}^{\mathrm{in}}} = \beta = \left(\frac{V_{\mathrm{ct,a}}^{\mathrm{in}}}{V_{\mathrm{ct,a}}^{\mathrm{out}}}\right)^{\mathrm{n_{ct}}}, \tag{2.3}$$

The subscripts indicate that the gas in question is air (a), and that the transformation takes place in the compression train (ct).

The assumption that air is an ideal diatomic gas implies the usage of the ideal gas law given by

$$p\,V = m\,R\,T, \tag{2.4}$$

where $R = 286.7^{\mathrm{J}}/_{\mathrm{kg\cdot K}}$ is the universal gas constant, p is the pressure of the gas, V is the volume occupied by the gas, m is the mass of the gas and T its temperature. Solving for V and substituting it into Equation (2.3) we obtain

$$\begin{aligned} p\,V = m\,R\,T \Rightarrow V = \frac{m\,R\,T}{p} \Rightarrow \left(\frac{V_{\mathrm{ct,a}}^{\mathrm{in}}}{V_{\mathrm{ct,a}}^{\mathrm{out}}}\right)^{n_{\mathrm{ct}}} &= \left(\frac{p_{\mathrm{ct,a}}^{\mathrm{out}}}{p_{\mathrm{ct,a}}^{\mathrm{in}}}\right)^{n_{\mathrm{ct}}} \left(\frac{T_{\mathrm{ct,a}}^{\mathrm{in}}}{T_{\mathrm{ct,a}}^{\mathrm{out}}}\right)^{n_{\mathrm{ct}}} \\ \Rightarrow \left(\frac{V_{\mathrm{ct,a}}^{\mathrm{in}}}{V_{\mathrm{ct,a}}^{\mathrm{out}}}\right)^{n_{\mathrm{ct}}} &= \beta^{n_{\mathrm{ct}}} \left(\frac{T_{\mathrm{ct,a}}^{\mathrm{in}}}{T_{\mathrm{ct,a}}^{\mathrm{out}}}\right)^{n_{\mathrm{ct}}}. \end{aligned} \tag{2.5}$$

Inserting Equation (2.3) in (2.5) and doing some algebra we get the following expression:

$$T_{\mathrm{ct,a}}^{\mathrm{out}} = \beta^{(\mathrm{n_{ct}}-1)/\mathrm{n_{ct}}} T_{\mathrm{ct,a}}^{\mathrm{in}}, \tag{2.6}$$

which is the air temperature after the compressor train. However, to calculate the air temperature after each compressor ($T_{\mathrm{out,c}}$), the exponent of the compression ratio needs to be divided by the number of compressors. Thereby the air temperature after one compressor stage is given by

$$T_{\mathrm{c,a}}^{\mathrm{out}} = \beta^{(\mathrm{n_{ct}}-1)/4\mathrm{n_{ct}}} T_{\mathrm{ct,a}}^{\mathrm{in}} = \beta_{\mathrm{c}}^{\mathrm{n_{ct}}-1/\mathrm{n_{ct}}} T_{\mathrm{ct,a}}^{\mathrm{in}}, \tag{2.7}$$

where $\beta_{\mathrm{c}} = \beta^{1/4}$ is the compression ratio of one compressor.

Finally, the power consumed by each compressor follows the equation

$$P_{\mathrm{c}} = \frac{1}{\eta_{\mathrm{c}}}\,\dot{m}_{\mathrm{c,a}}\,c_{\mathrm{p,a}}\,T_{\mathrm{ct,a}}^{\mathrm{in}}\left(\beta_{\mathrm{c}}^{\mathrm{n_{ct}}-1/\mathrm{n_{ct}}} - 1\right), \tag{2.8}$$

which results from the analysis of a polytropic compression process [57, 58]. In the last expression $\eta_{\mathrm{c}} = 88\ \%$ is the efficiency of each compressor, $\dot{m}_{\mathrm{c,a}} = 120\ ^{\mathrm{kg}}/_{\mathrm{s}}$ is the air mass flow and $c_{\mathrm{p,a}} = {}^{7}/_{2}\,R_{\mathrm{a}}$ is the specific heat capacity of a diatomic ideal gas at constant pressure. The nominal power consumed by the compression train is 85 MW, which is constant along the charging stage since all the variables are considered to be constant over time.

The air temperature that comes out from each heat exchanger (HX) during the compression stage is given by the expression

$$T_{\mathrm{HX,a}}^{\mathrm{out}} = T_{\mathrm{HX,a}}^{\mathrm{in}} + \eta_{\mathrm{HX}}(T_{\mathrm{HX,HTF}}^{\mathrm{in}} - T_{\mathrm{HX,a}}^{\mathrm{in}}). \tag{2.9}$$

Where $\eta_{\mathrm{HX}} = 70\ \%$ is the efficiency of the HX, $T^{\mathrm{in}}_{\mathrm{HX,a}}$ is the air temperature entering into the HX, $T^{\mathrm{in}}_{\mathrm{HX,HTF}}$ is the HTF's temperature arriving to each HX, and $T^{\mathrm{out}}_{\mathrm{HX,a}}$ is the temperature of the air after the HX. It is important to note that the heat exchangers are connected in parallel, so $T^{\mathrm{in}}_{\mathrm{HX,HTF}}$ is the same for each of them.

The HTF's output temperature from the HX is $T^{\mathrm{out}}_{\mathrm{HX,HTF}}$, and it follows that

$$T^{\mathrm{out}}_{\mathrm{HX,HTF}} = T^{\mathrm{in}}_{\mathrm{HX,HTF}} + \eta_{\mathrm{HX}}(T^{\mathrm{in}}_{\mathrm{HX,a}} - T^{\mathrm{in}}_{\mathrm{HX,HTF}}).$$

The HTF's mass flow depends on the temperature differences of the air and the HTF's inflow and outflow through the HX, as it is shown in the following expression

$$\dot{m}_{\mathrm{c,HTF}} = \frac{(T^{\mathrm{out}}_{\mathrm{HX,a}} - T^{\mathrm{in}}_{\mathrm{HX,a}})c_{\mathrm{p,a}}\dot{m}_{\mathrm{c,a}}}{(T^{\mathrm{in}}_{\mathrm{HX,HTF}} - T^{\mathrm{in}}_{\mathrm{HX,HTF}})c_{\mathrm{p,HTF}}}. \tag{2.10}$$

The temperature $T^{\mathrm{out}}_{\mathrm{HX,a}}$ depends on the energy losses of the thermal energy storage (TES) stage, and it has to comply with the required inlet temperature of the expansion stage.

2.2 TES Stage

The TES system is one of the greatest challenges in an AA-CAES plant since it has to store enough thermal energy to re-heat the extracted air from the cavern. A solid sensible heat storage[1] made of concrete is a good technological option regarding investment and maintenance costs [56]. Thereby we considered a cylindrical TES made of high temperature concrete with a height $h_{\mathrm{TES}} = 40\,\mathrm{m}$ and a radius $r_{\mathrm{TES}} = 11\,\mathrm{m}$. This concrete has a density $\rho_{\mathrm{TES}} = 2750\ {}^{\mathrm{kg}}/_{\mathrm{m}^3}$, a specific heat capacity $c_{\mathrm{p,TES}} = 916\ {}^{\mathrm{J}}/_{\mathrm{kg\cdot K}}$, and a thermal conductivity $R_{\mathrm{TES}} = 1\ {}^{\mathrm{W}}/_{\mathrm{m\cdot K}}$. Zublin AG and the German Aerospace Centre (DLR) used this type of concrete to build and test a TES system for parabolic trough concentrators [54].

The heat exchange between the HTF and the solid TES takes place through immersed heat exchanger coils (see Fig. 2.2). There are two heat exchangers inside the TES, one that receives the hot HTF coming from the compression stage, and another one that receives the cold HTF, which heats up as it passes through the TES so as to re-heat the air in the expansion stage. The mass flow of the latter one is differentiated by using the subscript *load*. An energy balance of this system shows that

[1] This system stores and provides energy by heating or cooling a solid that does not change its phase during the process [59].

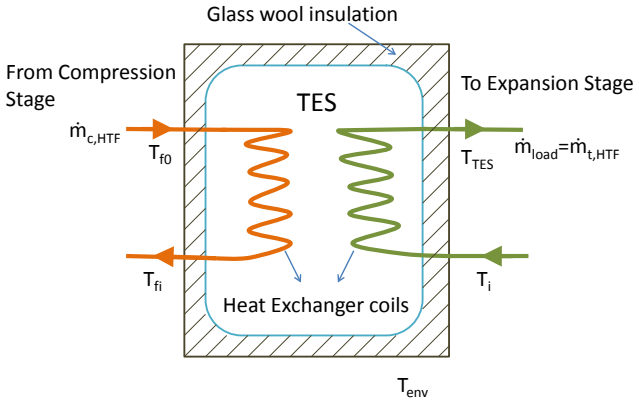

Figure 2.2: Scheme of a TES system with immersed heat exchanger coils [59].

$$(\rho_{\mathrm{TES}} V_{\mathrm{TES}} c_{\mathrm{p,TES}}) \frac{dT_{\mathrm{TES}}}{dt} = \dot{q}_{\mathrm{charging}} - \dot{q}_{\mathrm{discharging}} - \dot{q}_{\mathrm{env}}, \tag{2.11}$$

where $\dot{q}_{\mathrm{charging}}$ refers to the heat obtained throughout the compression stage of the CAES plant, $\dot{q}_{\mathrm{discharging}}$ refers to the heat used to re-heat the air extracted from the cavern during the expansion stage, and $\dot{q}_{\mathrm{env}}$ refers to the TES' energy losses. The first of these terms is given by the expression

$$\dot{q}_{\mathrm{charging}} = \dot{m}^{\mathrm{in}}_{\mathrm{TES,HTF}} c_{\mathrm{p,HTF}} (T_{\mathrm{f0}} - T_{\mathrm{fi}}), \tag{2.12}$$

where $\dot{m}^{\mathrm{in}}_{\mathrm{TES,HTF}} = \dot{m}_{\mathrm{c,HTF}}$ is the incoming mass flow of the HTF to the TES, T_{f0} and T_{fi} correspond to the temperature of the HTF that comes in and out of the TES, respectively (see Fig. 2.2).

Following the heat exchange theory [59] we can calculate $\dot{q}_{\mathrm{charging}}$ without the unknown T_{fi} by using the following expression

$$\frac{T_{\mathrm{f0}} - T_{\mathrm{fi}}}{T_{\mathrm{f0}} - T_{\mathrm{TES}}} = 1 - exp\{-(UA)_{\mathrm{inner}} / \dot{m}_{\mathrm{c,HTF}} c_{\mathrm{p,HTF}}\}, \tag{2.13}$$

where $(UA)_{\mathrm{inner}}$ is the inner TES' overall heat transfer coefficient (U_{inner}) multiplied by the area covered by the inner heat exchanger (A_{inner}). This product depends on the properties of the storage system. In Equation (2.13), T_{TES} is the temperature of the outgoing HTF that was heated in the TES (see Fig. 2.2).

By substituting the temperature difference $T_{\mathrm{f0}} - T_{\mathrm{fi}}$ term of Equation (2.12) into Equation (2.13) we obtain,

$$\dot{q}_{\text{charging}} = \dot{m}_{\text{c,HTF}} c_{\text{p,HTF}} (T_{\text{f0}} - T_{\text{TES}})[1 - exp\{-(UA)_{\text{inner}}/\dot{m}_{\text{c,HTF}} c_{\text{p,HTF}}\}]. \tag{2.14}$$

To calculate $\dot{q}_{\text{discharging}}$, we followed the same procedure as before to obtain the following expression,

$$\dot{q}_{\text{discharging}} = \dot{m}_{\text{load}} c_{\text{p,HTF}} (T_{\text{TES}} - T_i)[1 - exp\{-(UA)_{\text{inner}}/\dot{m}_{\text{load}} c_{\text{p,HTF}}\}], \tag{2.15}$$

where $\dot{m}_{\text{load}} = \dot{m}_{\text{t,HTF}}$ is the HTF's mass flow that exits the TES to re-heat the air extracted from the cavern. This mass flow remains constant through the heat exchangers of the expansion stage, and the energy balance of the latter ones yields its actual value (see Section 2.4).

The environmental losses considered in Equation (2.11) depend on the outer area of the TES (A_{outer}) as well as on the outer overall heat transfer coefficient (U_{outer}). We considered an insulated TES so as to reduce the heat losses by using an exterior cover of glass wool with a thickness of $d_{wool} = 10\,cm$, which has a thermal conductivity of $R_{\text{ins}} = 0.055\,\text{W/m·K}$. To calculate U_{outer} we considered that the concrete wall of the TES has a thickness of $d_{\text{TES}} = 1.0\,\text{m}$. This coefficient is calculated through the expression

$$U_{\text{outer}} = \frac{R_{\text{TES}} R_{\text{ins}}}{d_{\text{TES}} R_{\text{ins}} + d_{wool} R_{\text{ins}}}. \tag{2.16}$$

With the result from the last equation now we can calculate the energy losses through the following equation

$$\dot{q}_{\text{env}} = (UA)_{\text{outer}} (T_{\text{TES}} - T_{\text{env}}), \tag{2.17}$$

where A_{outer} is the outer surface cylindrical shaped TES.

Substituting Equations (2.14), (2.15) and (2.17) into Equation (2.11) yields

$$\begin{gathered}(\rho_{\text{TES}} \cdot V_{\text{TES}} \cdot c_{\text{p,TES}}) \frac{dT_{\text{TES}}}{dt} = \\ \dot{m}_{\text{c,HTF}} c_{\text{p,HTF}} (T_{\text{f0}} - T_{\text{TES}})[1 - exp\{-(UA)_{\text{inner}}/\dot{m}_{\text{c,HTF}} c_{\text{p,HTF}}\}] \\ -\dot{m}_{\text{load}} c_{\text{p,HTF}} (T_{\text{TES}} - T_i)[1 - exp\{-(UA)_{\text{e}}/\dot{m}_{\text{load}} c_{\text{p,HTF}}\}] \\ -(UA)_{\text{outer}} (T_{\text{TES}} - T_{\text{env}}),\end{gathered} \tag{2.18}$$

which describes the temperature change over time of the heated HTF that is leaving the TES.

This stage does not take into account any energy or mass losses that may take place in the pipes transporting the HTF.

2.3 Air Storage Stage

The storage of compressed air into a geological formation is a crucial stage in an AA-CAES plant. The stability of the underground storage depends on its mechanical and thermal properties, which at the same time are needed to assess the energy and mass losses of the stored air. The model of this stage only considers the energy losses associated with the heat exchange between the air and the cavern wall, hence the thermal properties of the latter one are important for the simulation of the losses. We considered a rock-salt cavern with a $NaCl$ compound, which translates into a thermal conductivity $a_{\mathrm{rs}} = 7.1\,{}^{\mathrm{W}}/_{\mathrm{m\cdot K}}$ [60], a specific heat capacity $c_{\mathrm{p,rs}} = 920\,{}^{\mathrm{J}}/_{\mathrm{kg\cdot K}}$, a heat transfer coefficient to air $\alpha_{\mathrm{a,w}} = 0.1\,{}^{\mathrm{W}}/_{\mathrm{m^2\cdot K}}$ and a density $\rho_{\mathrm{rs}} = 2100\,{}^{\mathrm{kg}}/_{\mathrm{m^3}}$. Following the specifications of the McIntosh plant, the underground storage is a salt cavern with a volume $V_{\mathrm{sc}} = 560,000\ \mathrm{m}^3$. The model approximates this salt cavern as a cylinder with height $h_{\mathrm{sc}} = 200\ \mathrm{m}$ and cross-section area $A_{\mathrm{sc}} = 2800\ \mathrm{m}^2$.

Within the cavern, air temperature varies during charging and discharging phases due to the heat transfer with the cavern walls and changes in pressure. Considering air as an ideal diatomic gas, the cavern as a cylinder and a uniform distribution of the air temperature and pressure, the change over time of the air temperature can be described by the following expression

$$\frac{dT_{\mathrm{sc,a}}}{dt} = \frac{1}{m_{\mathrm{sc,a}}}\left(1 - \frac{1}{k}\right)\left(\dot{m}^{\mathrm{in}}_{\mathrm{sc,a}} T^{\mathrm{in}}_{\mathrm{sc,a}} - \dot{m}^{\mathrm{out}}_{\mathrm{sc,a}} T^{\mathrm{out}}_{\mathrm{sc,a}}\right) + \frac{\alpha_{\mathrm{a,w}} A_{\mathrm{w}} (T_{\mathrm{w}} - T_{\mathrm{sc,a}})}{m_{\mathrm{sc,a}} c_{\mathrm{p,a}}}, \tag{2.19}$$

with $T_{\mathrm{sc,a}}$ being the air temperature inside the cavern, $k = {}^{\mathrm{c_{p,a}}}/_{\mathrm{c_{v,a}}} = 1.4$ being the ratio of specific heat capacities for a diatomic ideal gas, $\dot{m}^{\mathrm{in}}_{\mathrm{sc,a}}$ and $\dot{m}^{\mathrm{out}}_{\mathrm{sc,a}}$ being the inner and outer air mass flows to and from the salt cavern, respectively. As for the other variables, the $m_{\mathrm{sc,a}}$ term represents the air mass at a given time, A_{w} is the cavern wall surface that is in contact with the air, and T_{w} is the wall's temperature at a certain time. The derivation of Equation (2.19) is shown in Appendix A. The subscript *sc* used for previous variables corresponds to the salt cavern environment.

Since a salt dome formation is not necessarily cylindrical due to cracks and fissures in the rock, the inner surface's area follows the equation

$$A_{\mathrm{a,w}} = A_{\mathrm{L}}\left(A_{\mathrm{sc}} + \pi d_{\mathrm{sc}} h_{\mathrm{sc}}\right), \tag{2.20}$$

where $A_{\mathrm{L}} = 1.8$ is an enlargement factor that considers these irregularities within the cavern, and $d_{\mathrm{sc}} = 59.71\ \mathrm{m}$ is the cavern's diameter.

However, not all the variables in Equation (2.19) are known. To solve this equation, we need to know the wall's temperature T_{w} and the air mass $m_{\mathrm{sc,a}}$ at every time step of the process. The air mass is described by the differential equation

$$\frac{dm_{\mathrm{sc,a}}}{dt} = \dot{m}_{\mathrm{sc,a}}^{\mathrm{in}} - \dot{m}_{\mathrm{sc,a}}^{\mathrm{out}}, \tag{2.21}$$

which states that the total air mass flow within the cavern is determined by the substraction between the air in- and outflow.

The calculation of T_{w} requires an analysis of the heat transfer between the air and the cavern wall, which is described by geostationary heat conduction in a semi-infinite body. This physical process is represented by the heat equation or Fourier's Equation for constant heat conduction coefficients:

$$\frac{\partial T_{\mathrm{rs}}}{\partial t} = r_{\mathrm{rs}} \nabla^2 T_{\mathrm{rs}} + \frac{\tilde{\dot{q}}}{\rho c_{\mathrm{p}}}. \tag{2.22}$$

The absence of an inner heat source at the cavern wall eliminates the right term of the last equation, having as a result

$$\frac{\partial T_{\mathrm{rs}}}{\partial t} = r_{\mathrm{rs}} \nabla^2 T_{\mathrm{rs}}, \tag{2.23}$$

where r_{rs} is the diffusivity (m^2/s) that depends on the wall's properties, and is calculated as follows

$$r_{\mathrm{rs}} = \frac{a_{\mathrm{rs}}}{\rho_{\mathrm{rs}} c_{\mathrm{p,rs}}}. \tag{2.24}$$

Since the cavern is approximated through a cylinder, it makes sense to use cylindrical coordinates for Equation (2.23). For simplicity, we will assume that the cavern is an infinite cylinder in order to work with the one dimensional heat equation. Hence, equation (2.23) becomes

$$\frac{\partial T_{\mathrm{rs}}}{\partial t} = r_{\mathrm{rs}} \left(\frac{\partial^2 T_{\mathrm{rs}}}{\partial r^2} + \frac{1}{r} \frac{\partial T_{\mathrm{rs}}}{\partial r} \right), \tag{2.25}$$

where r is a distance measured from the cavern wall to a point inside the rock.

The solution of this last equation is presented in Appendix B. The idea of this solution is to discretise space derivatives so as to have a differential equation that solely depends on time, since this can be integrated easily through the Simulink platform. Once T_{w} is calculated, all the variables in Equation (2.19) are known for each time step and this equation can be integrated.

The pressure of the air inside the cavern $p_{\mathrm{sc,a}}$ is described in the ideal gas law (Eq. (2.4)). Since the volume of the cavern is constant, the pressure is determined by the change in mass and temperature in every time step.

2.4 Expansion Stage

This stage is formed by an expansion train formed by a high pressure turbine (HPT) followed by a low pressure turbine (LPT), together with the necessary heat exchangers to reheat the extracted air from the cavern. Before entering the HPT, the extracted air passes through a HX to increase its temperature. Once it enters the HPT, it generates electricity and its pressure and temperature drop. After this, the air passes through another HX to increase once again its temperature before entering the LPT, which generates electricity with the remaining pneumatic stored energy expanding the air until it reaches atmospheric pressure. The air massflow along the expansion stage is constant and equal to $\dot{m}_{\mathrm{e,a}} = 240\,\mathrm{kg/s}$. Since the air used in this stage is extracted from the cavern, we assumed that $\dot{m}^{\mathrm{out}}_{\mathrm{sc,a}} = \dot{m}_{\mathrm{e,a}}$.

When air is withdrawn from the cavern it is almost at ambient temperature, hence the HTF reheats it when it passes through the first heat exchanger. The HTF's inlet temperature into the HX depends on the TES losses and goes from $430 - 480\,^{\circ}\mathrm{C}$, which increases the air temperature to a value between $395\,^{\circ}\mathrm{C}$ and $425\,^{\circ}\mathrm{C}$. In this stage, the air temperature increases due to the heat transfer with the HXs following the same equations as the ones shown for the compression stage (Eq. (2.9)).

The mass flow of the HTF passing through the HXs is also calculated doing an energy balance, as we did in the compression stage. The value of $\dot{m}_{\mathrm{t,HTF}}$ determines the mass flow of the HTF that will go into the TES to recover the heat as shown in Fig. 2.2. Thus, this mass flow is given by the following expression

$$\dot{m}_{\mathrm{e,HTF}} = \frac{(T^{\mathrm{out}}_{\mathrm{HX,a}} - T^{\mathrm{in}}_{\mathrm{HX,a}}) c_{\mathrm{p,a}} \dot{m}_{\mathrm{e,a}}}{(T^{\mathrm{in}}_{\mathrm{HX,HTF}} - T^{\mathrm{in}}_{\mathrm{HX,HTF}}) c_{\mathrm{p,HTF}}}, \tag{2.26}$$

which is the same as Equation (2.10) but with sub-indices associated with the expansion stage.

The specifications of each turbine follow previous CAES models [41, 45]. The HPT has an efficiency of $\eta_{\mathrm{HPT}} = 79\ \%$ and a compression ratio $\beta_{\mathrm{HPT}} = 2.5$. The LPT turbine has an efficiency of $\eta_{\mathrm{LPT}} = 82\ \%$ and a compression ratio $\beta_{\mathrm{LPT}} = 18.4$. f In this case the air pressure drops as it passes through each turbine according to the following expression

$$p^{\mathrm{out}}_{\mathrm{t,a}} = p^{\mathrm{in}}_{\mathrm{t,a}}\, \beta^{-1}, \tag{2.27}$$

where the compression ratio β varies depending on the type.

The expansion process is also polytropic, with a polytropic index $n_{\mathrm{t}} = 1.1$. The combination of this assumption, together with the fact that air is treated as an ideal gas, provides a simple equation that describes the decrease in air temperature as it passes through each turbine. This expression is

similar to the one presented for the compressor train in Equation (2.7) and its derivation follows the same line of thought:

$$T_{\mathrm{t,a}}^{\mathrm{out}} = \beta^{1-\mathrm{n_t}/\mathrm{n_t}} T_{\mathrm{t,a}}^{\mathrm{in}}, \tag{2.28}$$

where again the compression ratio β is different for each turbine.

An analysis of a polytropic expansion process shows the electric power obtained from expanding hot air into a turbine [57, 58]. This power is described through the following expression

$$P_{\mathrm{t}} = \eta_{\mathrm{t}}\, \dot{m}_{\mathrm{t,a}}\, c_{\mathrm{p,a}}\, T_{\mathrm{t,a}}^{\mathrm{in}} \left(1 - \beta^{\mathrm{n_t}-1/\mathrm{n_t}}\right), \tag{2.29}$$

where the efficiency η_{t} and the compression ratio β vary according to the turbine. In the previous equation $\dot{m}_{\mathrm{t,a}} = \dot{m}_{\mathrm{e,a}}$ is the air massflow through the turbines, and $T_{\mathrm{t,a}}^{\mathrm{in}}$ represents the air temperature as it enters into each turbine.

The power calculated in Equation (2.28) decreases with time since $T_{\mathrm{t,a}}^{\mathrm{in}}$ varies due to the energy losses associated with the cavern wall and the TES system. The nominal power produced by the expansion train is 64 MW, which corresponds to the sum of the nominal powers of each of the turbines (see Appendix C).

The following section presents the results generated by simulating the AA-CAES model, which integrates the information described in the last four sections.

2.5 Model results

This chapter shows the evolution over time of the main physical properties of the model as a result of simulating our AA-CAES model. It also presents how this plant looses energy when it is in an idle state, that is to say, when neither compression nor expansion is taking place.

A quick review of the last four sections shows that the system dynamics of the constructed model is mainly governed by four differential equations. These equations describe the change over time of the TES and salt cavern's temperature (Eqs. (2.18) and (2.19)), the air massflows (Eq. (2.21)) and the temperature of the cavern wall (Eq. 2.23). The initial states of the first three equations are scalars. As for the fourth one, the discretisation of the cavern requires a vector $\bar{T}_{\mathrm{rs},0}$ as initial state in order to solve the heat equation. This vector describes the initial temperature profile of the rock-salt surrounding the cavern and its dimension depends on how fine is the discretisation of the cavern wall. The details of this are discussed in Appendix B.

Thus, the initial state of the whole model can be represented as a concatenation of $\bar{T}_{\mathrm{rs},0}$ with a three entry vector $\bar{x}_0$ such as the following

$$\bar{x}_0 = [T_{\text{sc,a,0}}, \quad T_{\text{TES,0}}, \quad m_{\text{a,0}}], \tag{2.30}$$

where $T_{\text{sc,a,0}}$ is the initial temperature of the air inside the cavern, $T_{\text{TES,0}}$ is the initial TES' temperature, and $m_{\text{sc,a,0}}$ is the initial a mass inside the cavern.

The model structure is such that it needs two inputs besides the initial state in order to work. These inputs tell the simulation to compress or expand air through two variables constrained to the inertial $[0, 1] \subset \mathbb{R}$. These two variables allow four operation states for the AA-CAES plant: a) Compress, b) expand, c) idle or d) compress and expand at the same time. The two variables can be expressed by a vector $\bar{u} = [u_1 \quad u_2] \in \mathbb{R}^2$, where the first entry corresponds to air compression and the second one corresponds to its expansion. This structure allows an easier management of the plant in case an external agent provides an operation strategy. This will be used more extensively in Chapter 4, where an optimal operation strategy of the plant is calculated by an MPC controller.

A complete charge followed by a complete discharge of the plant shows how the main physical properties of the model change over time. This is shown in the following two subsections. For more information on the code used for the simulations presented on this section refer to Appendix D.

2.5.1 Charging the plant

As stated in a previous paragraph, an initial state is required to start the simulation in any operation state. Before compression, the air is at ambient temperature ($293\,K$) and atmospheric pressure (1 bar). The rock-salt and the air in the cavern are in thermodynamic equilibrium, having a temperature of $T_{\text{sc,a,0}} = 293\,K$. This assumption means that the vector $\bar{T}_{\text{rs,0,d}}$ will have $T_{\text{sc,a,0}}$ in all its entries. The air mass inside the cavern at the initial state is the same that we would have in a container of $560,000\,\text{m}^3$ at ambient temperature and at a pressure $p_{\text{sc,a,0}} = 46$ bar, which is the minimum allowed pressure in the cavern. This mass can be calculated with the ideal gas expression (Eq. (2.4)), which yields $m_{\text{sc,a,0}} = 3.07 \cdot 10^7\,kg$. At this state the TES is in equilibrium with its surroundings, having therefore a temperature $T_{\text{TES,0}} = 293\,K$. Hence, the initial state before compression is

$$\bar{x}_{0,c} = \left[293, \quad 293, \quad 3.07 \cdot 10^7\right]. \tag{2.31}$$

With this assumptions and taking $\bar{u} = [1 \quad 0]$, the compressor takes $t_{\text{c,max}} = 22.97\text{h}$ to "fill" the cavern with air. In other words, $t_{\text{c,max}}$ is the time that the compressor needs to inject enough air into the cavern as to increase the pressure to $p_{\text{sc,a}} = 65$ bar, which is the maximum permitted pressure (see Fig. 1.5). To run the simulation, the cavern wall was discretised into 12

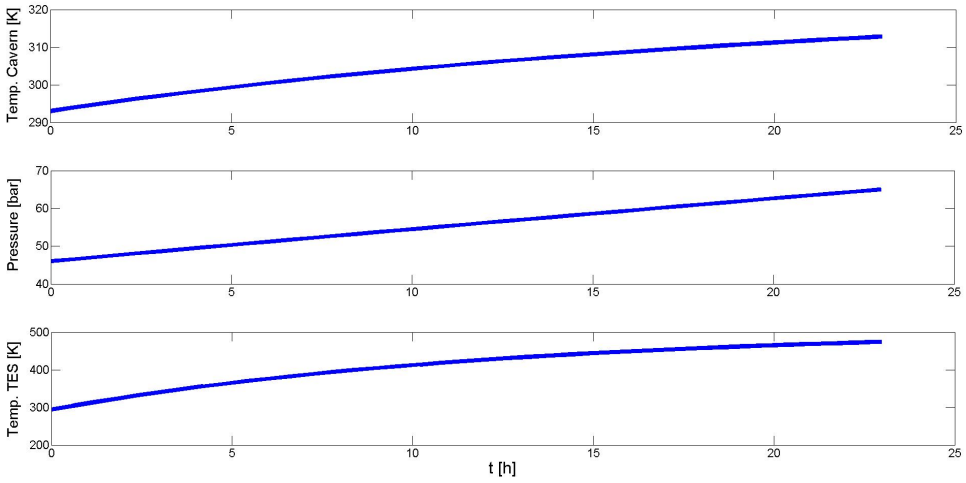

Figure 2.3: Evolution over time of the air temperature (top) and pressure (middle) inside the cavern, together with the TES temperature (bottom) during compression.

segments separated by $dx = 0.11\,\mathrm{m}$, covering a distance of $1.32\,\mathrm{m}$. Thereby, the vector $\bar{T}_{\mathrm{rs,0,d}}$ has twelve entries that are equal to $T_{\mathrm{sc,a,0}}$.

Figure 2.3 shows the time evolution of air properties inside the cavern (top and middle), together with the temperature evolution over time of the TES (bottom). The results concerned to the cavern wall and its surroundings are shown in Appendix A. The mass of air injected into the cavern during this operation state and the consumed electricity by the compression's train are shown in Figure 2.4.

On the one hand Figures 2.3 (middle) and 2.4 show a linear behaviour with respect to time. This means that the non-linear behaviour of the TES and cavern's temperature do not have a big effect on these three variables during this time span. The fact that the air mass differential equation (Eq. (2.21)) does not consider any mass losses explains the linear behaviour of this variable. The pressure of the air inside the cavern (Figure 2.3, middle) is of particular importance for the compression stage since the plant should stop compressing air whenever the pressure inside the cavern reaches 65 bar. However, the change in pressure seems to be linear during the compression time. This is explained due to the small temperature variation of the air during this time ($\sim 10\,K$), which is dwarfed by the air mass variation ($\sim 1 \cdot 10^7\,kg$).

On the other hand, the air and TES' temperature shown at the top and bottom of Figure 2.3, respectively, show a non-linear behaviour. The time-dependent losses present in the differential Equations (2.19) and (2.18)

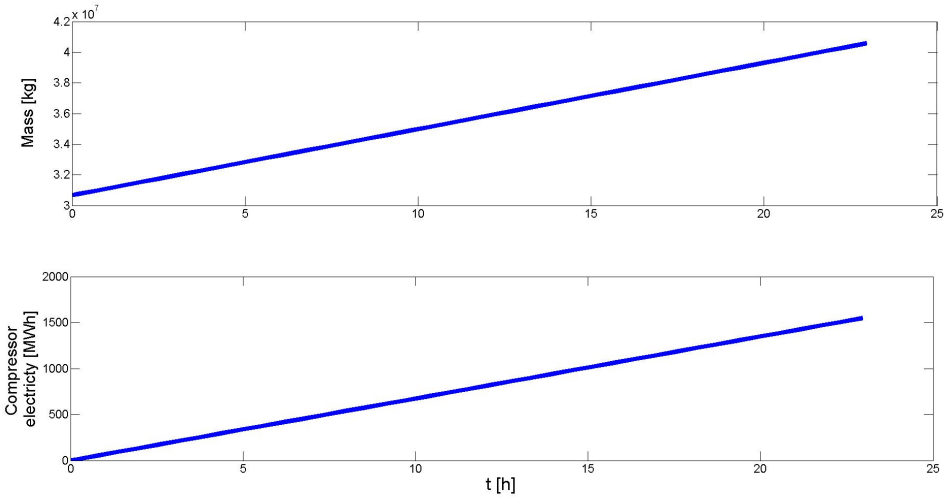

Figure 2.4: Evolution over time of the air mass inside the cavern (top) and the electricity consumed by the compressor's train (bottom) during compression.

explain the shape of these curves. In both cases, the temperature cannot increase linearly in time due to the heat exchange that takes place between both storage modules and its surroundings.

The cavern wall and its temperature profile depend on the temperature of the air inside the cavern. Since these three temperatures have the same order of magnitude, a change in the later one affects the other two in great extent. This explains the time evolution of T_{w} and $\bar{T}_{\mathrm{rs}}$ (see Appendix A).

2.5.2 Discharging the plant

Once the plant is fully charged we will proceed to discharge it so as to show what are the dynamics of this process. The final state of the model after fully charging the AA-CAES plant serves then as the initial state for the expansion stage. Before the expansion begins, the air temperature inside the cavern is $T_{\mathrm{sc,a}} = 312.80\,K$, the TES' temperature is $T_{\mathrm{TES}} = 474.14\,K$, and the air mass inside the cavern is $m_{\mathrm{sc,a}} = 4.06 \cdot 10^7\,kg$. The vector $\bar{T}_{\mathrm{rs,0,e}}$ is given by the temperature profile that the rock-salt had when the cavern became full, that is, when $t = 22.97$ h. Figure 2.5 shows this temperature profile in more detail.

The other three initial states before expansion are represented by the following vector

$$\bar{x}_{0,e} = [312.80, \quad 474.14, \quad 4.06 \cdot 10^7]. \tag{2.32}$$

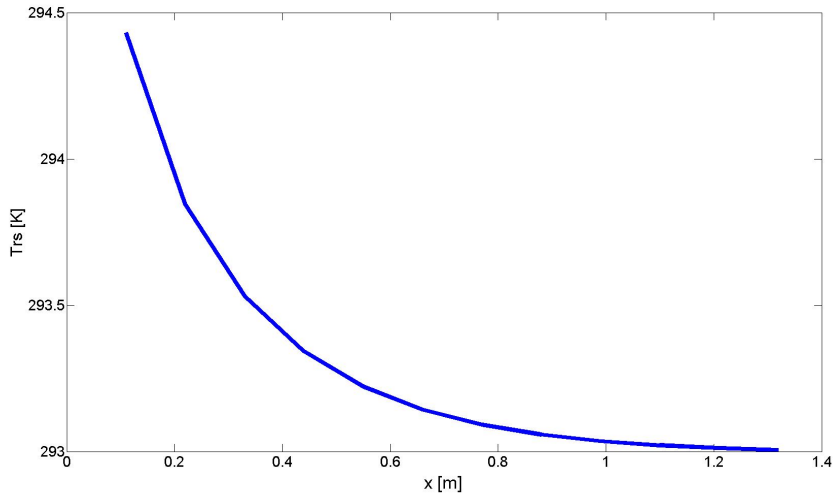

Figure 2.5: Temperature profile of the rock-salt surrounding the cavern after compression stage finished.

Considering $\bar{T}_{\mathrm{rs,0,e}}$ and $\bar{x}_{0,e}$ as initial states together with the input vector $\bar{u} = [0 \quad 1]$, the expansion train takes $t_{\mathrm{e,max}} = 10.88\,\mathrm{h}$ to "empty" the cavern. In other words, $t_{\mathrm{e,max}}$ is the time for the pressure of the air inside the cavern to decrease from 65 bar to 46 bar.

The results of a full expansion are shown in Figures 2.6 and 2.7.

The heat losses during the expansion stage are not as big as in the compression stage as it is shown in Figures 2.3 (top) and 2.6 (top). This behaviour is because the air massflow in the former stage is twice as big as the one in latter one. Hence, the air does not loose enough energy in the eleven hours of expansion compared to the twenty three hours of compression.

However, the air inside the cavern does exchange some energy with the cavern wall during expansion (see Appendix A). Therefore, the wall receives heat from the air until this last one cools down due to the expansion process.

Figures 2.4 (bottom) and 2.7 (bottom) provide the AA-CAES plant's electricity consumption and production, respectively. This information allows us to quantify the plant's overall efficiency by using the following expression

$$\eta_{\mathrm{Overall}} = \frac{Elec_{\mathrm{e}}}{Elec_{\mathrm{c}}} = \frac{885.96\ MWh}{1548.43\ MWh} = 0.57, \tag{2.33}$$

where $Elec_{\mathrm{e}}$ and $Elec_{\mathrm{c}}$ are the electricity produced by the expansion train and consumed by the compression train, respectively. Thus, the overall efficiency of this plant is 57 %, considering a full charge followed by a total discharge. An important remark is that this efficiency is not constant for

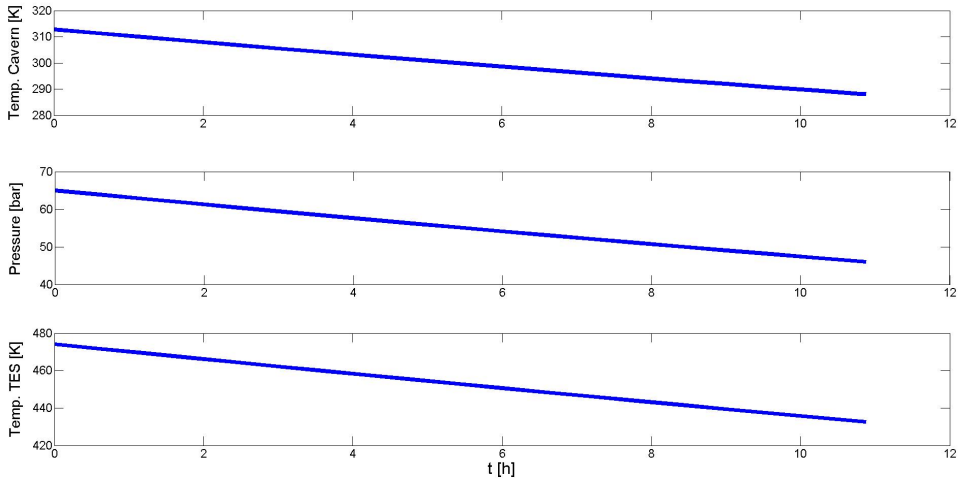

Figure 2.6: Evolution over time of the air temperature (top) and pressure (middle) inside the cavern, together with the TES temperature (bottom) during expansion.

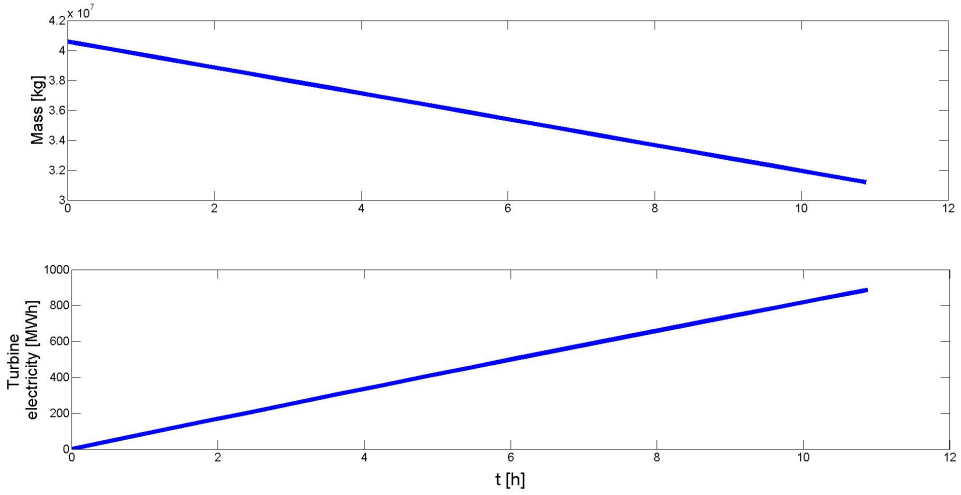

Figure 2.7: Evolution over time of the air mass inside the cavern (top) and the electricity produced by the turbines (bottom) during expansion.

all the operation states. If the plant's operator chooses to leave the plant idle for a certain amount of time before the expansion takes place, energy will be lost due to heat losses and the efficiency will decrease. Hence, the efficiency calculated above is the maximum overall efficiency.

The following subsection shows the heat losses that take place when the AA-CAES plant is idle.

2.5.3 Idle heat losses

In comparison with the previous operation states (compression and expansion), the idle state does not consume or produce any electricity, however the state-of-charge (SOC) of the plant is reduced due to the time-dependent energy losses.

The time-dependent differential equations describing this model only consider energy losses related to the heat transfer of the air with the cavern and of the TES with its surroundings, as it is shown in Sections 2.1, 2.2, 2.3 and 2.5. As for the time-independent losses, associated with the turbines, the compressors and the HX's, they are accounted for by its efficiencies. Following these assumptions it is clear that this model is a simplified version of what actually happens. Nevertheless, the omission of all the other losses associated with piping for example, reduces the complexity of the model without loosing valuable information.

To show how our AA-CAES model changes over time through this operating state, we charged the plant completely and then left it idle for 48 h. The procedure employed here is the same as for the expansion stage but instead of expanding, the model was running without withdrawing any air from the cavern. This means that the initial state $\bar{x}_{0,i} = \bar{x}_{0,e}$, the vector $\bar{T}_{\mathrm{rs,0,i}} = \bar{T}_{\mathrm{rs,0,e}}$, and $\bar{u} = [0 \quad 0]$.

The results obtained by using this operation state are shown in Figure 2.8.

Other results that are interesting to pursue are related to the actual power output losses that take place due to the heat transfer during the idle operating state. We quantified this by comparing how much energy is available in the plant before and after being idle for different time periods. This results from charging and discharging the plant completely, leaving it idle a certain amount of time in between the former operation states. The electricity produced by the expansion train can then be compared with the one obtained when the plant was discharged immediately after charging. The repetition of this process for different idle times gives a good idea of how the electricity output is affected by this parameter. We did this process for an idle time of $1-100$h, using the same initial vectors as for the expansion state.

Figure 2.9 shows the plant's electric output for different idle times on an absolute (top) and relative (middle) scales, together with the decrease of

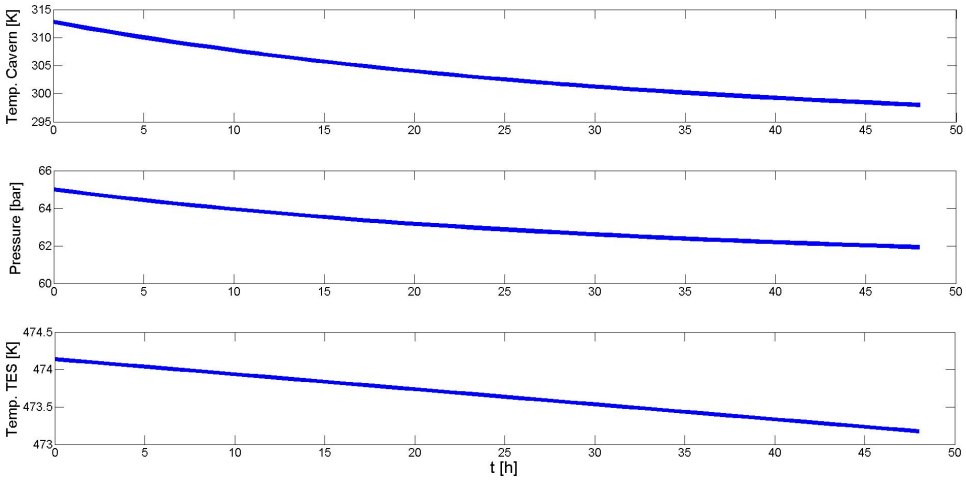

Figure 2.8: Evolution over time of the air temperature (top) and pressure (middle) inside the cavern, together with the TES temperature (bottom) during Idle state.

the plant's efficiency (bottom).

Even though Figure 2.9 shows the absolute energy losses of the plant (top), it is also important to know its power losses for every hour of idle time. The calculation of these losses is similar to the one did for the energy losses, and yields an approximate of 3 $^{\mathrm{MW}}/_{\mathrm{h}}$.

The relative losses presented in Figure 2.9 (middle), account for the percentage of energy lost for each idle time with respect with the maximum electric output of the compression train.

As shown in the bottom graph of Figure 2.9, the efficiency of the plant decreases as the idle time increases. However, this curve has a higher derivative for smaller idle times than for larger ones. This can be explained by the fact that for smaller idle times the temperature difference between the heat sources and the heat sinks is larger, having thereby a larger heat transfer. However, as the idle time increases, the temperature difference becomes smaller and there is a logarithmic growth of the electricity losses.

So far the main three operation strategies for the AA-CAES plant were presented in previous Subsections. However, there is still one more possibility for the plant's operation, which takes place when the compressor train and the expansion train are working at the same time. From the modeling point of view, this strategy does not present any new information compared to what is shown in Subsections 2.5.1 and 2.5.2. However, if time-varying electricity prices are considered for choosing the operation strategy of the plant, this operation state is rather interesting since a simultaneous com-

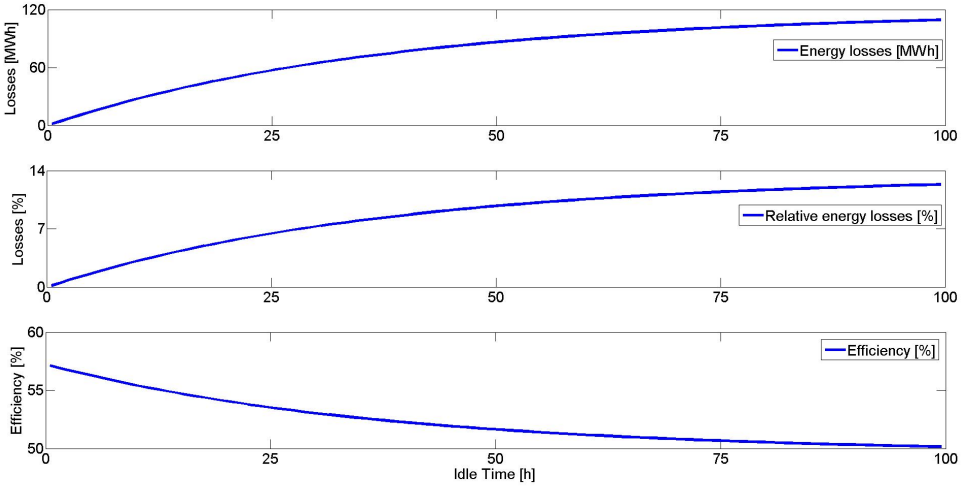

Figure 2.9: Energy and efficiency losses of the AA-CAES model for an idle state.

pression and expansion would only make sense when electricity prices are negative.

The results obtained from this model provide a first insight of the AA-CAES plant's performance, which can be used to analyze the feasibility of its possible applications. In other words, this model is a simple tool to show how this technology will behave in future energy systems while storing intermittent renewable energy sources, providing ancillary services or leveling the load of the electricity supply. In these energy systems, the AA-CAES plants will be operating within the electricity spot markets by storing energy when the prices are low and releasing it when the prices are high. However, in order to make a profit within these markets, the operators of these plants need to identify proper strategies to decide when to compress and when to expand air.

Following this line of thought, Chapter 3 presents model predictive control (MPC) as an optimization scheme for the operation strategy of our AA-CAES model, while Chapter 4 shows the results obtained.

Chapter 3

Model Predictive Control (MPC)

Model predictive control (MPC) theory combines concepts of optimal control and predictive control theory. This theory is a popular feedback control scheme for constrained optimization problems, which accounts for external disturbances and modeling uncertainties. The main idea of MPC algorithms is to designate a broad range of control methods that explicitly use a model to predict the process output at future time instants (horizon), calculating at the same time a control sequence of the process by minimizing an objective function [61]. Furthermore, its main advantage relies on its capability to handle constraints by explicitly considering them inside the controller design [62]. A concrete advantage for the use of MPC is that the controller can use a linear representation of the AA-CAES model to predict the future plant outputs.

This chapter describes a methodology to identify an optimal operation strategy for our AA-CAES model, which is constrained to the physical limitations of the system. This methodology uses Yalmip as an MPC controller, which is a MATLAB toolbox for optimization problems [63]. The first section of this chapter gives an introduction to the main ideas behind MPC theory. The second section deals with linear models used by the MPC controller to predict future system states. The third section presents an explicit representation of MPC. The fourth section gives some information about Yalmip as an MPC controller. Finally, the fifth subsection shows the application of the latter one on our AA-CAES model and the assumptions needed for this.

3.1 MPC Background

MPC algorithms solve an open-loop optimal control problem for a system state $x(t)$ of a given process/plant model at a sampling time t. These al-

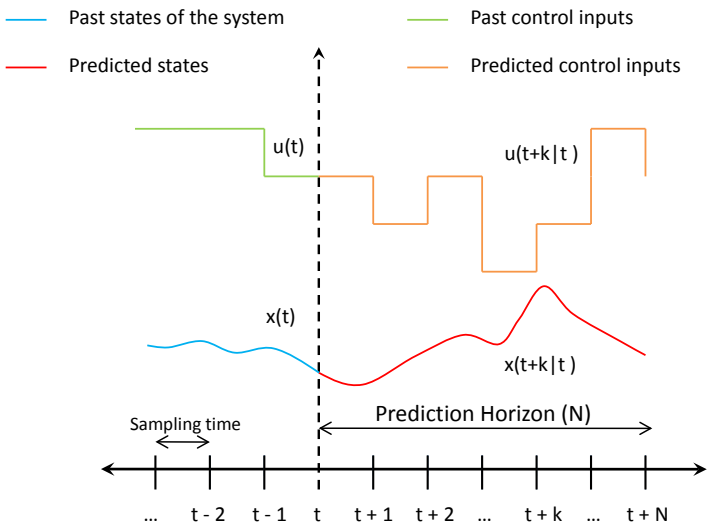

Figure 3.1: General MPC strategy.

gorithms follow a receding horizon strategy, where at each sampling time instant t, the prediction horizon N is moved towards the future, i.e. $[t, t+N]$ [61].

The MPC controller uses a model to predict at each sampling time t the system states $x(t+k \mid t)$[1] for $k \in \{1, ..., N\}$. These predictions depend on the known values at time t (past inputs and outputs). At the same time, the controller calculates a trajectory of control inputs $u(t+k \mid t)$, which is optimized by minimizing a cost function that penalizes the model states and control inputs. Only the first term of the control signal $u(t \mid t)$ is implemented into the process, which now yields a new state $x(t+1)$. This updated information from the process is used by the MPC controller to solve a new open-loop optimal control problem, yielding the next control signal $u(t+1 \mid t+1)$ [64].

Figure 3.1 shows a representation of the MPC strategy described above. This figure only shows the prediction of the control inputs and states for one prediction horizon, however following the receding horizon strategy, N will move towards the future every time the controller yields a new control input $u(t+1 \mid t+1)$.

To implement the strategy described above, the MPC controller follows the structure shown in Figure 3.2. This figure illustrates how the model calculates the predicted states based on past and current information and on the predicted control inputs. The optimizer calculates the latter ones by

[1] This notation indicates the value of the variable at the time $t+k$ calculated at time t [61].

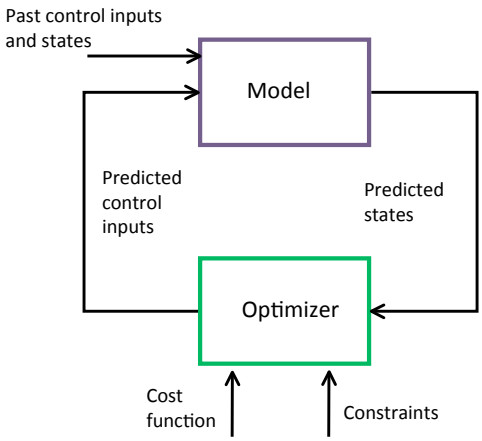

Figure 3.2: Basic MPC structure [61].

taking into account a cost function and the constraints of the system.

As Figure 3.2 reveals, the model is the cornerstone of an MPC scheme. It is crucial for the model to fully capture the dynamics of the process in order to produce accurate predictions of the states. Since MPC is a set of different methodologies, there are several types of models that can be used for different formulations [61]. For the purpose of this thesis, we are going to focus on the state-space models, and in particular, on the state-space representation of discrete-time linear time invariant (LTI) systems. The motivation of using these type of models comes from the fact that the AA-CAES is governed mainly by four differential equations, which can be linearized into an LTI state-space representation.

The next section explains in more detail the above mentioned discrete-time LTI systems, which will work as a model in the MPC controller used for the optimization of the AA-CAES plant's operation strategy.

3.2 LTI and PWA systems

The essence of MPC is to optimize forecasts of process behaviour through the manipulable control inputs. Since the forecasts come from a model used by the controller, the model is the essential part of the MPC [65]. Since the model for the AA-CAES plant can be linearized in a state-space form, we are going to focus on the utilization of state-space representations of linear models within the MPC controller. Using state-space linear models for the MPC controller has the advantages of easy generalization of multivariable

systems, ease of analysis of closed-loop properties, and online computation [65]. Within the linear models, we will focus on its discrete-time state-space representation because it is convenient to implement in MATLAB.

A discrete-time linear time-invariant (LTI) system is described in state-space form by the following expressions

$$\bar{x}(t+1) = \mathbf{A} \cdot \bar{x}(t) + \mathbf{B} \cdot \bar{u}(t), \tag{3.1}$$

$$\bar{y}(t) = \mathbf{C} \cdot \bar{x}(t) + \mathbf{D} \cdot \bar{u}(t), \tag{3.2}$$

where $\bar{x} \in \mathbb{R}^n$ is the discrete state vector, $\bar{u} \in \mathbb{R}^m$ the discrete control input vector, $\bar{y} \in \mathbb{R}^l$ the discrete system output, $\mathbf{A} \in \mathbb{R}^{n \times n}$, $\mathbf{B} \in \mathbb{R}^{n \times m}$, $\mathbf{C} \in \mathbb{R}^{n \times l}$ and $\mathbf{D} \in \mathbb{R}^{l \times m}$. The initial state of the system is $\bar{x}(0) = [x_1(0), \ldots, x_n(0)]^T = \bar{x}_0$.

The states $\bar{x}$ and inputs $\bar{u}$ in Equations (3.1) and (3.2) are subject to the following constraints

$$\bar{x} \in \mathbb{X} \in \mathbb{R}^n, \qquad \bar{u} \in \mathbb{U} \in \mathbb{R}^m, \tag{3.3}$$

where $\mathbb{X}$ and $\mathbb{U}$ are compact polyhedral sets containing the origin in their interior. With these assumptions, the MPC controller can determine an optimal control input by considering the following constrained finite-time optimal control (CFTOC) problem

$$J_N^*(\bar{x}_0) = min \left[\|\mathbf{Q}_\mathrm{f} \cdot \bar{x}(k+N)\|_\ell + \sum_{k=0}^{N-1} \left(\|\mathbf{R} \cdot \bar{u}(k)\|_\ell + \|\mathbf{Q} \cdot \bar{x}(k)\|_\ell \right) \right] \tag{3.4}$$

subject to the constraints

$$\bar{x}(k) \in \mathbb{X}, \qquad \forall k \in \{1, \ldots, N\}, \tag{3.5}$$

$$\bar{x}(k+N) \in \mathcal{X}_{set}, \tag{3.6}$$

$$\bar{u}(k) \in \mathbb{U}, \qquad \forall k \in \{1, \ldots, N-1\}, \tag{3.7}$$

$$\bar{x}(k+1) = \mathbf{A} \cdot \bar{x}(k) + \mathbf{B} \cdot \bar{u}(k), \quad \forall k \in \{1, \ldots, N-1\}, \tag{3.8}$$

$$\begin{cases} \mathbf{Q} = \mathbf{Q}' \succeq 0,\ \mathbf{Q}_\mathrm{f} = \mathbf{Q}_\mathrm{f}' \succeq 0,\ \mathbf{R} = \mathbf{R}' \succ 0, & if \ \ \ell = 2, \\ rank(\mathbf{Q}) = n,\ rank(\mathbf{R}) = m, & if \ \ \ell \in \{1, \infty\}, \end{cases} \tag{3.9}$$

where Equation (3.6) is a user defined set-constraint on the final state that should be chosen to guarantee the stability of the closed-loop system [66]. Equation (3.4) represents the objective function, which can be linear

or quadratic when $\ell \in \{1, \infty\}$ or $\ell = 2$, respectively. The matrix $\mathbf{Q}$ is the cost term for the system state $\bar{x}(k)$, $\mathbf{R}$ is the cost term for the control input $\bar{u}(t)$, and $\mathbf{Q}_\mathrm{f}$ is the cost term for the calculated system state at the prediction horizon $\bar{x}(k+N)$. The control input matrix resulting from solving the CFTOC problem is $\bar{u}^* \equiv [\bar{u}(0)^T, \ldots, u(N-1)^T]^T \in \mathbb{R}^{m \times N}$.

Linear time-invariant (LTI) systems can be extended to piece-wise affine (PWA) systems with ease [67]. The latter ones are the most simplest extension of linear systems and they can model non-linear and non-smooth processes [67, 68]. This is relevant for the previously presented AA-CAES model since the dynamics of each operation state are different. Hence, the implementation of PWA systems will allow us to have three linear models for each operation state of the plant.

A general discrete-time PWA system in its state-space representation is given by the equations

$$\begin{array}{rl} \bar{x}(k+1) & = \mathbf{A}_i \bar{x}(k) + \mathbf{B}_i \bar{u}(k) + \bar{f}_i \\ \bar{y}(k) & = \mathbf{C}_i \bar{x}(k) + \mathbf{D}_i \bar{u}(k) + \bar{g}_i \end{array} \forall \begin{bmatrix} \bar{x}(k) \\ \bar{u}(k) \end{bmatrix} \in \Omega_i \quad i \in I, \tag{3.10}$$

where the convex polyhedra $\Omega_i \subset \Omega \in \mathbb{R}^{n+m}$ are defined by a finite number of linear inequalities for the inputs and states of the system. The vectors and matrices $\bar{x}$, $\bar{u}$, $\mathbf{A}$, $\mathbf{B}$, $\mathbf{C}$, $\mathbf{D}$ have the same dimensions as the ones described above for the LTI systems. The set $I = \{1, \ldots, d\} \subset \mathbb{N}$ represents the possible dynamics of the linear system, where d is the number of different dynamics. The first term in Equation (3.10) together with its restrictions, is usually abbreviated as $\bar{x}(k+1) = f_{PWA}(\bar{x}(k), \bar{u}(k))$ [67, 69].

Now that two types of linear systems are available, the constrained finite-time optimal control (CFTOC) problem presented for LTI systems can be extended to PWA systems as well, adding its corresponding constraints. Thus, using the same cost function as the one presented in Equation (3.4), the CFTOC problem for an LTI or PWA system is subject to the following constraints

$$\begin{cases} \bar{x}(0) = \bar{x}_0 \quad (LTI) \\ \bar{x}(k+1) = \mathbf{A} \cdot \bar{x}(k) + \mathbf{B} \cdot \bar{u}(k) \\ \\ \bar{x}(0) = \bar{x}_0 \quad (PWA) \\ \bar{x}(k+1) = f_{PWA}(\bar{x}(k), \bar{u}(k)) \\ \quad \forall\ [\bar{x}(k), \bar{u}(k)]^T \in \Omega \end{cases} \tag{3.11}$$

$$\bar{x} \in \mathbb{X} \in \mathbb{R}^n, \qquad \bar{u} \in \mathbb{U} \in \mathbb{R}^m$$

$$\begin{cases} \mathbf{Q} = \mathbf{Q}' \succeq 0,\ \mathbf{Q}_\mathrm{f} = \mathbf{Q}'_\mathrm{f} \succeq 0,\ \mathbf{R} = \mathbf{R}' \succ 0, & if\ \ \ell = 2, \\ \quad rank(\mathbf{Q}) = n,\ rank(\mathbf{R}) = m, & if\ \ \ell \in \{1, \infty\}. \end{cases}$$

Before implementing the MPC theory to the AA-CAES non-linear model, the following section presents an alternative approach to the classical MPC theory to reduce the computational time of the calculations.

3.3 Yalmip

Yalmip is a MATLAB toolbox used to model and solve optimization problems that take place in control and systems theory [63]. There are two main motivations to use Yalmip to optimize the operation strategy of our AA-CAES model. The first one is that Yalmip is interfaced with the already existing multi-parametric toolbox (MPT) from MATLAB, which enables convenient definition and solution of these type of problems. The second one comes from the fact that this toolbox is consistent with standard MATLAB syntax. The latter one is important since the modeling of the plant and its linearization were done in this programming platform, making the implementation of the already written subroutines into Yalmip a straightforward step.

The decision variables of the optimization problem are represented in Yalmip by *sdpvar* objects, which can be used as regular variables using most of MATLAB's commands. The constraints can be declared by constructing sets of conditions that can be concatenated with each other. The most commonly used constraints in Yalmip are element-wise, semidefinite and equality constraints.

Finally, the last thing that Yalmip needs for solving the CFTOC problem is the objective function. This can be constructed by imposing weights on the decision variables using MATLAB's most common operators.

There are two formulations to implement a model of the system in question for the prediction of its future states. The first one is to do it explicitly, by inserting the model inside the controller routine. With this approach the optimization problem lies on the decision variables and the initial state of the system. The second formulation is an implicit one. Here the optimization is done over the decision variables and the state predictions, while the system dynamics of the system are included using equality constraints. For example, for an LTI system, we would like to include the constraints shown in Equation (3.10) as a part of our constraint set. For the purpose of this thesis we will work with the latter formulation. This is because it helps us to cope with any discrepancies that the linear model of our AA-CAES plant may have with the non-linear model.

To solve the CFTOC Yalmip uses the command *solvesdp*, which has an entry for the objective function and another one for the set of constraints. There is an option to compile the numerical model once using the *optimizer* command, which allows us to save the time that *solvesdp* spends on converting the Yalmip model to the numerical format on every time step.

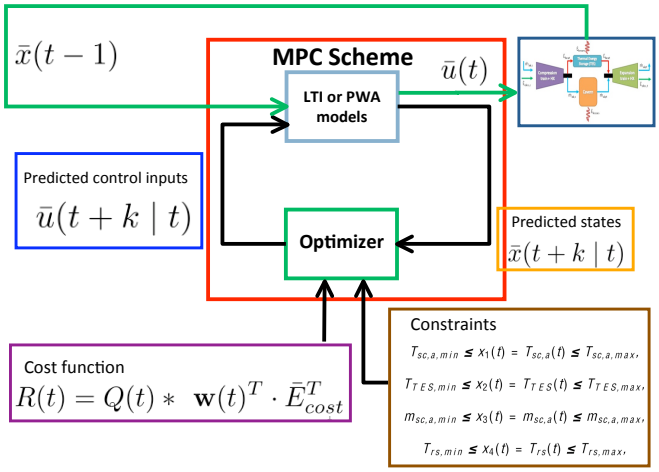

Figure 3.3: Basic MPC structure [61].

As a final part of this chapter, the next section presents the implementation of Yalmip to obtain an optimal operation strategy for our AA-CAES model.

3.4 MPC implementation on an AA-CAES model

The calculation of an optimal operation strategy for our AA-CAES model using Yalmip follows the structure depicted in Figure (3.3), which is a modified version of the general MPC structure (see Figure 3.2). In this case, the optimizer is Yalmip and the model is given by a state-space representation of our AA-CAES model (see Chapters 2 and 3). A reference trajectory is given by the actual non-linear AA-CAES model, which receives as input the optimal operation strategy $\bar{u}(t)$. This input is calculated by the MPC controller at each time step. The last state of the plant $\bar{x}(t-1)$ is calculated by the non-linear model itself on the previous time step, and it is used as an input for the linear model. The constraints of the optimizer are given by the physical limitations of the AA-CAES plant, while the cost function considers weighted control inputs together with varying electricity prices.

3.4.1 AA-CAES linear model

The linearization of the AA-CAES model seems to be straightforward due to the fact that the system dynamics are governed mainly by four time-dependent differential equations. However, on the one hand different operation states of the plant suggest that the dynamics of the system would be

different at each of them (expansion, compression and idle). On the other hand it is important to note that the price of electricity in a power market varies hourly and this suggests the use of a discrete-time linear model for the MPC controller. These two constraints on the dynamics of the system suggest the utilization of discrete-time PWA systems in Equation (3.10). Nevertheless, the first assumption can also be omitted and this would exhort us to use a discrete-time LTI system.

The linearization of the model during each operation strategy was done by MATLAB's function *dlinmod* using a sampling time of $t_s = 3600\ s$. However, to calculate the matrices $\mathbf{A}_i$, $\mathbf{B}_i$, $\mathbf{C}_i$ and $\mathbf{D}_i$ in Equation (3.10), this MATLAB function needs as an input a state of the system that will be linearized. As explained in Subsection 2.5.2, the states of the non-linear model are represented by a vector that has more than four entries due to the discretisation of the cavern's wall. To avoid this problem, we only consider one point for this calculation, which means that $N_C = 1$ (see Appendix B). This simplification provides a more intuitive state of the plant that corresponds to one entry per differential equation. Hence, $\bar{x}(t) \in \mathbb{R}^4$ and it is given by

$$\bar{x}(t) = [T_{\text{sc,a}}, \quad T_{\text{TES}}, \quad m_{\text{sc,a}}, \quad , T_{\text{rs}}], \tag{3.12}$$

where each of the entries are the main variables of each of the time-dependent differential equations employed in our AA-CAES model (see Chapter 2).

The resulting states after compression or expansion were calculated by the AA-CAES model after compressing or expanding enough air as to leave the cavern half-full, respectively. In other words, the states of the plant were extracted when $p_{\text{sc,a}} = 55.5$ bar. As for the idle operation, the state of the system corresponded to a completely charged plant that was idle for $t = 10\ hours$.

With the coefficients of the state-space linear models for each operation state of the plant, Yalmip is now able to predict the future states $\bar{x}(t+k \mid t)$. The next step for the optimization of the operation strategy of the plant, is to implement Yalmip using these discrete-time PWA or LTI systems by imposing constraints and defining a cost function.

3.4.2 Yalmip implementation

Once a model is available for the MPC controller, Yalmip requires that we define the decision variables, the constraints for the latter ones and a cost function.

As discussed above, the decision variables need to be declared as *sdpvar* objects within this MATLAB toolbox. In this case these variables are the states of the system $\mathbf{x}(t) \in \mathbb{R}^{4\times N}$ and the control inputs $\mathbf{u}(t) \in \mathbb{R}^{2\times N}$, which are the concatenation of the vectors $\bar{x}(t+k \mid t)^T \in \mathbb{R}^4$ and $\bar{u}(t+k \mid t)^T \in \mathbb{R}^2$

calculated N times for each time step t, respectively. These matrices are given by

$$\mathbf{x}(t) = \begin{pmatrix} x_1(t+1) & \dots & x_1(t+N) \\ x_2(t+1) & \dots & x_2(t+N) \\ x_3(t+1) & \dots & x_3(t+N) \\ x_4(t+1) & \dots & x_4(t+N) \end{pmatrix}, \tag{3.13}$$

and

$$\mathbf{u}(t) = \begin{pmatrix} u_1(t+1) & \dots & u_1(t+N) \\ u_2(t+1) & \dots & u_2(t+N) \end{pmatrix}, \tag{3.14}$$

where N is the prediction horizon and it is measured in hours. This variable is moved into the future by Yalmip by following the receding horizon strategy.

Now that Yalmip recognizes which are the decision variables of this CFTOC problem, it needs to know the objective function. For the construction of this function it is important to remember the main objective of this optimization, which is to calculate an operation strategy that maximizes the revenue of an AA-CAES plant operating in a power market. Therefore, the objective function would need to yield a monetary result. This is done by multiplying the amount of power consumed or produced by the AA-CAES plant in one hour, with the market's price of electricity on that same hour. The idea is that this product will work as a weight for each operation strategy suggesting the optimizer when to expand, compress or to go idle. The time-dependent objective function is given by

$$R(t) = Q(t) * \left[\mathbf{w}(t)^T \cdot \bar{E}_{\text{cost}}^T\right], \tag{3.15}$$

where $R(t)$ is the revenue of the plant at time t and it is measured in Euros, $Q(t)$ is the hourly power price and it is measured in $^{\text{EUR}}/_{\text{MW}}$. The time t is measured in hours. The term $\bar{E}_{\text{cost}}^T$ is a three-entry vector that considers the hourly electricity produced or consumed by the AA-CAES plant for each operation state and is measured in MW. Finally, $\mathbf{w}(t)^T \in \mathbb{R}^{3\times N}$ is a matrix that represents the operating state of the plant (compression, expansion and idle) at time t.

The time-series $Q(t)$ represents the hourly electricity prices of any power market. These prices are assumed to be perfectly predictable up to the prediction horizon N of the MPC controller.

As for the construction of $\bar{E}_{\text{cost}}^T$, this is a constant vector over time with the nominal power of the compression and the expansion trains as its first two entries, and the idle power losses as the third one. This vector is in MW and is given by

$$\bar{E}_{\text{cost}}^{T} = \begin{pmatrix} -64 \\ 85 \\ -3 \end{pmatrix}, \tag{3.16}$$

where the negative sign means that power is being consumed or lost, while the positive sign means that power is being produced.

The matrix $\mathbf{w}(t)^T$ is constructed by adding one more column to $\mathbf{u}(t)$ that takes into account the operation state idle by multiplying $(1-u_1(t)) * (1-u_2(t))$. This matrix is given by the following expression

$$\mathbf{w}(t)^T = \begin{pmatrix} u_1(t+1) & u_2(t+1) & (1-u_1(t+1)) * (1-u_2(t+1)) \\ \vdots & \vdots & \vdots \\ u_1(t+N) & u_2(t+N) & (1-u_1(t+N)) * (1-u_2(t+N)) \end{pmatrix}, \tag{3.17}$$

where $u_1, u_2 \in [0,1] \subset \mathbb{R}$ are the entries of the input matrix $\mathbf{u}(t)$.

It is worth noting that since MPC controllers work with minimization problems we multiplied the objective function by -1 to obtain a maximization of the revenue.

Finally, we need to define the constraints of the decision variables for Yalmip to be able to solve the CFTOC problem. As mentioned above, we are going to use the implicit formulation of the linear model in Yalmip, which means that the state-space representation of our plant will be written as a constraint.

The constraints associated to the decision variable $\mathbf{x}(t)$ depend on the physical restrictions of the AA-CAES model itself, which are determined by the maximum and minimum capacities of the cavern and the TES system. Since $\mathbf{x}(t)$ is constructed concatenating $\bar{x}(t+k \mid t) \in \mathbb{R}^4$, there will only be four constraints associated to $\mathbf{x}(t)$, which are given by

$$\begin{aligned} T_{\text{sc,a,min}} \leq \quad & x_1(k) = T_{\text{sc,a}}(t) \leq \quad T_{\text{sc,a,max}}, \\ T_{\text{TES,min}} \leq \quad & x_2(k) = T_{\text{TES}}(t) \leq \quad T_{\text{TES,max}}, \\ m_{\text{sc,a,min}} \leq \quad & x_3(k) = m_{\text{sc,a}}(t) \leq \quad m_{\text{sc,a,max}}, \\ T_{\text{rs,min}} \leq \quad & x_4(k) = T_{\text{rs}}(t) \leq \quad T_{\text{rs,max}}, \end{aligned} \tag{3.18}$$

where these minima and maxima correspond to a completely full or completely empty AA-CAES plant, respectively.

As for the constraints for the input decision variable $\mathbf{u}(t)$, they need to restrict the values of the operation strategy given by Yalmip so the non-linear model can interpret them correctly. The main constraint for the vector $\bar{u}(t) = [u_1 \quad u_2]$ is that $u_1, u_2 \in [0, 1] \subset \mathbb{R}$. To ensure this, the following constraints were considered

$$0 \leq u_1,\ u_2 \leq 1, \ \wedge\ 0 \leq u_1 + u_2 \leq 1. \tag{3.19}$$

The second constraint in Equation (3.19) ensures that we will only have the three desired operations states (compression, expansion and idle).

For the implementation of the model we followed two main approaches. The first one was to use one linear model instead of three, making the assumption that the dynamics of the system are similar for the three operation states. In this case, the model used to predict the states of the system $\bar{x}(t+1)$ follows the LTI system state-space representation shown in Equation (3.1). The model used was the one obtained while compressing, and it was added to the already existing constraints set.

The second approach was to use one model for each operation state of the plant, in other words, a state-space representation of a PWA system where the set $I = \{1, 2, 3\}$ in Equation (3.10). For the implementation of this approach Yalmip needs a binary decision variable $\mathbf{b}(t)$ that will determine when to use what model on each time-step t. This variable is constructed by concatenating the three-entry vector $\bar{b}(t+k)^T$ for $k \in \{1, \ldots, N\}$, as shown by the following expression

$$\mathbf{b}(t) = \begin{pmatrix} b_1(t+1) & \ldots & b_1(N) \\ b_2(t+1) & \ldots & b_2(N) \\ b_3(t+1) & \ldots & b_3(N) \end{pmatrix}, \tag{3.20}$$

where $b_1, b_2, b_3 \in \{0, 1\}$ correspond to compression, expansion and idle operation states, respectively.

This new decision variable allows Yalmip to manage constraints with logic implications through the command *implies*. In other words, b_1, b_2, b_3 are forced to be true (1) or false (0) by a set of linear inequalities imposed over the control input $\bar{u}(t)$ and the states of the system $\bar{x}(t)$. These constraints determine whether the plant is compressing, expanding or idle. For the states of the system, a comparison between the present ($T_{\text{TES}}(t)$) and future ($T_{\text{TES}}(t+1)$) temperature of the TES system shows what is the operation state of the plant. This assessment is also done by comparing the entries of the control inputs u_1 and u_2. Hence, the constraints with logic implications for the PWA systems are

$$
\begin{aligned}
(x_2(t+1) > x_2(t)) \;&\rightarrow\; (b_1 = 1 \;\wedge\; b_2 = b_3 = 0),\\
(u_1(t) > u_2(t)) \;&\rightarrow\; (b_1 = 1 \;\wedge\; b_2 = b_3 = 0),\\
(b_1 = 1 \;\wedge\; b_2 = b_3 = 0) \;&\rightarrow\; (\bar{x}(t+1) = \mathbf{A}_{\mathrm{c}}\bar{x}(k) + \mathbf{B}_{\mathrm{c}}\bar{u}(k)),
\end{aligned}
$$

$$
\begin{aligned}
(x_2(t+1) < x_2(t)) \;&\rightarrow\; (b_2 = 1 \;\wedge\; b_1 = b_3 = 0),\\
(u_1(t) < u_2(t)) \;&\rightarrow\; (b_2 = 1 \;\wedge\; b_1 = b_3 = 0),\\
(b_2 = 1 \;\wedge\; b_1 = b_3 = 0) \;&\rightarrow\; (\bar{x}(t+1) = \mathbf{A}_{\mathrm{e}}\bar{x}(k) + \mathbf{B}_{\mathrm{e}}\bar{u}(k)),
\end{aligned}
\tag{3.21}
$$

$$
\begin{aligned}
(x_2(t+1) - x_2(t) \leq 10^{-3}) \;&\rightarrow\; (b_3 = 1 \;\wedge\; b_1 = b_2 = 0),\\
(u_1(t) * u_2(t) \leq 10^{-3}) \;&\rightarrow\; (b_3 = 1 \;\wedge\; b_1 = b_2 = 0),\\
(b_3 = 1 \;\wedge\; b_1 = b_2 = 0) \;&\rightarrow\; (\bar{x}(t+1) = \mathbf{A}_{i}\bar{x}(k) + \mathbf{B}_{i}\bar{u}(k)),
\end{aligned}
$$

where the first set of constraints corresponds to the compression state, the second one to the expansion state and the third one to the idle state. The first equation of each of these three sets of constraints follows the assumption that $x_2(t) = T_{\mathrm{TES}}(t)$ will increase over time when compressing, decrease when expanding and stay relatively constant while being idle. The second equation in each of these sets follows the definition of the operation states given in Section 2.5. This last inequality constraint prevents Yalmip from using the wrong model in case the control input does not match with the comparison between $x_2(t)$ and $x_2(t+1)$. The subindices c, e and i correspond to compression, expansion and idle linear models, respectively. For more information on the code used for this implementation refer to Appendix D.

Now the definition of the CFTOC problem is complete. To start with the optimization Yalmip needs an initial state of the AA-CAES plant, which is calculated using the state-of-charge (SOC) through the variable SOC. The initial state $\bar{x}_0(t) \in \mathbb{R}^4$ given to Yalmip is the result of charging the plant completely and then discharging it for a time $t = (1 - SOC) * t_{\mathrm{e,max}}$ (see Subsection (2.5.2)). This will ensure that the TES system has already been charged and its not "cold" or at ambient temperature.

The following chapter shows the results of the optimization for the operation strategy of our AA-CAES model following the approaches presented in this section.

Chapter 4

Optimal Operation Strategies for an AA-CAES Model

There are several studies on how CAES plants can cope with the intermittency of renewable energy sources, specially from wind, so as to provide more reliable power output [5, 12, 14, 24, 31, 58]. However, little attention has been given in literature to the management of these plants while dealing with fluctuating electricity prices in power markets. The importance of this subject is compelling due to the high interest on the adoption of AA-CAES systems, which would become part of the present electric power systems operating within the existing power markets. Thus, to ensure its profitability, these storage plants will have to follow an operation strategy that copes with fluctuating electricity prices. Although a previous study has applied computer-based methodologies to optimize the operation strategy of a CAES plant [70], nothing has been done with respect to the AA-CAES concept. The main difference between the adiabatic and diabatic CAES operation strategies is that in the first one, the energy losses need to be considered in the optimization strategy, while in the second one they are not relevant due to the use of natural gas for reheating the air.

Before entering into the approaches used for the optimization, the following subsection gives a more detailed insight of the used price profiles to calculate the revenue-maximizing operation strategies.

Electricity price time-series

The objective function of the MPC controller uses a time-series of electricity prices to weight the decision variable $\mathbf{w}(t)$, which helps the controller to decide when the AA-CAES model will expand, compress or go idle depending on the state-of-charge of the plant and the future electricity prices.

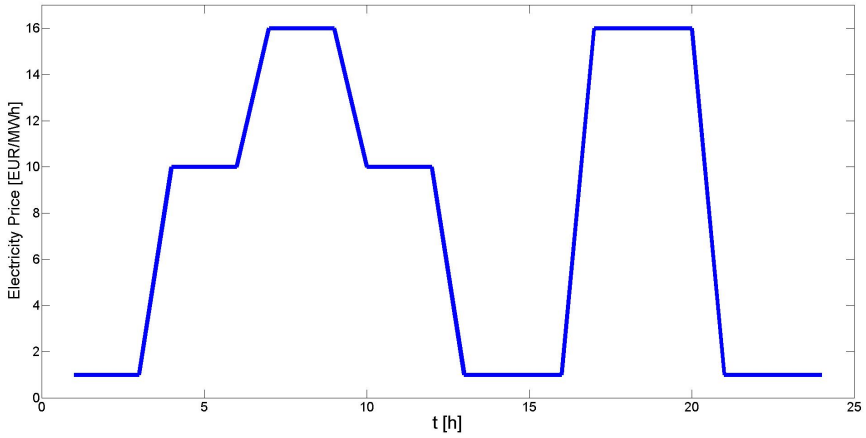

Figure 4.1: Flat price profile.

The main idea of introducing a real price time-series is to show how the AA-CAES plant can behave in the presence of a variable electricity price to maximize its profit. At a first glance, we would expect the plant to compress when the prices are low and expand when they are high, but the situation is not as easy, even though this approach should be followed in principle by the MPC controller.

A first question that arrives while having a price time-series is what would be the operation state of the storage system when prices are not at its maximum nor minimum within the prediction horizon of that time step. A possible answer is to make the plant to go into the idle state. This would make sense as long as the monetary losses involved with the idle operation state are smaller than the gains produced in future expansions. This last argument is the main reason why the consideration of the losses in our AA-CAES model is important for the calculation of an optimal operation strategy.

We considered two price time-series for the optimization. The first one is a flat price profile with three different prices on a lapse of 24 h (see Fig. 4.1). The idea of having three prices is to associate one price with each operation state, so the controller will try to expand at the high price (EUR 16), send the idle signal at the middle one (EUR 10), and compress at the low one (EUR 1). This will allow the controller to calculate an optimal operation strategy by easily recognizing any changes in electricity prices. The objective of this profile is to make a first test of the MPC controller to see if it is really maximizing the cost function or not. This means that if the controller decides to expand or compress air while the prices are low or high, respectively, then there is a problem with the optimizer.

The second price time-series corresponds to the hourly electricity prices

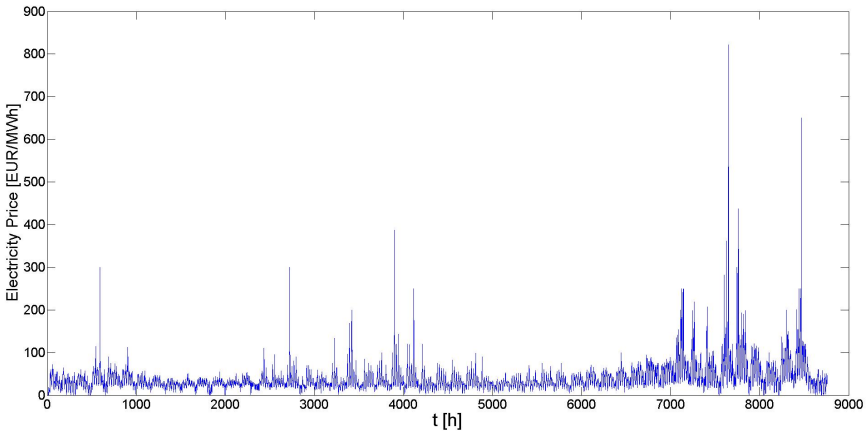

Figure 4.2: EPEX's hourly electricity prices for 2007 [71].

of the European Power Exchange's (EPEX) market for 2007 [71] (see Fig. 4.2). The use of a real price profile allows us to assess how the MPC controller optimizes the operation strategy of the plant with very different prices along the day. In the actual optimization of the plant we will not use the whole year profile, since the idea is only to see if the optimization is done correctly by the MPC controller. The maximum amount of time that will be used from this time-series will be one week.

It is important to note that the prices are considered to be perfectly predictable up to the prediction horizon of the MPC controller. This means that the optimizer will always know what prices follow in the future through the receding prediction horizon strategy.

In this context, with an already developed model for an AA-CAES system and an electricity price profile, the calculation of an optimal operation strategy is straightforward. However, the optimization approach needs to cope with the non-linearities of the AA-CAES model and its multiple physical constraints, together with the hourly changing electricity prices.

The following two sections present the optimal operation strategies calculated by Yalmip through the implementation of two different approaches. The first one uses a state-space representation of a discrete-time LTI system as a linear model inside the MPC controller, while the second one uses a discrete-time PWA system. The latter one has three different state-space models that correspond to each of the operating states of the plant (see Subsection 3.4.2).

4.1 Optimization strategy (LTI system)

In this first approach, the MPC controller used a state-space representation of a discrete-time LTI system to calculate the optimal operation strategy of the AA-CAES plant. The main assumption under this approach is that the dynamics of the system are not that different between the operation states, so one of the three linearized models is good enough for the MPC controller to make its predictions. Therefore, we used the linear model obtained while the plant was compressing (see Subsection 3.4.1).

All the same, a simplification was made within the LTI system. Instead of calculating the complete state of the system $\bar{x}(t)$ by the linear model for every time step t, the model focused on the air temperature inside the cavern $T_{\mathrm{sc,a}}$. Thus, the simplified linear model is given by

$$x_{1,\mathrm{c}}(t+1) = \bar{A}_{1,\mathrm{c}} \cdot \bar{x}(t) + \bar{B}_{1,\mathrm{c}} \cdot \bar{u}(t), \tag{4.1}$$

where $\bar{A}_{1,\mathrm{c}}$ and $\bar{B}_{1,\mathrm{c}}$ are the first rows of the matrices $\mathbf{A}$ and $\mathbf{B}$, respectively. Where the latter ones are part of the discrete-time LTI system obtained by *dlinmod* (MATLAB function) during compression.

It is worth mentioning that the use of one linear model simplifies the complexity of the CFTOC problem within Yalmip due to the avoidance of a binary decision variable. Thus, if the initial assumption is correct, this would be a more efficient way of calculating the operation strategy of the plant.

Within this approach, the first optimization calculated by Yalmip was using the flat price profile presented before (see Figure 4.1), in order to evaluate the performance of the optimizer. The initial state-of-charge for this optimization was $SOC = 0.5$, which determines the initial state of the plant $\bar{x}_0$ by completely charging it and then discharging it for $t = (0.5) * 11.87\,h = 5.94$ h (see end of Subsection 3.4). Yalmip calculated the optimal operation strategy for this 24 h price profile using a prediction horizon of $N = 15$ h.

Figure 4.3 shows the flat price profile (top), the optimal operation strategy calculated by Yalmip for the above-mentioned conditions (middle), and the revenue of the plant (bottom). The revenue of the plant calculated by the MPC controller after operating for 24 h was EUR 7977.

In the operation strategy of the plant presented in Figure 4.3 (middle), the red and blue bars show a normalized version of the electric power consumed or produced by the plant on each hour. As the legend suggests, the red bars correspond to expansion and the blue ones to compression, however the maximum of each operation state is different due to the different nominal powers of the compression and expansion trains (see Sections 2.1 and 2.4). The absence of bars on an hour means that the plant is idle.

The middle graph of Figure 4.3 shows that the operation strategy of the plant follows the price profile, compressing when the prices are EUR 1

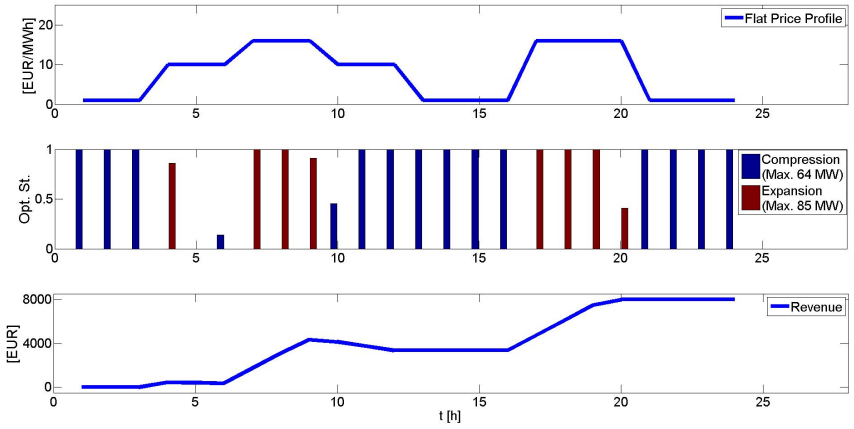

Figure 4.3: Optimal operation strategy for the LTI system using a flat price profile ($SOC = 0.5$ and $N = 15$ h).

or EUR 10, and expanding when the prices are EUR 16. The fact that it compresses when the price is EUR 10 is an indication that the plant needs to increase the SOC as much as possible in order to profit the most when the prices are high. It is worth noting that the optimizer chooses to compress or expand partially depending on future prices. The idle operation state is also present in this graph at hour 5, where the price is EUR 10 and the optimizer is looking into the next 15 h, where it notices that high prices will be available so it "saves" some air inside the cavern to use it later on. At this point, going idle makes sense since the prices will be lower in the future and it is not worth to spend money on "expensive" electricity if better price offers will be available in the future. This kind of decisions made by the optimizer exploit the assumption that all the pricing information is known within the prediction horizon.

Since the optimizer calculated a reasonable operation strategy for the flat price profile, we decided to implement the EPEX electricity prices for 2007 into the MPC scheme. We calculated two operation strategies shown in Figures 4.4 and 4.5, which correspond to a state-of-charge $SOC = 0.3$ and 0.6 respectively. The initial state of the plant $\bar{x}_0$ for both SOC's was calculated similarly as for the flat price profile optimization. Yalmip calculated the hourly optimal operation strategy for seven days or 168 h, using a prediction horizon of $N = 15$ h.

The operation strategies presented in Figures 4.4 and 4.5 (middle), follow the given price profile on almost every hour, expanding when the prices are at its maximum and compressing or going idle at low or at intermediate prices, respectively.

The revenue of the AA-CAES system at the end of the week was EUR

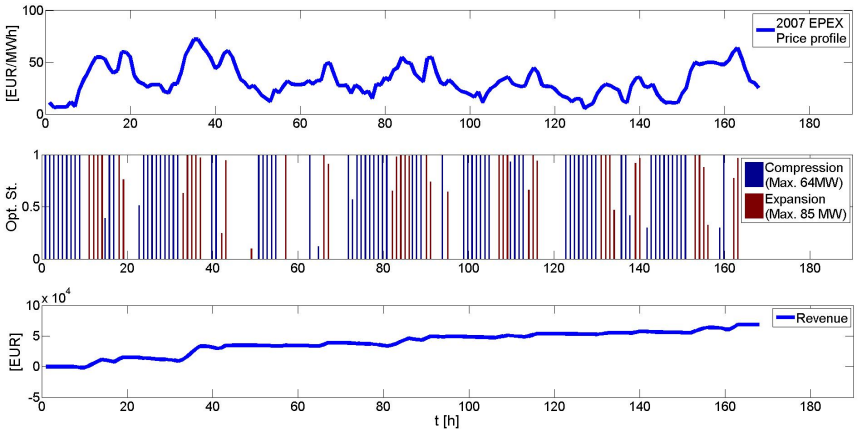

Figure 4.4: Optimal operation strategy for a $SOC = 0.3$ and $N = 15\,\mathrm{h}$ using the EPEX price profile for 2007.

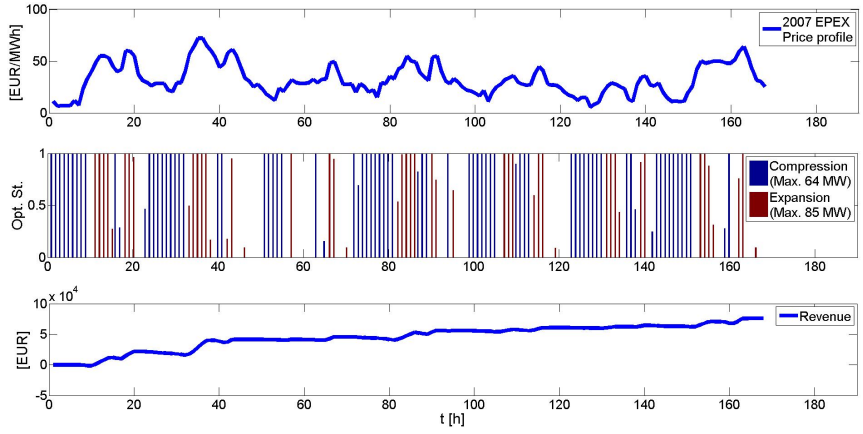

Figure 4.5: Optimal operation strategy for a $SOC = 0.6$ and $N = 15\,\mathrm{h}$ using the EPEX price profile for 2007.

68760 and EUR 75970 for a $SOC = 0.3$ and $SOC = 0.6$, respectively. A comparison between these revenues and the profiles shows that the profiles are almost the same but the revenue ends up being higher at the end of the week for the $SOC = 0.6$. This can be understood since more energy is available for a higher state-of-charge, thus less money has to be spent to charge the plant. It is hard to show that this is the best outcome possible since the optimizer is always looking forward into the future, due to the receding horizon strategy. This means that at the end of the week, the MPC controller will calculate an operation strategy taking into account future states and prices. Hence, the results obtained for the latest hours of the week would be optimal considering the future, but not for the week itself.

Another thing that is important to point out in Figures 4.4 and 4.5 is that the plant goes idle in approximately the same hours of the week (see middle graphs). This means that no matter what initial SOC we put into the plant, the optimizer will identify the same hours to go idle. However, a more detailed inspection shows that the graph in Figure 4.5 makes small expansions in some of these "idle times", which take place since the plant has more energy to discharge and the prices are sufficiently low to increase the revenue.

As a final remark, the optimal operation strategy calculated by Yalmip for this discrete-time system followed the assumption that the temperature in the thermal energy storage (TES) should increase, decrease or stay relatively constant while the AA-CAES plant is compressing, expanding or idle, respectively (see Section 4.1). This assumption is justified by the results shown previously in Section 2.5. As Figure 2.3 (bottom) shows, the temperature of the TES does increase for every hour while compressing. The opposite is shown in Figure 2.6 (bottom), where the temperature of this system decreases during expansion. As for the idle operation state, there are time-dependent losses that cause a decrease of the temperature of the TES, as shown in the differential equation that presents the dynamics of this storage system (see Eq. 2.18). Nevertheless, these losses are relatively small when accounted for per hour as shown in Figure 2.8 (bottom); hence, the assumption that the temperature of this system is almost constant can be maintained.

Following the results presented in this section, it is now compelling to extend the optimization to the more general approach, where the state-space representation of the PWA system is used as a linear model inside the optimizer. The following section presents the results obtained by Yalmip under this approach.

4.2 Optimization strategy (PWA system)

This second approach deals with a state-space representation of a discrete-time PWA system for the optimization of the operation strategy of our AA-CAES model (see Subsections 3.4.1 and 3.4.2). In this case Yalmip needs a binary decision variable $\mathbf{b}(t)$ so as to change between models through constraints with logic implications (see Subsection 3.4.2).

We applied the same simplification as before to this formulation, where only the first variable of the linear model is calculated by using the first rows of the matrices defining each model. This simplification yields the following linear models

$$\begin{aligned} x_{1,\mathrm{c}}(t+1) &= \bar{A}_{1,\mathrm{c}} \cdot \bar{x}(t) + \bar{B}_{1,\mathrm{c}} \cdot \bar{u}(t), \\ x_{1,e}(t+1) &= \bar{A}_{1,e} \cdot \bar{x}(t) + \bar{B}_{1,e} \cdot \bar{u}(t), \\ x_{1,i}(t+1) &= \bar{A}_{1,i} \cdot \bar{x}(t) + \bar{B}_{1,i} \cdot \bar{u}(t), \end{aligned} \tag{4.2}$$

where the sub-indices c, e and i correspond to the linear models we calculated while the AA-CAES plant was compressing, expanding or idle, respectively. This simplification makes that the MPC controller only concentrates on one variable out of four, reducing the computational effort considerably.

As for the previous linear model, the optimization was done for a flat price profile during a time frame of 24 h, using a prediction horizon of $N = 15$h and an initial state-of-charge of $SOC = 0.5$. The same initial conditions were chosen for this optimization in order to compare the results and assess which linear model performs better for this optimization.

The operation strategy calculated by the optimizer is presented in Figure 4.6, where the flat price profile is presented (top), together with the operation strategy of the plant (middle) and its revenue (bottom). In this case, the revenue of the plant for the period of 24 h was EUR 5760.

The operation strategy presented in Figure 4.6 (middle) shows that the MPC controller was not able to calculate the best operation strategy. One the one hand, the optimizer tells the plant to compress when the prices are at its highest value (EUR 16) in the 8th hour, which makes no sense if the revenue should be maximized. This shows a failure in the optimizer since instead of expanding as much as possible for high prices, it decides to waste its energy on the middle prices (EUR 10), emptying the cavern without having enough for the future high prices. This shows that the forecast ability of the optimizer within the prediction horizon is not very accurate. On the other hand, the idle states are too frequent for such a small period of time. If the optimizer forecasts would have been correct, it would have compressed enough air to be able to supply electricity when the prices were at its maximum, instead it proposed an idle operation state. Finally, comparing this operation strategy with the one shown in Figure 4.3,

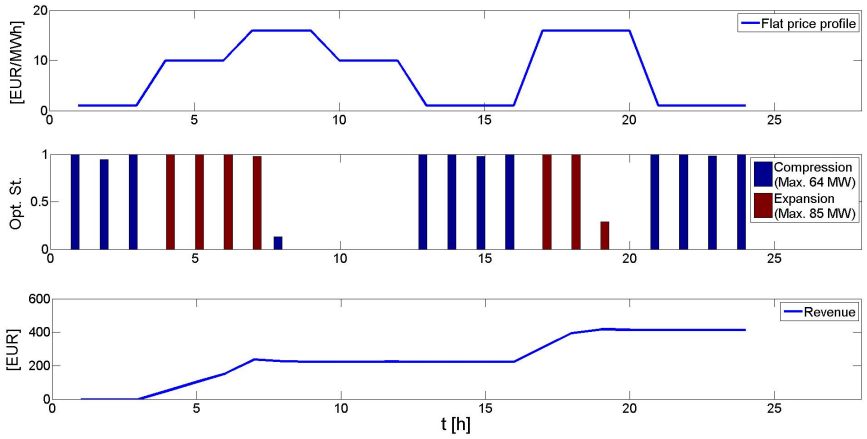

Figure 4.6: Optimal operation strategy for the PWA system using a flat price profile ($SOC = 0.5$ and $N = 15$ h).

the former one performs worse in a sense that it does not take advantage of high prices to increase its revenue. Additionally, the revenue obtained in this operation strategy is considerably lower than the one calculated for the LTI system.

The problems encountered above are exacerbated by the fact that the calculation time for the PWA system was more than twenty times longer than for the LTI system. This is related to the introduction of the binary variable $\mathbf{b}(t)$, which increases to a great extent the computational effort for this optimization.

Following these results for a price profile where only three different prices were available, we did not go further for the calculation of an optimization strategy following the EPEX electricity prices. It can be inferred that if the optimizer did not perform well for a simple price profile, it will not improve its performance using a more complex price time-series.

Chapter 5

Conclusions

The main outcomes of this master thesis comprehend two different fields of study, thermodynamics being the first one, and optimal control the second one. Thermodynamics was the main tool for the modeling of an AA-CAES plant, providing the physics to describe the dynamics of the system. As for optimal control, it took part on the calculation of an operation strategy that can work as a benchmark for the future inclusion of these storage systems into the present power market regimes.

The results of the model presented in Section 2.5 show how the main variables of the plant evolve over time for each operation state (compression, expansion and idle). The increase and decrease of the air temperature inside the cavern is non-linear, and this is due to the heat exchange that takes place between the air and the wall of the rock-salt cavern. The modeling of this heat transfer was done through the heat equation by using a discretisation of the cavern.

A similar explanation follows the non-linear behaviour of the concrete-made TES system, where energy is being lost due to the heat exchange with the environment. The dynamics of the system were modeled by taking into account the energy balance of the plant and following the equations of an immersed coil as heat exchanger.

An insulation layer was considered for the TES system, covering completely the concrete block and reducing considerably the heat transfer. This layer was chosen to be made of glass wool because this is a very common material to insulate buildings and big surfaces. Nevertheless, other materials with smaller heat transfer coefficients can bring better solutions to prevent energy losses in this system. The thickness of the insulation wall d_{wall}, and thus the amount of glass wool considered for this insulation was determined without considering any costs on the insulation material, which could present a problem for its implementation. Since the objective of the thesis was to provide a thermodynamical model of an AA-CAES plant together with its energy losses, we permitted ourselves to exclude the economic analysis of

its components. Nevertheless, this analysis is very important if we expect a future implementation of these storage systems within the present electric power systems, even though this can only take place with a considerable cooperation between academia and industry.

As for the salt-cavern no artificial insulation was considered due to its big volume, which is in the order of 10^5 m^3. However, there are two main parameters that regulate the heat transfer between the air and the cavern wall that play a big role. These are the enlargement factor A_{L} and the thickness of the wall Δr. Even though the thickness of the wall is important in order to regulate the energy transfer through the Biot-number Bi^+ (see Appendix B), the enlargement factor plays a more relevant role since it multiplies the term related to the energy losses of the cavern (see Eq. (2.19)). Thus, a variation of these parameters regulates the energy losses encountered inside the cavern.

Several modifications can be done to our AA-CAES model to make it closer to reality, but this would also increase its complexity which is not necessarily the best for the objective of this thesis. Further steps include a more sophisticated model of the cavern, where the heat equation is not simplified to one dimension but considers all three dimensions. Another improvement can take place in the expansion and compression trains, where better turbines and compressors can be implemented to calculate the thermodynamic properties of air. This is also true for the heat exchangers, where a 70 % efficiency was considered, making omission of the complex physics involved in the flux of the HTF inside them.

With respect to the optimization strategy, the main goal was to show how an AA-CAES plant can maximize its revenue from price arbitrage while minimizing ocurring idle losses.

Following Sections 4.1 and 4.2, the optimization results show that Yalmip can yield an operation strategy that follows the given price profiles when a state-space representation of a discrete-time LTI system is used to predict future states of the plants. The results for the PWA systems were not as encouraging as the previous ones but another MPC scheme or even another optimization method could be implemented in the future for the inclusion of these linear models.

It is important to discuss the fact that in the present power market regimes electricity prices are not known in advance. In this case we assumed a scenario with perfect information, where the electricity prices are known for every hour of the day allowing the MPC controller to make forecasts of the state of the plant regardless of the prediction horizon. The calculated optimization strategies can work as a benchmark to show how an AA-CAES plant would work for varying electricity prices. As a further step, a forecasting model for electricity prices can be used to calculate the optimal operation strategy for the forthcoming hours. In this case, the operator of the plant would know how much energy can be withdrawn for each hour of the day,

at the same time that the revenue is maximized.

Another assumption made with respect to the prices has to do with the fact that the capacity of the plant is too small as to affect future market prices. This assumption is valid in case this plant would be considered as a part of the European power exchange market, since its nominal output power (85 MW) is very small compared to the whole electricity generation sector of this market. This assumption would change whenever bigger systems are considered, but for the moment this is not the horizon of the industry.

It is important to remember that for the calculation of the operation strategies, the non-linear model of the AA-CAES was an input for the MPC scheme. This provided the controller with a reference trajectory at each time step, which helped for the linear model calibration. In other words, the controller improved its prediction of the future states by comparing between its output and the reference trajectory. This can justify the use of a single model into the MPC controller instead of three, since in case the model used is not the appropriate for the operation state, this can be corrected by the controller itself. This is a good alternative for the optimization of this plant without losing valuable information.

Fostering the implementation of large-scale storage systems such as AA-CAES systems to cope with RES intermittency is crucial for the future of the electric power systems. In addition, AA-CAES is a technology that can provide additional electricity storage capacity in places where other technologies cannot be implemented.

This thesis achieves to present a general model where the main dynamics of these systems are considered without losing any information on the inflicted energy losses. At the same time, an operation strategy is provided as a benchmark to manage these systems in case they are integrated into the present electricity markets. The results presented in this work are far from offering the best and only solution for the problems related to the AA-CAES modeling or its optimal control. However, they present a first simplified model tailored for power system generation studies.

Appendix A

Air temperature

The air temperature inside the cavern varies due to the change of the air pressure and the heat flux through the wall [72]. Hence, the change over time of the air temperature is given by:

$$\frac{dT_{\mathrm{sc,a}}}{dt} = \left(\frac{dT_{\mathrm{sc,a}}}{dt}\right)_{\mathrm{adiabatic}} + \left(\frac{dT_{\mathrm{sc,a}}}{dt}\right)_{\mathrm{isobaric}}. \tag{A.1}$$

The adiabatic term of the previous equation can be obtained using the adiabatic relation between pressure and volume of a gas (2.2), together with the ideal gas law (2.4). Combining these last two equations we get

$$\frac{T^{\frac{k}{k-1}}}{p} = constant, \tag{A.2}$$

where $k = 1.4$ is the ratio of the specific heat capacities for an ideal diatomic gas. Derivation (A.2) over time gives

$$\frac{dT}{dt} = \frac{T}{p}\left(1 - \frac{1}{k}\right)\frac{dp}{dt}, \tag{A.3}$$

where the pressure's derivative with respect to time is unknown. Following the ideal gas relation (2.4) once again, and remembering that the volume of the cavern is constant over time, we can obtain this derivative as follows

$$\frac{dp}{dt} = \frac{d}{dt}\left(\frac{mRT}{V}\right) = \frac{R}{V}\frac{d}{dt}\left(mT\right) = \frac{R}{V}\left(\dot{m}_{in}T_{in} - \dot{m}_{\mathrm{out}}T_{\mathrm{out}}\right). \tag{A.4}$$

Substituting Equation (A.4) in Equation (A.3) and doing some algebra we get

$$\left(\frac{dT_{\mathrm{sc,a}}}{dt}\right)_{\mathrm{adiabatic}} = \frac{1}{m_{\mathrm{sc,a}}}\left(1 - \frac{1}{k}\right)\left(\dot{m}^{\mathrm{in}}_{\mathrm{sc,a}}T^{\mathrm{in}}_{\mathrm{sc,a}} - \dot{m}^{\mathrm{out}}_{\mathrm{sc,a}}T^{\mathrm{out}}_{\mathrm{sc,a}}\right). \tag{A.5}$$

The second term of Equation (A.1) is a result of applying the heat balance of the air [72]. This isobaric term is given by

$$\left(\frac{dT_{\mathrm{sc,a}}}{dt}\right)_{\mathrm{isobaric}} = \frac{\dot{q}_{\mathrm{a,w}} A_{\mathrm{w}}}{\rho_{\mathrm{a}} c_{\mathrm{p,a}} V_{\mathrm{sc}}} = \frac{\alpha_{\mathrm{a,w}} A_{\mathrm{w}} (T_{\mathrm{w}} - T_{\mathrm{a}})}{m_{\mathrm{sc,a}} c_{\mathrm{p,a}}}, \tag{A.6}$$

where $\dot{q}_{\mathrm{a,w}}$ is the heat flux from the air to the cavern, A_{w} is the cavern surface in contact with the stored air and T_{w} is the cavern wall temperature.

Adding Equations (A.5) and (A.6) we get

$$\frac{dT_{\mathrm{sc,a}}}{dt} = \frac{1}{m_{\mathrm{sc,a}}} \left(1 - \frac{1}{k}\right) \left(\dot{m}^{\mathrm{in}}_{\mathrm{sc,a}} T^{\mathrm{in}}_{\mathrm{sc,a}} - \dot{m}^{\mathrm{out}}_{\mathrm{sc,a}} T^{\mathrm{out}}_{\mathrm{sc,a}}\right) + \frac{\alpha_{\mathrm{a,w}} A_{\mathrm{w}} (T_{\mathrm{w}} - T_{\mathrm{sc,a}})}{m_{\mathrm{sc,a}} c_{\mathrm{p,a}}}.$$

Appendix B

Cavern temperature

The one dimensional Fourier's equation in cylindrical coordinates is the following:

$$\frac{\partial T_{\mathrm{rs}}}{\partial t} = r_{\mathrm{rs}} \left(\frac{\partial^2 T_{\mathrm{rs}}}{\partial r^2} + \frac{1}{r} \frac{\partial T_{\mathrm{rs}}}{\partial r} \right), \tag{B.1}$$

which can be discretised via the finite difference method. The main idea of this method is to replace continuous derivatives from a function $f(x)$, with difference formulas that involve solely the discrete values of this function.

For a discrete domain $[x_0, ..., x_i, ..., x_N]$ of a function $f(x)$, a Taylor series expansion of $f(x)$ around the point x_i is given by

$$f(x_i + \Delta x) = f(x_i) + \Delta x \frac{\partial f(x)}{\partial x}\bigg|_{x_i} + \frac{(\Delta x)^2}{2} \frac{\partial^2 f(x)}{\partial x^2}\bigg|_{x_i} + \frac{(\Delta x)^3}{3!} \frac{\partial^3 f(x)}{\partial x^3}\bigg|_{x_i} + \cdots \tag{B.2}$$

$$f(x_i - \Delta x) = f(x_i) - \Delta x \frac{\partial f(x)}{\partial x}\bigg|_{x_i} + \frac{(\Delta x)^2}{2} \frac{\partial^2 f(x)}{\partial x^2}\bigg|_{x_i} - \frac{(\Delta x)^3}{3!} \frac{\partial^3 f(x)}{\partial x^3}\bigg|_{x_i} + \cdots \tag{B.3}$$

where Δx is a change in x relative to x_i. To simplify the notation, $f(x_i + \Delta x) = f_{i+1}$, $f(x_i - \Delta x) = f_{i-1}$ and $f(x_i) = f_i$.

Subtracting Equation (B.3) from Equation (B.2) yields

$$f_{i+1} - f_{i-1} = 2\Delta x \frac{\partial f(x)}{\partial x}\bigg|_{x_i} + \frac{2\,(\Delta x)^3}{3!} \frac{\partial^3 f(x)}{\partial x^3}\bigg|_{x_i} + \cdots \tag{B.4}$$

Solving for the first derivative of $f(x)$ with respect to x, evaluated at x_i gives

$$\left.\frac{\partial f(x)}{\partial x}\right|_{x_i} = \frac{f_{i+1} - f_{i-1}}{2\Delta x} + \mathcal{O}(\Delta x^2), \tag{B.5}$$

where $\mathcal{O}(\Delta x^2)$ is the truncation error of the Taylor series. This last equation is the so-called central difference approximation of a first-order continuous derivative.

Adding Equations B.2 and (B.3) yields

$$f_{i+1} + f_{i-1} = 2f_i + (\Delta x)^2 \left.\frac{\partial^2 f(x)}{\partial x^2}\right|_{x_i} + \cdots \tag{B.6}$$

Solving for the second derivative of $f(x)$ gives

$$\left.\frac{\partial^2 f(x)}{\partial x^2}\right|_{x_i} = \frac{f_{i+1} - 2f_i + f_{i-1}}{(\Delta x)^2} + \mathcal{O}(\Delta x^2), \tag{B.7}$$

which is the central difference approximation of a second-order continuous derivative.

The space discretisation of Equation (B.1) results from applying Equations (B.5) and (B.7), and dropping the truncation errors:

$$\left.\frac{\partial T_{\mathrm{rs}}}{\partial t}\right|_{r_i} = r_{\mathrm{rs}} \left[\frac{T_{i+1} - 2T_i + T_{i-1}}{(\Delta r)^2} + \frac{1}{r_i}\left(\frac{T_{i+1} - T_{i-1}}{2\Delta r}\right)\right]. \tag{B.8}$$

After some algebra, the later equation can be re-arranged into the following one

$$\left.\frac{\partial T_{\mathrm{rs}}}{\partial t}\right|_{r_i} = \widehat{r_{\mathrm{rs}}} \left[T_{i+1}(g_i + 1) + T_{i-1}(1 - g_i) - 2T_i\right], \tag{B.9}$$

where $\widehat{r_{\mathrm{rs}}} = r_{\mathrm{rs}}/(\Delta r)^2$ and $g_i = \Delta r/2r_i$. Equation (B.9) has a discrete spatial domain $[r_1, ..., r_i, ..., r_{N_C}]$, where $N_C \in \mathbb{N}$.

Figure B.1 shows the discretisation of the salt-cavern together with its boundary conditions. Following Equation (B.9), for $i = 1$ and $i = N_C$ we get:

$$\left.\frac{\partial T_{\mathrm{rs}}}{\partial t}\right|_{r_1} = \widehat{r_{\mathrm{rs}}} \left[T_2(g_1 + 1) + T_0(1 - g_1) - 2T_1\right], \tag{B.10}$$

$$\left.\frac{\partial T_{\mathrm{rs}}}{\partial t}\right|_{r_{N_C}} = \widehat{r_{\mathrm{rs}}} \left[T_{N_C+1}(g_{N_C} + 1) + T_{N_C-1}(1 - g_{N_C}) - 2T_{N_C}\right], \tag{B.11}$$

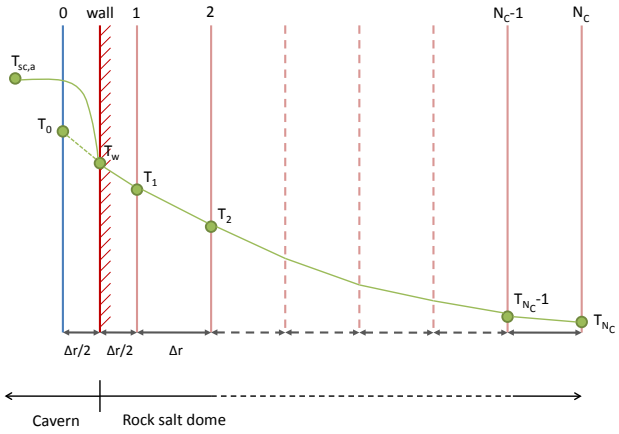

Figure B.1: Cavern's wall discretisation [36].

where T_0 and T_{N_C+1} are the temperatures of the boundary conditions. The calculation of these values is discussed below.

The matricial form of Equation (B.9) is:

$$\frac{d\mathbf{T}}{dt} = r_{\mathrm{rs}} \left[\mathbf{M} \cdot \mathbf{T} + \mathbf{P}\right], \tag{B.12}$$

where $\mathbf{T}$ and $\mathbf{P}$ are column vectors with N_C entries and $\mathbf{M}$ is a matrix with $[N_C \times N_C]$ entries. The column vector $\mathbf{T}$ represents the temperature of the cavern wall within the discrete domain at a certain point in time:

$$\mathbf{T} = \begin{pmatrix} \mathrm{T}(\mathrm{r}_1, \mathrm{t}) \\ \vdots \\ \mathrm{T}(\mathrm{r}_\mathrm{i}, \mathrm{t}) \\ \vdots \\ \mathrm{T}(\mathrm{r}_{\mathrm{N_C}}, \mathrm{t}) \end{pmatrix} = \begin{pmatrix} \mathrm{T}_1(\mathrm{t}) \\ \vdots \\ \mathrm{T}_\mathrm{i}(\mathrm{t}) \\ \vdots \\ \mathrm{T}_{\mathrm{N_C}}(\mathrm{t}) \end{pmatrix} \tag{B.13}$$

The matrix $\mathbf{A}$ represents the coefficients of each temperature in Equation (B.9) and it is given by

$$\mathbf{M} = \begin{pmatrix} -2 & g_1+1 & 0 & 0 & \cdots & 0 & 0 & 0 \\ 1-g_2 & -2 & g_2+1 & 0 & \cdots & 0 & 0 & 0 \\ 0 & 1-g_3 & -2 & g_3+1 & \cdots & 0 & 0 & 0 \\ \vdots & \vdots & \vdots & \vdots & \vdots & \vdots & \vdots & \vdots \\ 0 & 0 & 0 & 0 & \cdots & -2 & g_{N_C-2}+1 & 0 \\ 0 & 0 & 0 & 0 & \cdots & 1-g_{N_C-1} & -2 & g_{N_C-1}+1 \\ 0 & 0 & 0 & 0 & \cdots & 0 & 1-g_{N_C} & -2 \end{pmatrix}. \tag{B.14}$$

As for the column vector $\mathbf{P}$, it represents the boundary conditions for the cavern wall. On the left side of the wall, the air temperature is known and the heat is transferred between the air and the rock. On the right side of the wall, the temperature $T(r_{N_C+1}, t) = T_{\text{ambient}} = 293\,K$, assuming that the temperature at the end of the spatial domain will be equal to the ambient temperature of the wall. This column vector has the form:

$$\mathbf{P} = \begin{pmatrix} \Theta_1 \\ 0 \\ \vdots \\ 0 \\ \Theta_2 \end{pmatrix}, \tag{B.15}$$

where Θ_1 determines the boundary conditions for the air-sided wall, and Θ_2 provides the boundary conditions at the right side of the wall. For the later one we are assuming that the rock will be at its ambient temperature at the end of the spatial domain no matter what the temperature inside the cavern would be, hence $\Theta_2 = T_{\text{ambient}}(1 + g_{N_C})$.

The following boundary condition is applied for the transition between air and rock [36, 73]:

$$T_{\text{sc,a},k} Bi^+ = T_{0,k}\left(\frac{Bi^+}{2} + 1\right) + T_{1,k}\left(\frac{Bi^+}{2} - 1\right) \tag{B.16}$$

Where the sub-index k indicates that the temperatures are measured at the same time. The temperature $T_{\text{sc,a},k}$ is the temperature of the air inside the cavern at time k. The Biot-number Bi^+ is the ratio between the heat conduction inside the wall to the transfer coefficient at the surface. This later one is calculated as follows

$$Bi^+ = \frac{\alpha_{\text{a,w}} \Delta r}{r_{\text{rs}}}, \tag{B.17}$$

where $\alpha_{\text{a,w}}$ is the heat transfer coefficient from the air to the cavern wall, Δr is a change in space along the cavern wall, and r_{rs} is the thermal conductivity of the rock-salt.

Solving Equation (B.16) for $T_{\mathrm{sc,a},k}$ and subtracting $T_{1,k}$ yields

$$T_{\mathrm{sc,a},k} - T_{1,k} = (T_{0,k} - T_{1,k}) \left(\frac{1}{Bi^{+}} + \frac{1}{2} \right), \tag{B.18}$$

which solving for $T_{0,k}$ gives

$$T_0 = T_{0,k} = \frac{T_{\mathrm{sc,a},k}}{(\frac{1}{Bi^{+}} + \frac{1}{2})} + T_{1,k} \left(1 - \frac{1}{(\frac{1}{Bi^{+}} + \frac{1}{2})} \right). \tag{B.19}$$

Substituting Equation (B.19) into Equation (B.10) and re-arranging the terms we get

$$\left. \frac{\partial T_{\mathrm{rs}}}{\partial t} \right|_{r_1} = \widehat{r_{\mathrm{rs}}} \left[T_2(g_1 + 1) + T_{\mathrm{sc,a}} \frac{(1 - g_1)}{(\frac{1}{Bi^{+}} + \frac{1}{2})} + T_1 \left(-2 + (1 - g_1) \left(1 - \frac{1}{(\frac{1}{Bi^{+}} + \frac{1}{2})} \right) \right) \right], \tag{B.20}$$

where the temperature of the air inside the cavern ($T_{\mathrm{sc,a}}$) is unknown in every time step of the simulation.

Following the coefficients of Equation (B.20), Θ_1 in vector $\mathbf{P}$ is given by $T_{\mathrm{sc,a}}$'s coefficient, while the factor multiplying T_1 is the new entry $\mathbf{M}_{1,1}$ of the matrix $\mathbf{M}$. Thereby the vector $\mathbf{P}$ is given by:

$$\mathbf{P} = \begin{pmatrix} \mathrm{T_{sc,a}} \dfrac{(1 - \mathrm{g_1})}{(\dfrac{1}{\mathrm{Bi^{+}}} + \dfrac{1}{2})} \\ 0 \\ \vdots \\ 0 \\ T_{\mathrm{ambient}}(1 + g_{N_C}) \end{pmatrix}. \tag{B.21}$$

However, the solution of Equation (B.12) will provide a temperature profile that starts with T_1, while Equation (2.19) requires the temperature of the wall T_{w}.

The temperature of the wall is calculated by the arithmetic mean of the temperatures T_1 and T_0 [73], as follows

$$T_{\mathrm{w}} = \frac{T_1 + T_0}{2}. \tag{B.22}$$

Substituting Equation (B.19) into Equation (B.22) we get

$$T_{\mathrm{w}} = \frac{T_{\mathrm{sc,a}}}{2 \left(\frac{1}{Bi^{+}} + \frac{1}{2} \right)} + T_1 \left(1 - \frac{1}{2 \left(\frac{1}{Bi^{+}} + \frac{1}{2} \right)} \right), \tag{B.23}$$

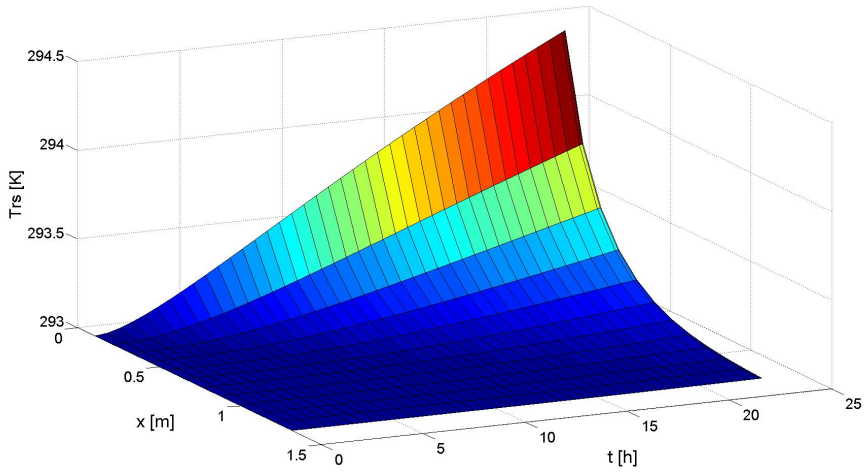

Figure B.2: Evolution over time of the rock-salt's temperature profile surrounding the cavern during compression.

which is an expression to obtain the temperature of the wall in each time step of the simulation.

The profile of the cavern wall obtained through solving equation (B.12) is shown in Figures B.2 and B.3 for compression and expansion states, respectively.

The temperature of the wall after compression, expansion and idle is shown in Figure B.4 at the top, middle and bottom, respectively.

The curve shown in Figure B.4 (middle), has a smaller slope at the beginning of the expansion stage compared to the final slope. This is explained by the fact that at the initial state, the air temperature inside the cavern has a higher temperature than that of the cavern wall.

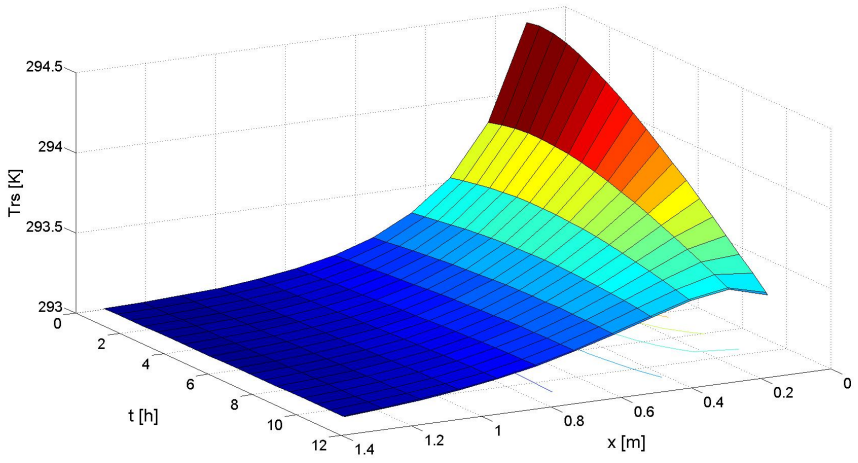

Figure B.3: Evolution over time of the rock-salt's temperature profile surrounding the cavern during expansion.

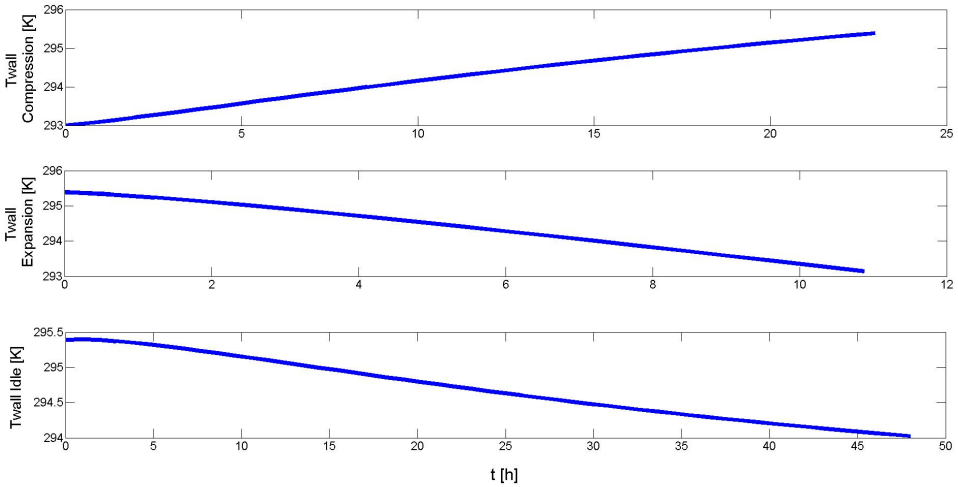

Figure B.4: Evolution over time of the cavern wall during compression (top), expansion (middle) and idle states (bottom).

Appendix C

Simulink Diagrams

This appendix shows the diagrams of the AA-CAES model and its main components in MATLAB's Simulink.

Figure C.1 shows the main structure of the model, where compression and expansion blocks include the compression and expansion trains together with its heat exchangers. The valve block regulates the mass flows of air for the compressor block ($\dot{m}_{\mathrm{sc,a}}$), and the expansion block ($\dot{m}_{\mathrm{e,a}}$), depending on the air pressure inside the cavern. If this pressure is higher than 65 bar or lower than 46 bar then both mass flows become zero.

Figure C.2 has two circular addition blocks that receive outputs from the heat exchangers and the compressors. The circular addition block at the top calculates the total mass flow of the heat transfer fluid that goes through the heat exchangers, while the one at the bottom calculates the total electrical power consumed by the compressor train.

Figure C.3 presents the same structure as the compression block (Fig. C.2), but in this case only two heat exchangers are present together with the high (HPT) and low pressure (LPT) turbines. The inputs of this block, as shown in Figure C.1, come from the TES, the cavern and the valve blocks.

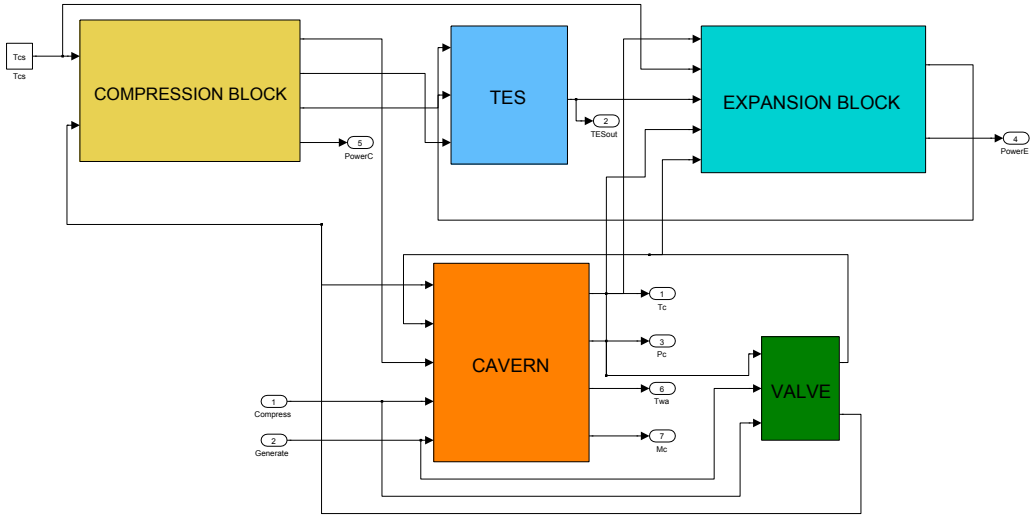

Figure C.1: Main diagram of the AA-CAES model, TES: Thermal Energy Storage.

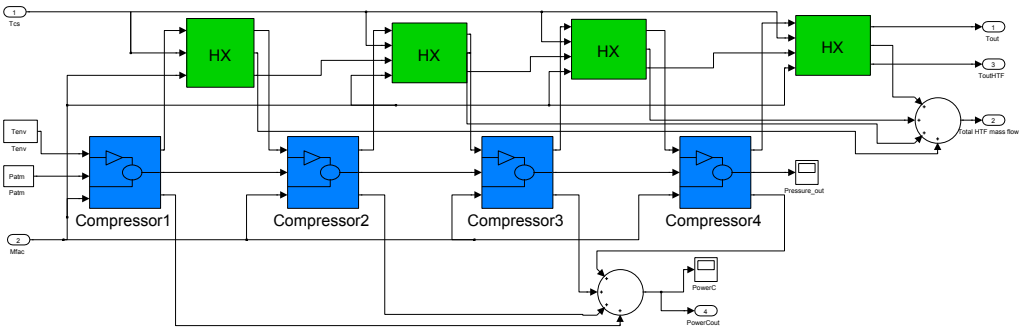

Figure C.2: Diagram of the compression train together with the heat exchangers (HX).

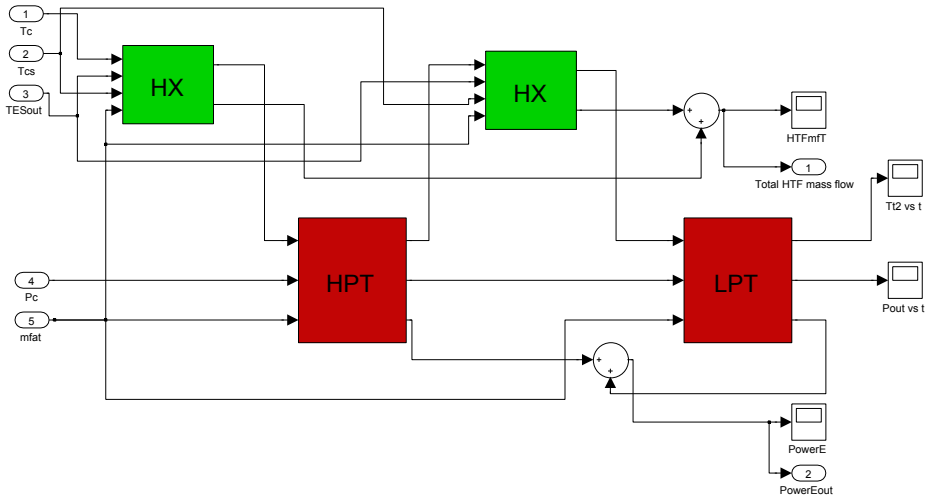

Figure C.3: Diagram of the expansion train together with the heat exchangers (HX). HPT: High Pressure Turbine, LPT: Low Pressure Turbine.

Appendix D

Source code

The codes we used to calculate the main results of this work are presented in this Appendix. Since the main platform used to program was MATLAB, all the following codes have the same syntax. As a remark, it is important to remember that within this syntax the symbol % at the beginning of a line indicates that this is a commented line. These codes are here as a guideline to see how the AA-CAES model was implemented. However, in case the reader wants to reproduce the results presented in this thesis, it is better to use the CD that contains all the information needed for these codes to run.

Charge-Discharge Code

Contents

- Main parameters
- Constants
- Compressor values
- Heat Exchanger values
- Cavern
- Thermal Energy Storage made of concrete (TES)
- Turbine
- Calculation of Cavern wall temperature
- Running the simulation
- Managing the plant

This program charges and discharges the plant completely to see how it performs for a complete cycle.

```
clear all
close all
warning off;
```

```
Nfor=100; % Maximum number of hours that the plant will be idle
Nstep=1; % Increase on the idle time after each step of the for loop

for ifor=1:Nfor
```

Main parameters

```
Pmax = 65; % Maximum allowed  pressure in the cavern [bar]
Pmin = 46;  % Minimum allowed  pressure in the cavern [bar]
massflowratio = 2;
% Mass flow of the turbine / Mass flow of the compressor
Tchargeh=85; % Time  the compressor will be on [h]
Tdischargeh=85; % Time  the turbine will be on [h]
Tidleh1=0.5; % Time the  plant will be idle [h]
```

Constants

```
Tenv=293;
% Ambient temperature [K]
Tcs=293; % Temperature of the cold storage [K]
Patm=1.013*10^5;
% Atmospheric pressure [Pa]
Ra = 286.7;
% Gas constant [J/(kg*K)]
cva=Ra*(5/2); % Cv of air for a  diatomic gas []
cpa=cva+Ra; % Cp of air for a  diatomic gas []
k=cpa/cva; % Cp/Cv for air as an ideal diatomic gas []
lambda=(k-1)/k;
```

Compressor values

```
mfac=120; % Massflow from air [kg/s]
polyc=1.6; % Polytropic exponent for compression
lambdac=(polyc-1)/polyc;
etac=0.88; % Compressor efficiency
EnergyC0=0; % Initial energy consu med by the compressor [J]
betac1=3.8; % p_n/p_0 Compression ratio of compressor one
betac2=2.6; % p_n/p_0 Compression ratio of compressor two
betac3=2.4; % p_n/p_0 Compression ratio of compressor three
betac4=Pmax/(betac1*betac2*betac3);
% p_n/p_0 Compression ratio of compressor four
betac=betac1*betac2*betac3*betac4;
```

Heat Exchanger values

```
effhxc=0.7; % Heat exchanger efficiency
cph2o=4181.3; % Specific heat for water at constant -
% pressure [J/(kg*K)]

% Heat transfer fluid (HTF). Liquid sodium was chosen as HTF
% because of its high temperature range (100C-760C)

cp_HTF=1260;
% Specific heat capacity at constant pressure [J/(kg*K)]
rho_HTF=570;
% Density of the heat transfer fluid [kg/m^3]
```

Cavern

```
Vc = 560000;
% Cavern volume [m^3] (McIntosh size)
Hc=200;
% Height of the cavern [m]
Ac=Vc/Hc;
% Cross-section area of the cavern [m^2]
dc=(4*Ac/pi)^(1/2);
% Diameter of the cavern [m]

Ae=1.8; % Enlargement factor []
Twa0 = Tenv;
% Temperature of the air sided wall at  time 0 [K]
Ta0 = Tenv;
% Temperature of the air at time 0 [K]
Pa0 = 46*10^5;
% Initial pressure of the air in the cavern [Pa]
Minitial = Pa0*Vc/(Ra*Ta0);
% Minimum mass in the cavern [kg]
Aaw=(pi*dc*Hc+2*Ac)*Ae;
% Area of contact between air and -
% cavern [m^2]

l = 5;
% Conductivity of the rock-salt [W/(m*K)]
rho = 2100; % Densitiy of the rock-salt  [kg/m^3]
crs = 920; % Specific heat capacity of the rock-salt [J/(kg*K)]
Long = 1.25;
% Deepness of the cavern to explore [m]
```

```
dwall = 1; % Thickness of the cavern's wall through which -
% air will transfer heat [m]
alaw = 1/dwall; % heat transfer coefficient fluid-cavern-
%  [W/(K*m^2)]
```

Thermal Energy Storage made of concrete (TES)

```
Ssc_TES=0.66;
% Specific storage capacity of the TES [kWh/(m^3*K)]
rho_TES=2750;
% Density of concrete [kg/m^3]
cp_TES=916;
% Specific Heat capacity of the TES (concrete) [J/(Kg*K)]
TES0=294;
% Starting temperature for the TES [K]
Tin_TES=Tenv;
% Inlet temperature for the TES [K]
Tout_TES=TES0;
% Outlet temperature of the TES [K]
deltaT_TESmin=Tout_TES-Tin_TES;
% Difference between inlet and outlet temperatures from the
%  expansion side [K]
h_TES=40; % Height of the TES [m]
r_TES=22/2; % Radius of the TES [m]
V_TES=h_TES*pi*r_TES^2; % Volume of the TES [m^3]
Energy_TESmin=V_TES*Ssc_TES*deltaT_TESmin/1000;
% Maximum amount of thermal energy that will be stored in -
% the TES [MWh]
m_TES=Energy_TESmin*10^6*3600/(cp_TES*deltaT_TESmin);
% Mas of the TES [kg]
Rconcrete=1;
% Thermal conductivity of the concrete [W/(m*K)]
Rwool=0.055;
% Thermal resistance of Glass-wool [W/(m*K)]
dconcrete=1;
% Thickness of the outer concrete wall [m]
dwool=0.10;
% Thickness of the insulation layer for the TES [m]
U_TES=(Rconcrete*Rwool)/(dconcrete*Rwool+dwool*Rconcrete);
% Overall heat transfer coefficient (out) [W/(m^2*K)]
A_TES=2*r_TES*pi*h_TES+pi*r_TES^2;
% Area of the TES exposed to the environment [m^2]
Ar=1.5; % Conversion factor for the heat exchanger inside -
% the TES []
```

```
dinnerconcrete=0.005; % Wall of the inner heat exchanger [m]
U1_TES=Rconcrete/dinnerconcrete;
% Overall heat transfer coefficient (in) [W/(m^2*K)]
```

Turbine

```
mfat=massflowratio*mfac; % Turbine mass flow [kg/s]
polyt=1.1; % Polytropic expansion coefficient []
lambdat=(polyt-1)/polyt;
EnergyE0=0; % Initial energy produced by the turbine [J]

% High Pressure Turbine (HPT)

betaHPT=2.5; % Expansion ratio of the turbines []
etaHPT=0.79; % Efficiency gas turbine []
PopHPT=43;
% Operational pressure so the turbine can start [bar]

% Low Pressure Turbine (LPT)

betaLPT=Pmin/betaHPT;
% Expansion ratio of the turbines []
etaLPT=0.82;
% Efficiency gas turbine []
PopLPT=15;
% Operational pressure so the turbine can start [bar]

betat=betaHPT*betaLPT;
etat=etaHPT*etaLPT;
```

Calculation of Cavern wall temperature

```
dx=0.11;
x=dx:dx:Long+dx;
N=length(x);

% define the ratio r (Fourier's number)
r = l/(rho*crs)/dx/dx;


% define the ratio g (dimensionless location)
for i=1:N

    g(i) = dx/(2*x(i));
```

```
end

% define the Biot number (left)
Bi = alaw/l*dx;

% Matrix A is a tridiagonal matrix that is obtained through -
% the differential equation:
% dT/dt=r*[T(i+1,m)*(g+1)+T(i-1,m)*(1-g)-2*T(i,m)]

Diagup=zeros(N-1,N-1);
Diagdown=zeros(N-1,N-1);

for i=1:N-1

    Diagup(i,i)=(g(i)+1);
    Diagdown(i,i)=(1-g(i+1));

end


A=[-2*eye(N) + [zeros(N-1,1),Diagup;
zeros(1,N)] + [zeros(N-1,1),Diagdown;
zeros(1,N)]'];

A(1,1) = -2+(1-g(1))*(1-1/(1/Bi+1/2));

% Vector P is the vector that is added to consider the boundary-
% conditions. Since this vector has the value of the wall tempe-
% rature at the beginning and the value of the rock-salt at the -
% end, then we are decomposing it in two vectors P=P1+P2

Twinf=Tenv;

P1=[(1-g(1))/(1/Bi+1/2);zeros(N-1,1)];
P2=[zeros(N-1,1);1+g(N)];

% uinitial is the initial value for the temperature of the wall.
% When the cavern is empty this value is set as the ambient -
% temperature (Tamb).

uinitial=[Twa0*ones(N,1)];
Aux=[1;zeros(N-1,1)]';
```

Running the simulation

```
Generate=0; % 1 When the plant generates electrity, 0 when it's not
Compress=1; % 1 When the plant is compressing air, 0 when it's not
Tcharge=Tchargeh*3600; % Charging time [s]
sim('simCAESlinmod_regP_noE',Tcharge,[],[]) % Loading Simulink Simulation
```

Managing the plant

```
LPc1=length(Pc);
ltout=length(tout);

PowerC1=PowerC;
PowerAC=PowerC1(1,2);

Ta0=Tc(LPc1,2);
TES0=TESout(LPc1,2);
Pa0=Pc(LPc1,2);

Twa0=Twa(ltout,2);
Minitial=Mc(LPc1,2);
Twacompress=Twa(:,2);

uinitial=xout(ltout,4:N+3)';
Twinf=xout(ltout,N+3);


% Calculating the power consumed

Compress=0;
Generate=1;

% Tidle=Tidleh1*3600;
Tdischarge=Tdischargeh*3600; % Discharge time [s]

sim('simCAESlinmod_regP_noE',Tdischarge,[],[])
% Loading Simulink Simulation

LPc2=length(Pc);
PowerE1=PowerE;
PowerAE=PowerE1(1,2);

EfficiencyPA=PowerAE/PowerAC
% Calculation of the efficiency of the plant
```

Idle losses Code

Contents

This program calculates the idle losses for different idle times.

```
clear all
close all
warning off;

Nfor=100; % Maximum number of hours that the plant will be idle
Nstep=1; % Increase on the idle time after each step of the for loop

for ifor=1:Nfor
```

Main parameters

```
Pmax = 65; % Maximum allowed  pressure in the cavern [bar]
Pmin = 46;  % Minimum allowed  pressure in the cavern [bar]
massflowratio = 2;
% Mass flow of the turbine / Mass flow of the compressor
Tchargeh=85; % Time  the compressor will be on [h]
Tdischargeh=85; % Time  the turbine will be on [h]
Tidleh1=0.5; % Time the  plant will be idle [h]
```

Constants

```
Tenv=293;
% Ambient temperature [K]
Tcs=293; % Temperature of the cold storage [K]
Patm=1.013*10^5;
% Atmospheric pressure [Pa]
Ra = 286.7;
% Gas constant [J/(kg*K)]
cva=Ra*(5/2); % Cv of air for a  diatomic gas []
cpa=cva+Ra; % Cp of air for a  diatomic gas []
k=cpa/cva; % Cp/Cv for air as an ideal diatomic gas []
lambda=(k-1)/k;
```

Compressor values

```
mfac=120; % Massflow from air [kg/s]
polyc=1.6; % Polytropic exponent for compression
lambdac=(polyc-1)/polyc;
etac=0.88; % Compressor efficiency
EnergyC0=0; % Initial energy consu med by the compressor [J]
betac1=3.8; % p_n/p_0 Compression ratio of compressor one
betac2=2.6; % p_n/p_0 Compression ratio of compressor two
betac3=2.4; % p_n/p_0 Compression ratio of compressor three
betac4=Pmax/(betac1*betac2*betac3);
% p_n/p_0 Compression ratio of compressor four
betac=betac1*betac2*betac3*betac4;
```

Heat Exchanger values

```
effhxc=0.7; % Heat exchanger efficiency
cph2o=4181.3; % Specific heat for water at constant -
% pressure [J/(kg*K)]

% Heat transfer fluid (HTF). Liquid sodium was chosen as HTF
% because of its high temperature range (100C-760C)

cp_HTF=1260;
% Specific heat capacity at constant pressure [J/(kg*K)]
rho_HTF=570;
% Density of the heat transfer fluid [kg/m^3]
```

Cavern

```
Vc = 560000;
```

```
% Cavern volume [m^3] (McIntosh size)
Hc=200;
% Height of the cavern [m]
Ac=Vc/Hc;
% Cross-section area of the cavern [m^2]
dc=(4*Ac/pi)^(1/2);
% Diameter of the cavern [m]

Ae=1.8; % Enlargement factor []
Twa0 = Tenv;
% Temperature of the air sided wall at  time 0 [K]
Ta0 = Tenv;
% Temperature of the air at time 0 [K]
Pa0 = 46*10^5;
% Initial pressure of the air in the cavern [Pa]
Minitial = Pa0*Vc/(Ra*Ta0);
% Minimum mass in the cavern [kg]
Aaw=(pi*dc*Hc+2*Ac)*Ae;
% Area of contact between air and -
% cavern [m^2]

l = 5;
% Conductivity of the rock-salt [W/(m*K)]
rho = 2100; % Densitiy of the rock-salt  [kg/m^3]
crs = 920; % Specific heat capacity of the rock-salt [J/(kg*K)]
Long = 1.25;
% Deepness of the cavern to explore [m]
dwall = 1; % Thickness of the cavern's wall through which -
% air will transfer heat [m]
alaw = l/dwall; % heat transfer coefficient fluid-cavern-
%  [W/(K*m^2)]
```

Thermal Energy Storage made of concrete (TES)

```
Ssc_TES=0.66;
% Specific storage capacity of the TES [kWh/(m^3*K)]
rho_TES=2750;
% Density of concrete [kg/m^3]
cp_TES=916;
% Specific Heat capacity of the TES (concrete) [J/(Kg*K)]
TES0=294;
% Starting temperature for the TES [K]
Tin_TES=Tenv;
% Inlet temperature for the TES [K]
```

```
Tout_TES=TES0;
% Outlet temperature of the TES [K]
deltaT_TESmin=Tout_TES-Tin_TES;
% Difference between inlet and outlet temperatures from the
%  expansion side [K]
h_TES=40; % Height of the TES [m]
r_TES=22/2; % Radius of the TES [m]
V_TES=h_TES*pi*r_TES^2; % Volume of the TES [m^3]
Energy_TESmin=V_TES*Ssc_TES*deltaT_TESmin/1000;
% Maximum amount of thermal energy that will be stored in -
% the TES [MWh]
m_TES=Energy_TESmin*10^6*3600/(cp_TES*deltaT_TESmin);
% Mas of the TES [kg]
Rconcrete=1;
% Thermal conductivity of the concrete [W/(m*K)]
Rwool=0.055;
% Thermal resistance of Glass-wool [W/(m*K)]
dconcrete=1;
% Thickness of the outer concrete wall [m]
dwool=0.10;
% Thickness of the insulation layer for the TES [m]
U_TES=(Rconcrete*Rwool)/(dconcrete*Rwool+dwool*Rconcrete);
% Overall heat transfer coefficient (out) [W/(m^2*K)]
A_TES=2*r_TES*pi*h_TES+pi*r_TES^2;
% Area of the TES exposed to the environment [m^2]
Ar=1.5; % Conversion factor for the heat exchanger inside -
% the TES []
dinnerconcrete=0.005; % Wall of the inner heat exchanger [m]
U1_TES=Rconcrete/dinnerconcrete;
% Overall heat transfer coefficient (in) [W/(m^2*K)]
```

Turbine

```
mfat=massflowratio*mfac; % Turbine mass flow [kg/s]
polyt=1.1; % Polytropic expansion coefficient []
lambdat=(polyt-1)/polyt;
EnergyE0=0; % Initial energy produced by the turbine [J]

% High Pressure Turbine (HPT)

betaHPT=2.5; % Expansion ratio of the turbines []
etaHPT=0.79; % Efficiency gas turbine []
PopHPT=43;
% Operational pressure so the turbine can start [bar]
```

```
% Low Pressure Turbine (LPT)

betaLPT=Pmin/betaHPT;
% Expansion ratio of the turbines []
etaLPT=0.82;
% Efficiency gas turbine []
PopLPT=15;
% Operational pressure so the turbine can start [bar]

betat=betaHPT*betaLPT;
etat=etaHPT*etaLPT;
```

Calculation of Cavern wall temperature

```
dx=0.11;
x=dx:dx:Long+dx;
N=length(x);

% define the ratio r (Fourier's number)
r = l/(rho*crs)/dx/dx;


% define the ratio g (dimensionless location)
for i=1:N

    g(i) = dx/(2*x(i));

end

% define the Biot number (left)
Bi = alaw/l*dx;

% Matrix A is a tridiagonal matrix that is obtained through -
% the differential equation:
% dT/dt=r*[T(i+1,m)*(g+1)+T(i-1,m)*(1-g)-2*T(i,m)]

Diagup=zeros(N-1,N-1);
Diagdown=zeros(N-1,N-1);

for i=1:N-1

    Diagup(i,i)=(g(i)+1);
    Diagdown(i,i)=(1-g(i+1));
```

```
end


A=[-2*eye(N) + [zeros(N-1,1),Diagup;
zeros(1,N)] + [zeros(N-1,1),Diagdown;
zeros(1,N)]'];

A(1,1) = -2+(1-g(1))*(1-1/(1/Bi+1/2));

% Vector P is the vector that is added to consider the boundary-
% conditions. Since this vector has the value of the wall tempe-
% rature at the beginning and the value of the rock-salt at the -
% end, then we are decomposing it in two vectors P=P1+P2

Twinf=Tenv;

P1=[(1-g(1))/(1/Bi+1/2);zeros(N-1,1)];
P2=[zeros(N-1,1);1+g(N)];

% uinitial is the initial value for the temperature of the wall.
% When the cavern is empty this value is set as the ambient -
% temperature (Tamb).

uinitial=[Twa0*ones(N,1)];
Aux=[1;zeros(N-1,1)]';
```

Running the simulation

```
Generate=0;
% 1 When the plant is expanding air, 0 when it's not
Compress=1;
% 1 When the plant is compressing air, 0 when it's not

Tcharge=Tchargeh*3600; % Simulation time [s]
sim('simCAES_regP',Tcharge,[],[])
% Runnig the Simulink Simulation


LPc1c=length(Pc);

Pa0charge=Pc(LPc1c,2);
Ta0charge=Tc(LPc1c,2);
TES0charge=TESout(LPc1c,2);
```

```
Minitialcharge=Mc(LPc1c,2);
Twacompress=Twa(:,2);

ltoutc=length(tout);
uinitialcharge=xout(ltoutc,4:N+3)';
Twinfcharge=xout(ltoutc,N+3);
Twa0charge=Twa(ltoutc,2);

% Calculating the power consumed

EnergyC1=EnergyC;
EnergyAC=EnergyC1(LPc1c,2);

PowerC1=PowerC;
PowerAC=PowerC1(1,2);

EAC(ifor)=EnergyAC;
PAC(ifor)=PowerAC;
```

Managing the plant

```
% Expanding

Pa0=Pa0charge;
Ta0=Ta0charge;
TES0=TES0charge;
Minitial=Minitialcharge;

uinitial=uinitialcharge;
Twinf=Twinfcharge;
Twa0=Twa0charge;

Compress=0;
Generate=1;

Tdischarge=Tdischargeh*3600;

sim('simCAES_regP',Tdischarge,[],[])
% Loading Simulink Simulation

% Calculating the power consumed

LPc2=length(Pc);
```

```
EnergyE1=EnergyE;
EnergyAEd=EnergyE1(LPc2,2);

PowerE1=PowerE;
PowerAEd=PowerE1(1,2);


EAEd(ifor)=EnergyAEd;
PAEd(ifor)=PowerAEd;

EfficiencyAd=EnergyAEd/EnergyAC;
EfficiencyPAd=PowerAEd/PowerAC;

EforAd(ifor)=EfficiencyAd*100;
EforPAd(ifor)=EfficiencyPAd;
```

Idle

```
Pa0=Pa0charge;
Ta0=Ta0charge;
TES0=TES0charge;
Minitial=Minitialcharge;

uinitial=uinitialcharge;
Twinf=Twinfcharge;
Twa0=Twa0charge;

Generate=0;
% 1 When the plant expanding air, 0 when it's not
Compress=0;
% 1 When the plant is compressing air, 0 when it's not

Tidleh=Tidleh1+Nstep*(ifor-1);
Tidlefor(ifor)=Tidleh;
Tidle=Tidleh*3600;

sim('simCAES_regP',Tidle,[],[])
% Loading Simulink Simulation
```

Managing the plant after idle

```
LPci=length(Pc);

Pa0idle=Pc(LPci,2);
```

```
Ta0idle=Tc(LPci,2);
TES0idle=TESout(LPci,2);
Minitialidle=Mc(LPci,2);

ltouti=length(tout);
uinitialidle=xout(ltouti,4:N+3)';
Twinfidle=xout(ltouti,N+3);
Twa0idle=Twa(ltouti,2);
```

Expanding after Idle

```
Pa0=Pa0idle;
Ta0=Ta0idle;
TES0=TES0idle;
Minitial=Minitialidle;

uinitial=uinitialidle;
Twinf=Twinfidle;
Twa0=Twa0idle;

Generate=1;
% 1 When the plant is expanding air, 0 when it's not
Compress=0;
% 1 When the plant is compressing air, 0 when it's not

sim('simCAES_regP',Tdischarge,[],[])
% Loading Simulink Simulation

LPc3=length(Pc);
EnergyE2=EnergyE;
EnergyAEi=EnergyE2(LPc3,2);
PowerE2=PowerE;
PowerAEi=PowerE2(1,2);

EAEi(ifor)=EnergyAEi;
PAEi(ifor)=PowerAEi;

EfficiencyAi=EnergyAEi/EnergyAC;
EfficiencyPAi=PowerAEi/PowerAC;
EforAi(ifor)=EfficiencyAi*100;
EforPAi(ifor)=EfficiencyPAi;
EnergyLosses=(EnergyAEd-EnergyAEi);
EnergyLossesPower=(PowerAEd-PowerAEi);
```

```
EnergyLosses_MWh=EnergyLosses/3600/10^6;
% Energy losses after idle [MWh]
EnergyLosses_MW=EnergyLossesPower/10^6;
% Energy losses after idle [MW]

Losses=EnergyLosses/EnergyAEd*100;
LossesPower=EnergyLossesPower/PowerAEd*100;
Lossesfor(ifor)=Losses;
LossesforPower(ifor)=LossesPower;
LossesAbsMWH(ifor)=EnergyLosses_MWh;
LossesAbsMW(ifor)=EnergyLosses_MW;
LossesAbs(ifor)=EnergyLosses;
LossesAbsPower(ifor)=EnergyLossesPower;
LAP=cat(2,Tidlefor',LossesAbsPower');
LAE=cat(2,Tidlefor',LossesAbs');

end
```

Plotting

```
% Plotting a graph with the relative and absolute losses of
% the plant, together with the efficiency decrease for diffe-
% rent idle times.

figure

subplot(3,1,1)
plot (Tidlefor,LossesAbsMWH)
ylabel('Losses [MWh]')

subplot(3,1,2)
plot (Tidlefor,Lossesfor)
ylabel('Losses [%]')

subplot(3,1,3)
plot (Tidlefor,EforAi)
xlabel('Idle Time [h]')
ylabel('Efficiency [%]')
```

LTI Optimization Code

Contents

- Model data
- Yalmip
- Plot

This program calculates the optimal operation strategy of our AA-CAES model using Yalmip as a MPC controller. The linear model used in this case is a state-space representation of a linear time invariant (LTI) system.

```
yalmip('clear')
close all
clear all
```

Model data

```
load('v1prices') % Loading the electricity prices of 2007
load('ssc_regP_noE') % Loading compression's linear model
load('sse_regP_noE') % Loading expansion's linear model
load('ssi_regP_noE') % Loading idle's linear model

Ac_Tempc = ssc.a(1,:); Bc_Tempc = ssc.b(1,:);
Ae_Tempc = sse.a(1,:); Be_Tempc = sse.b(1,:);
Aid_Tempc = ssi.a(1,:); Bid_Tempc = ssi.b(1,:);

SOC0=0.5; % Initial state of charge of the plant []
Tcmax=22.97; % Maximum compression's time [h]
Ttmax=11.87; % Maximum turbine's time [h]

Tdischargeh=(1-SOC0)*Ttmax;

CAESmanagey_regP_noE; % Program that gives the initial conditions -
% of the plant when the initial SOC is given.

InitPc1 = PowerAC/10^6;
% Maximum energy output of the compressor in 1 hour [MWh]
InitPt = PowerAE/10^6;
% Maximum energy output of the turbine in 1 hour [MWh]

eta_plant=0.5722; % CAES plant's efficiency []
Pid=3.09; % Energy Idle losses in 1 hour [MWh]
InitPc=InitPc1-Pid;
```

```
% Compression power considering the energy losses during 1 hour [MWh]

% The sampling time is 1 hour

Ecost = (1/InitPt)*[-InitPc , InitPt , -Pid]; % Vector used to calculate -
% the amount of money lost or earned according to the operation strategy
Ecost1 = [-InitPc , InitPt , -Pid];

nx = 4; % Number of states
nu = 2; % Number of inputs
%ns = 3; % Number of plant states (compressing, expanding, idle)
```

Yalmip

```
PredH = 15; % Prediction Horizon
TSAM = 24; % Hours that will be explored
%Q1 = v1prices(25:25+PredH+TSAM);

Tcgraph=ones(TSAM,1); % Prelocating
TESgraph=ones(TSAM,1); % Prelocating
Pressgraph=ones(TSAM,1); % Prelocating

Q1 = cat(2,ones(1,3),ones(1,3)*10,ones(1,3)*16,ones(1,3)*10,ones(1,4),
ones(1,4)*16,ones(1,4)); % Doing a flat price profile
Q1 = cat(2, Q1, Q1, Q1, Q1, Q1, Q1, Q1, Q1);

MinQ = min(Q1); % Minimum price in the chosen price interval (Q1)
MaxQ = max(Q1); % Maximum price in the chosen price interval (Q1)
Q2 = (1/(MaxQ-MinQ)) * (Q1-MinQ);
% Normalization of the prices in the chosen price interval (Q1)

Revenue=0; % Initial Revenue

for counterP=1:TSAM

    Q = Q2(counterP:PredH+counterP-1); % The price interval will -
    % change for each i since we want to move our prediction horizon -
    % on every hour.

    udec = sdpvar(repmat(nu,1,PredH),ones(1,PredH));
    % Decision variable that gives the operation strategy of the CAES plant
    xdec = sdpvar(repmat(nx,1,PredH+1),ones(1,PredH+1));
    % Decision variable used as a constraint. It represents the SOC.
```

```
    constraints = [];
    objective = 0;


    for kPH = 1:PredH

wdec{kPH} = cat(1,udec{kPH},(1-udec{kPH}(1))*(1-udec{kPH}(2)));

udifference = ( udec{kPH}(1) - udec{kPH}(2) );

objective = objective + Q(kPH)*Ecost*wdec{kPH} ; % Cost function

constraints = [constraints, Tcmin+4 <= xdec{kPH+1}(1) <= Tcmax ,
TTESmin <= xdec{kPH+1}(2) <= TTESmax ,
3 <= (1/10^7)*xdec{kPH+1}(3) <= 4.1 ,
uinitmin <= xdec{kPH+1}(4) <= uinitmax ];

constraints = [constraints, xdec{kPH+1}(1) == Ac_Tempc*xdec{kPH}
+ Bc_Tempc*udec{kPH}];

constraints = [constraints, 0 <= udec{kPH} <= 1 ,
0 <= sum(udec{kPH}) <= 1, 0 <= wdec{kPH} <= 1,
udec{kPH}(1)*udec{kPH}(2) <= 1e-3];

    end

    controller = optimizer(constraints, -objective ,
    sdpsettings('verbose',1),xdec{1},udec{1});

    counterP
    Tcgraph(counterP) = x0(1)*Tcgraph(counterP);
    TESgraph(counterP) = x0(2)*TESgraph(counterP);
    Pressgraph(counterP) = Pc(LPc2,2)/10^5*Pressgraph(counterP);

    u1 = controller{x0};


    Compress = u1(1);
    Generate = u1(2);

% The Simulation cannot use very small numbers at inputs, so whenever -
% the controller gives very small numbers then Generate and Compress -
% become zero through the following if's
```

```
    if Compress < 0.09

        Compress = 0;

    end

    if Generate < 0.09

        Generate = 0;

    end

    Ta0 = xsim0(LPc2,1);
    TES0 = xsim0(LPc2,2);
    Minitial = xsim0(LPc2,3);
    uinitial = xsim0(LPc2,4);

   [Time0,xsim0,Ysim0] = sim('simCAESY_regP_noE',3600,[],[]);

    LPc2 = length(Time0);

    ut(counterP,1) = Compress;
    ut(counterP,2) = Generate;

    w1 = cat(1,u1,(1-u1(1))*(1-u1(2)));

    Revenue = Revenue + Ecost1*w1*Q2(counterP);

    Revgraph(counterP) = Revenue;

    x0(1) = xsim0(LPc2,1);
    x0(2) = xsim0(LPc2,2);
    x0(3) = xsim0(LPc2,3);
    x0(4) = xsim0(LPc2,4);

end

data=cat(2,[1:TSAM]',ut,Q2(1:TSAM)'*(MaxQ-MinQ) + MinQ, Tcgraph,
Pressgraph)
```

Plot

Plotting the price profile used for the optimization, the optimal operation strategy, and the revenue achievedthrough the time TSAM.

```
figure

subplot(3,1,1)
plot (1:TSAM, Q2(1:TSAM)'*(MaxQ-MinQ) + MinQ)
ylabel('[Euro/MW]')

subplot(3,1,2)
bar(1:TSAM,ut)
ylabel('Opt. St.')

subplot(3,1,3)
plot(1:TSAM, Revgraph)
xlabel('Time [h]')
ylabel('[Euro]')
```

PWA Optimization Code

Contents

- Model data
- Yalmip
- Plot

This program calculates the optimal operation strategy of our AA-CAES model using Yalmip as a MPC controller. The linear model used in this case is a state-space representation of a piece-wise affinities (PWA) system.

```
yalmip('clear')
close all
clear all
```

Model data

```
load('v1prices') % Loading the electricity prices of 2007
load('ssc_regP_noE') % Loading compression's linear model
load('sse_regP_noE') % Loading expansion's linear model
load('ssi_regP_noE') % Loading idle's linear model

Ac_Tempc = ssc.a(1,:); Bc_Tempc = ssc.b(1,:);
Ae_Tempc = sse.a(1,:); Be_Tempc = sse.b(1,:);
Aid_Tempc = ssi.a(1,:); Bid_Tempc = ssi.b(1,:);

SOC0=0.5; % Initial state of charge of the plant []
Tcmax=22.97; % Maximum compression's time [h]
Ttmax=11.87; % Maximum turbine's time [h]

Tdischargeh=(1-SOC0)*Ttmax;

CAESmanagey_regP_noE; % Program that gives the
% initial conditions of the plant when the initial SOC is given.

LinAc=ssc.a; LinBc=ssc.b; LinCc=ssc.c; LinDc=ssc.d;
LinAe=sse.a; LinBe=sse.b; LinCe=sse.c; LinDe=sse.d;
LinAid=ssi.a; LinBid=ssi.b; LinCid=ssi.c; LinDid=ssi.d;

InitPc1 = PowerAC/10^6;
% Maximum energy output of the compressor in 1 hour [MWh]
InitPt = PowerAE/10^6;
% Maximum energy output of the turbine in 1 hour [MWh]
```

```
eta_plant=0.5722; % CAES plant's efficiency []
Pid=3.09; % Energy Idle losses in 1 hour [MWh]
InitPc=InitPc1-Pid;
% Compression power considering the -
% energy losses during 1 hour [MWh]

% The sampling time is 1 hour

Ecost = (1/InitPt)*[-InitPc , InitPt , -Pid];
% Vector used to calculate the amount of money lost or earned -
% according to the operation strategy
Ecost1 = [-InitPc , InitPt , -Pid];

nx = 4; % Number of states
nu = 2; % Number of inputs
ns = 3; % Number of plant states (compressing, expanding, idle)
```

Yalmip

```
PredH = 15; % Prediction Horizon
TSAM = 24; % Hours that will be explored
% Q1 = v1prices(25:25+PredH+TSAM);

% Q1 is the vector that has the hourly prices

Tcgraph=ones(TSAM,1); % Prelocating
TESgraph=ones(TSAM,1); % Prelocating
Pressgraph=ones(TSAM,1); % Prelocating

Q1 = cat(2,ones(1,3),ones(1,3)*10,ones(1,3)*16,
ones(1,3)*10,ones(1,4),ones(1,4)*16,ones(1,4));
% Doing a flat price profile
Q1 = cat(2, Q1, Q1, Q1, Q1, Q1, Q1, Q1, Q1);

MinQ = min(Q1);
% Minimum price in the chosen price interval (Q1)
MaxQ = max(Q1);
% Maximum price in the chosen price interval (Q1)
Q2 = (1/(MaxQ-MinQ)) * (Q1-MinQ); % Normalization of the -
% prices in the chosen price interval (Q1)


Revenue=0; % Initial Revenue
```

```
for counterP=1:TSAM

    Q = Q2(counterP:PredH+counterP-1);
    % The price interval will change for each i since we want to
    % move our prediction horizon on every hour
    udec = sdpvar(repmat(nu,1,PredH),ones(1,PredH));
    % Decision variable that gives the operation strategy of the plant
    xdec = sdpvar(repmat(nx,1,PredH+1),ones(1,PredH+1));
    % Decision variable used as a constraint. It represents the SOC
    ddec = binvar(repmat(ns,1,PredH),ones(1,PredH));
    % Decision variable used to manage the linear models

    constraints = [];
    objective = 0;


    for kPH = 1:PredH

wdec{kPH} = cat(1,udec{kPH},(1-udec{kPH}(1))
*(1-udec{kPH}(2)));

udifference = ( udec{kPH}(1) - udec{kPH}(2) );

objective = objective + Q(kPH)*Ecost*wdec{kPH} ;
% Cost function

constraints = [constraints,
implies(ddec{kPH}(1),  xdec{kPH+1}(2) > xdec{kPH}(2)) ,
implies(ddec{kPH}(2),  xdec{kPH+1}(2) < xdec{kPH}(2)) ,
implies(ddec{kPH}(3),
 -0.1 <= ( xdec{kPH}(2) - xdec{kPH+1}(2) ) <= 0.1) ,
implies(ddec{kPH}(1), xdec{kPH+1}(1) ==
Ac_Tempc*xdec{kPH} + Bc_Tempc*udec{kPH}) ,
implies(ddec{kPH}(2), xdec{kPH+1}(1) ==
Ae_Tempc*xdec{kPH} + Be_Tempc*udec{kPH}) ,
implies(ddec{kPH}(3), xdec{kPH+1}(1) ==
Aid_Tempc*xdec{kPH} + Bid_Tempc*udec{kPH}) ];

constraints = [constraints, Tcmin+4 <=
xdec{kPH+1}(1) <= (Tcmax) ,
TTESmin <= xdec{kPH+1}(2) <= TTESmax ,
3 <= (1/10^7)*xdec{kPH+1}(3) <= 4.1 ];
```

```
constraints = [constraints, 0 <= udec{kPH} <= 1 ,
0 <= sum(udec{kPH}) <= 1, 0 <= wdec{kPH} <= 1];

constraints = [constraints , sum(ddec{kPH}) == 1];

    end

    controller = optimizer(constraints, -objective ,
    sdpsettings('verbose',1),xdec{1},udec{1});

    counterP
    Tcgraph(counterP) = x0(1)*Tcgraph(counterP);
    TESgraph(counterP) = x0(2)*TESgraph(counterP);
    Pressgraph(counterP) = Pc(LPc2,2)/10^5
    *Pressgraph(counterP);

    u1 = controller{x0};

    Compress = u1(1);
    Generate = u1(2);

% The Simulation cannot use very small numbers at inputs,
% so whenever the controller gives very small numbers then
% Generate and Compress become zero through the follo-
% wing if's

    if Compress < 0.09

        Compress = 0;

    end

    if Generate < 0.09

        Generate = 0;

    end

    Ta0 = xsim0(LPc2,1);
    TES0 = xsim0(LPc2,2);
    Minitial = xsim0(LPc2,3);
    uinitial = xsim0(LPc2,4);

    [Time0,xsim0,Ysim0] = sim('simCAESY_regP_noE',
```

```
    3600,[],[]);
    LPc2 = length(Time0);

    ut(counterP,1) = Compress;
    ut(counterP,2) = Generate;

    w1 = cat(1,u1,(1-u1(1))*(1-u1(2)));
    Revenue = Revenue + Ecost1*w1*Q2(counterP);
    Revgraph(counterP) = Revenue;

    x0(1) = xsim0(LPc2,1);
    x0(2) = xsim0(LPc2,2);
    x0(3) = xsim0(LPc2,3);
    x0(4) = xsim0(LPc2,4);

end

data=cat(2,[1:TSAM]',ut,Q2(1:TSAM)'*(MaxQ-MinQ)+ MinQ,
Tcgraph, Pressgraph)
```

Plot

```
% Plotting the price profile used for the optimization, the -
% optimal operation strategy, and the revenue achieved through -
% the time TSAM.


figure

subplot(3,1,1)
plot (1:TSAM, Q2(1:TSAM)'*(MaxQ-MinQ) + MinQ)
xlabel('Time [h]')
ylabel('[Euro/MW]')

subplot(3,1,2)
bar(1:TSAM,ut)
xlim([0 TSAM])
xlabel('Time [h]')
ylabel('Opt. St.')

subplot(3,1,3)
plot(1:TSAM, Revgraph)
xlabel('Time [h]')
ylabel('[Euro]')
```

Bibliography

[1] P. B. Weisz. Basic Choices and Constraints on Long-Term Energy Supplies. *Physics Today*, 57(7):47–55, July 2004.

[2] A. M. Mcfarlane. Energy: The Issue of the 21st Century. *ELEMENTS*, 3(3):165–170, 2007.

[3] International Energy Agency. Key World Energy Statistics 2009. Technical report, International Energy Agency, Paris, France, 2009.

[4] H-H. Rogner. An Assessment of World Hydrocarbon Resources. *Annual Review of Energy and the Environment*, 22(1):217–262, 1997.

[5] J. B. Greenblatt, S. Succar, D. C. Denkenberger, R. H. Williams, and R. H. Socolow. Baseload wind energy: modeling the competition between gas turbines and compressed air energy storage for supplemental generation. *Energy Policy*, 35(3):1474 – 1492, 2007.

[6] I. Dincer. Renewable energy and sustainable development: a crucial review. *Renewable and Sustainable Energy Reviews*, 4(2):157 – 175, 2000.

[7] R. M. Dell and D. A. J. Rand. Energy storage – a key technology for global energy sustainability. *Journal of Power Sources*, 100(1-2):2 – 17, 2001.

[8] M. Ringel. Fostering the use of renewable energies in the european union: the race between feed-in tariffs and green certificates. *Renewable Energy*, 31(1):1 – 17, 2006.

[9] S. Van der Linden. Bulk energy storage potential in the USA, current developments and future prospects. *Energy*, 31(15):3446 – 3457, 2006. ECOS 2004 - 17th International Conference on Efficiency, Costs, Optimization, Simulation, and Environmental Impact of Energy on Process Systems.

[10] M. J. Tinkler. Electricity storage: A key component of our emerging future. Toronto, Ontario, May 2009. THIRD INDUSTRIAL REVOLUTION: Canadian Executive Roundtable Meeting.

[11] J. Makansi and J. Abboud. Energy storage: The missing link in the electricity value chain. Whitepaper, May 2002.

[12] A. Cavallo. Controllable and affordable utility-scale electricity from intermittent wind resources and compressed air energy storage (CAES). *Energy*, 32(2):120 – 127, 2007.

[13] EPRI and U.S. Department of Energy. EPRI - DOE Handbook of Energy Storage for Transmission and Distribution Applications. Technical report, Electric Power Reseach Institute, Palo Alto, CA, and the U.S. Department of Energy, Washington, DC, 2003.

[14] P. Denholm and R. Sioshansi. The value of compressed air energy storage with wind in transmission-constrained electric power systems. *Energy Policy*, 37(8):3149 – 3158, 2009.

[15] J. Slowe. Emerging electricity storage technologies. *Cogeneration and On-Site Power Production*, pages 69 – 71, sept-oct 2008.

[16] J. Kondoh, I. Ishii, H. Yamaguchi, A. Murata, K. Otani, K. Sakuta, N. Higuchi, S. Sekine, and M. Kamimoto. Electrical energy storage systems for energy networks. *Energy Conversion and Management*, 41(17):1863 – 1874, 2000.

[17] H. Ibrahim, A. Ilinca, and J. Perron. Energy storage systems–characteristics and comparisons. *Renewable and Sustainable Energy Reviews*, 12(5):1221 – 1250, 2008.

[18] A. Ter-Gazarian and Institution of Electrical Engineers. *Energy storage for power systems / A. Ter-Gazarian*. P. Peregrinus on behalf of the Institution of Electrical Engineers, Stevenage, 1994.

[19] B. Sorensen. Dependability of wind energy generators with short-term energy storage. *Science*, 194:935–937, November 1976.

[20] F. R. Kalhammer and T. R. Schneider. Energy storage. *Annu. Rev. Energy*, 1:311–343, 1976.

[21] B. Roberts. Capturing grid power. *IEEE Power and Energy Magazine*, pages 32–41, july-august 2009.

[22] W. F. Pickard, A. Q. Shen, and N. J. Hansing. Parking the power: Strategies and physical limitations for bulk energy storage in supply-demand matching on a grid whose input power is provided by intermittent sources. *Renewable and Sustainable Energy Reviews*, 13(8):1934 – 1945, 2009.

[23] P. F. Ribeiro. Energy storage systems for advanced power applications. *Proceedings of the IEEE*, 89(12):1744–1756, 2001.

[24] P. Denholm, E. Ela, B. Kirby, and M. Milligan. The role of energy storage with renewable electricity generation. Technical report, Golden, Colorado, January 2010.

[25] D. Connolly. A review of energy storage technologies for the integration of fluctuating renewable energy. Technical report, August 2009.

[26] AMERICAN SOCIETY OF CIVIL ENGINEERS. *Hydroelectric pumped storage technology.* The american society of civil engineers, New-York, 1996. Prepared by the Task Committee on Pumped Storage of the Committee on the Hydropower of the Energy Division of the ASCE.

[27] AMERICAN SOCIETY OF CIVIL ENGINEERS. *Compendium of Pumped Storage Plants in the United States.* The american society of civil engineers, New-York, 1993.

[28] Electricity Storage Association. Pumped Hydro. *www.electricitystorage.org/site/technologies/pumped-hydro*, Accessed on March 23th, 2010.

[29] S. Succar and R. H. Williams. Compressed air energy storage: Theory, resources, and applications for wind power. Technical report, Princeton Environmental Institute, Princeton, New Jersey, April 2008.

[30] A. J. Giramonti, R. D. Lessard, W. A. Blecher, and E. B. Smith. Conceptual design of compressed air energy storage electric power systems. *Applied Energy*, 4(4):231 – 249, 1978.

[31] A. J. Cavallo. Energy storage technologies for utility scale intermittent renewable energy systems. *Journal of Solar Energy*, 123:387–389, November 2001.

[32] F. S. Aschner. *PLANNING FUNDAMENTALS OF THERMAL POWER PLANTS.* Israel University Press, Jerusalem, Israel, 1978.

[33] *Huntorf CAES: more than 20 years of successful operation*, Orlando, FL, 23-25 April 2001.

[34] M. J. Moran and H. N. Shapiro. *Fundamentals of Engineering Thermodynamics; 5th ed.* Wiley, Chichester, England, 2006.

[35] B. Calaminus. Innovative Adiabatic Compressed Air Energy Storage System of EnBW in Lower Saxony. In *2nd International Renewable Energy Storage conference (IRES II)*, Bonn, Germany, 2007.

[36] L. Nielsen and R. Leithner. Modelling and dynamic simulation of an underground cavern for operation in an innovative compressed air energy

storage plant. *5th International Conference on Energy, Environment, Ecosystems and Sustainable Development (EEESD '09)*, 2009.

[37] Ridge Energy Storage and Grid Services L.P. The Economic Impact of CAES on Wind in TX, OK, and NM. Technical report, Ridge Energy Storage and Grid Services L.P., June 2005.

[38] Ben M. Enis, P. Lieberman, and I. Rubin. Operation of hybrid wind-turbine compressed-air system for connection to electric grid networks and cogeneration. *Wind Engineering*, 27(6):449–459, 2003.

[39] C. Jakiel, S. Zunft, and A. Nowi. Adiabatic compressed air energy storage plants for efficient peak load power supply from wind energy: the European project AA-CAES. *International Journal of Energy Technology and Policy*, 5:296–306(11), 6 August 2007.

[40] J. Sears. Thermal and Compressed-Air Energy Storage (TACAS). In *Electricity Storage Association Annual Meeting*, Toronto, Ontario, May 2005.

[41] I. Arsie, V. Marano, G. Rizzo, G. Savino, and M. Moran. Energy and Economic Evaluation of a Hybrid CAES/Wind Power Plant with Neural Networks-Based Wind Speed Forecasting. In *Proc. of ECOS 2006*, Aghia Pelagia, Crete (Greece), July 12-14 2006. 19th Intn. Conf. on Effciency, Cost, Optimization, Simulation and Environmental Impact of Energy Systems.

[42] S. Lemofouet, A. Rufer, I. Cyphelly, P. Barrade, and F. Grasser. Principle of a hibrid compressed air and supercapacitors energy storage system with maximum efficiency point tracking. *http://www.scientificcommons.org/22456389*, 2003.

[43] S. Zunft, C. Jakiel, M. Koller, and C. Bullough. Adiabatic compressed air energy storage for the grid integration of wind power. 2006.

[44] W. F. Pickard, N. J. Hansing, and A. Q. Shen. Can large-scale advanced-adiabatic compressed air energy storage be justified economically in an age of sustainable energy? *Journal of Renewable and Sustainable Energy*, 1(3):033102–1 – 033102–10, 2009.

[45] G. Grazzini and A. Milazzo. Thermodynamic analysis of CAES/TES systems for renewable energy plants. *Renewable Energy*, 33(9):1998 – 2006, 2008.

[46] Fifth EU Framework Programme. Advanced Adiabatic Compressed Air Energy Storage (AA-CAES), 2002. Project reference: ENK6-CT-2002-00611.

[47] S. M. Schoenung and W. V. Hassenzahl. Short v. long term energy storage analysis. T, November 2002. THIRD INDUSTRIAL REVOLUTION: Canadian Executive Roundtable Meeting.

[48] Electricity Storage Association. Electricity Storage Technologies. *www.electricitystorage.org/ESA/technologies*, Accessed on October 3th, 2010.

[49] World Wind Energy Association. World Wind Energy Report 2009. Technical report, World Wind Energy Association, Bonn, Germany, March 2010.

[50] D. J. Swider. Compressed air energy storage in an electricity system with significant wind power generation. *Energy Conversion, IEEE Transactions on*, 22(1):95 –102, March 2007.

[51] J.K. Kaldellis, D. Zafirakis, and K. Kavadias. Techno-economic comparison of energy storage systems for island autonomous electrical networks. *Renewable and Sustainable Energy Reviews*, 13(2):378 – 392, 2009.

[52] P. Denholm, G. L. Kulcinski, and T. Holloway. Emissions and energy efficiency assessment of baseload wind energy systems. *Environmental Science and Technology*, 39(6):1903–1911, 2005.

[53] RWE. AA-CAES Project. *www.rwe.com/web/cms/en/113648/rwe /press-news/press-release/?pmid=4004404*, Accessed on October 10th, 2010.

[54] D. Laing, W. Steinmann, R. Tamme, and C. Richter. Solid media thermal storage for parabolic trough power plants. *Solar Energy*, 80(10):1283 – 1289, 2006. Solar Power and Chemical Energy Systems (SolarPACES'04).

[55] D. Laing, D. Lehmann, and C. Bahl. Concrete storage for solar thermal power plants and industrial process heat. 2008.

[56] D. Laing, D. Lehmann, M. Fiss, and C. Bahl. Test results of concrete thermal energy storage for parabolic trough power plants. *Journal of Solar Energy Engineering*, 131(4):041007, 2009.

[57] S. Lemofouet-Gatsi. *Investigation and Optimisation of Hybrid Electricity Storage Systems Based on Compressed Air and Super Capacitors.* PhD thesis, EPFL, October 2006.

[58] I. Arsie, V. Marano, G. Nappi, and G. Rizzo. A Model of a Hybrid Power Plant with Wind Turbines and Compressed Air Energy Storage. *Proc. of ASME Power Conference*, 2005.

[59] S.P. Sukhatme and J.K. Nayak. *SOLAR ENERGY: Principles of Thermal Collection and Storage*. Tata McGraw-Hill, India, New Delhi, 2008.

[60] S. L. Subhash and G. S. Jitendra. *High Thermal Conductivity Materials*. Springer, 233 Spring Street, New York, NY 10013, USA, 2006.

[61] E. F. Camacho and C. Bordons. *Model Predictive Control*. Springer Verlag, Berlin, 2004.

[62] M. Khalid and A.V. Savkin. A model predictive control approach to the problem of wind power smoothing with controlled battery storage. *Renewable Energy*, 35(7):1520 – 1526, 2010. Special Section: IST National Conference 2009.

[63] J. Löfberg. Yalmip : A toolbox for modeling and optimization in MATLAB. In *Proceedings of the CACSD Conference*, Taipei, Taiwan, 2004.

[64] C. V. Rao and J. B. Rawlings. Linear programming and model predictive control. *Journal of Process Control*, 10(2-3):283 – 289, 2000.

[65] J.B. Rawlings. Tutorial overview of model predictive control. *Control Systems Magazine, IEEE*, 20(3):38 –52, jun. 2000.

[66] D. Q. Mayne, J. B. Rawlings, C. V. Rao, and P. O. M. Scokaert. Constrained model predictive control: Stability and optimality. *Automatica*, 36(6):789 – 814, 2000.

[67] A. Ulbig, M. D. Galus, S. Chatzivasileiadis, and G. Andersson. General frequency control with aggregated control reserve capacity from time-varying sources: The case of phevs. In *IREP Symposium ï¿œ Bulk Power System Dynamics and Control VIII*, Búzios, RJ, Brazil, August 2010.

[68] C. Ebenbauer, T. Raff, and F. Allgöwer. Dissipation inequalities in systems theory: An introduction and recent results. In R. Jeltsch and G. Wanner, editors, *Invited Lectures of the International Congress on Industrial and Applied Mathematics 2007*, pages 23–42, 2009.

[69] M. Kvasnica, P. Grieder, M. Baotic, and F.J. Christophersen. *Multi-Parametric Toolbox (MPT)*. Institut für Automatik, ETH - Swiss Federal Institute of Technology, ETH, CH-8092 Zürich.

[70] H. Lund, G. Salg, B. Elmegaard, and A. N. Andersen. Optimal operation strategies of compressed air energy storage (CAES) on electricity spot markets with fluctuating prices. *Applied Thermal Engineering*, 29(5-6):799 – 806, 2009.

[71] European Power Exchange Spot Societas Europaea. European Power Exchange Market Data. *www.epexspot.com/en/market-data*, 2007.

[72] Y. Zimmels, F. Kirzhner, and B. Krasovitski. Design criteria for compressed air storage in hard rock. *Energy and Environment*, 13(6):851 – 872, 2002. Special Issue 3rd International Conference on Thermal Engineering: Theory and Applications.

[73] N. Elsner, S. Fischer, and J. Huhn. *Grundlagen der Technischen Thermodynamik, Band 2: Wärmeübertragung.* Akademie Verlag, Berlin, 1993.